Thèse n° 9080

Single-Chain Nanoparticles for Intracellular Drug Delivery

Présentée le 8 avril 2022

Faculté des sciences et techniques de l'ingénieur
Laboratoire des nanomatériaux supramoléculaires et interfaces - Chaire Constellium
Programme doctoral en science et génie des matériaux

pour l'obtention du grade de Docteur ès Sciences

par

Suiyang LIAO

Acceptée sur proposition du jury

Prof. V. Subramanian, président du jury
Prof. F. Stellacci, directeur de thèse
Prof. D. Irvine, rapporteur
Prof. E. Meijer, rapporteur
Prof. A. Anastasaki, rapporteuse

École
polytechnique
fédérale
de Lausanne

2022

C'est le temps que tu as perdu pour ta rose qui fait ta rose si importante.

— Antoine de Saint-Exupéry

Le Petit Prince

献给我的妈老汉儿

Acknowledgements

This PhD chapter of my life is measured by its length, 4.5 years, and by its width, the people whom I had the pleasure to encounter and whom my most sincere gratitude goes to…

My supervisor, Prof. Francesco Stellacci, without whom none of this would be possible. Thank you for the open-mindedness, for the sharing spirit, for the critical thinking, for the trust and support, for indulging my curiosity, and for being a role model!

The jury of my thesis: Prof. Athina Anastasaki, Prof. Bert Meijer, Prof. Darrell J. Irvine, and Prof. Vivek Subramanian for taking time to evaluate my work and challenging/inspiring me with insightful questions during the exam.

Prof. Harm-Anton Klok for the scientific discussion and the valuable suggestions. Prof. Horacio Cabral for hosting me in Todai and introducing me to the field of drug delivery. Prof. Renato Zenobi for hosting me in ETHZ and teaching me mass spectrometry.

The scientific infrastructure of EPFL, especially Luciano Abriata, Romain Guiet, Kelvin Lau, Natalia Gasilova, Daniel Ortiz, Laure Menin, André Mozes, Miguel Garcia, Jacques Morisod and Yann Lavanchy. Thank you!

The entire team of SuNMIL for sharing thoughts about work and life, for the support during drying times, for the lunchtime chats … especially Matteo$^{\text{my man}}$, Zhi$^{\text{big brother}}$, Lixia$^{\text{cell master}}$, Ahmet, Anna, Lukasz, Colleen, Quy, Paulo, and Chiara.

All the master/bachelor students who offered me opportunities to teach in the lab or classroom. The pleasure was truly mine.

All my friends. Xiangwei, Hao, Jing, Tzu-Hsien, Xiaoyu, Xiaotong, Ye, Anqi, Jiangtao, Aysu, Huachuan, Mou, Kasimir… for always being there for me.

XY, for understanding the little child inside the man.

My parents, 立琼&世林, for everything.

S.L.
Morges, 28th Feb. 2022

Abstract

Single-chain nanoparticles (SCNPs) are a type of polymeric nanoparticles formed by collapsing/folding individual polymer chains via intra-molecular interactions. Their emergence holds promise to construct sub-20 nm polymeric nanoparticles with defined structure.

Challenges remain for controllable construction of SCNPs. First, soft nanostructures like SCNPs are prone to deformation and cannot be well represented by geometrical terms such as size and shape; instead, a topological description is more proper. Second, SCNP formation by stochastic pairing of the functionalities from the same linear precursor leads to stochastic outcomes. Versatile synthetic approaches as well as novel analytical tools are needed to gain control on the SCNP topologies. Third, it remains an open question how SCNPs' topology affects their properties, such as their interaction with cells.

This thesis investigates SCNP folding and their interaction with cells from the topological point of view.

We first show that the SCNP topology can be tuned. The effect from two key factors (the initial chain conformation and the length of the cross-linkers) on the formation of SCNPs were experimentally investigated. A suite of analytical tools was developed and applied to characterize the SCNP topology, which was then correlated to SCNPs' cytotoxicity profile. We then show that cellular uptake discriminates SCNP topological isomers. SCNPs cross-linked with disulfide bonds were transformed into topological isomers by reshuffling the disulfide pairs. The nuances of different topologies were captured by the unparallel sensitivity of analytical ultracentrifugation. The glucocorticoid induced GFP translocation assays showed that the SCNPs' topology was essential for their ability to access the cytosol.

The overall work presented in the thesis provides new perspectives on SCNPs' formation, characterization, and interaction with cells from the topological point of view.

Keywords: SCNPs; topology; topological isomer; topological defects; characterization; drug delivery

Riassunto

Le nanoparticelle a catena singola (SCNP) sono un tipo di nanoparticelle polimeriche formate dal collasso/ripiegamento di singole catene polimeriche tramite interazioni intramolecolari. Questo approccio promette di costruire nanoparticelle polimeriche inferiori a 20 nm con una struttura definita.

Restano comunque delle difficoltà per la sintesi controllata di SCNP. In primo luogo, le nanostrutture soffici come le SCNP sono soggette a deformazione e non possono essere ben rappresentate da termini geometrici come dimensioni e forma; è necessaria, invece, una prospettiva topologica. In secondo luogo, la formazione di SCNP mediante l'accoppiamento stocastico delle funzionalità dello stesso precursore lineare porta a risultati imprevedibili; per ottenere il controllo sulle topologie delle SCNP sono necessari approcci sintetici facili e versatili, nonché nuovi strumenti analitici. Terzo, in che modo la topologia delle SCNP influisce sulle loro proprietà, come la loro interazione con le cellule?

Questa tesi indaga il ripiegamento delle SCNP e la loro interazione con le cellule dal punto di vista topologico.

Per prima cosa mostriamo che la topologia delle SCNP può essere controllata. L'effetto di due fattori chiave (la conformazione iniziale della catena e la lunghezza dei reticolanti) sulla formazione delle SCNP è stato studiato sperimentalmente. Sono stati inoltre sviluppati e applicati una serie di strumenti analitici per caratterizzare la topologia delle SCNP, che è stata quindi correlata al profilo di citotossicità delle SCNP. Mostriamo quindi che l'assorbimento cellulare discrimina gli isomeri topologici di SCNP. Le SCNP reticolate con legami disolfuro sono state trasformate in isomeri topologici rimescolando le coppie disolfuro. Le sfumature di diverse topologie sono state identificate dall'impareggiabile sensibilità dell'ultracentrifugazione analitica. I test di traslocazione di GFP indotti da glucocorticoidi hanno mostrato che la topologia delle SCNP è essenziale per la loro capacità di accedere al citosol.

Il lavoro complessivo presentato nella tesi fornisce nuove prospettive sulla formazione, la caratterizzazione e l'interazione con le cellule delle SCNP dal punto di vista topologico.

Parole chiave: SCNP; topologia; isomero topologico; difetti topologici; caratterizzazione; somministrazione farmaci

Table of Contents

Acknowledgements iii
Abstract v
Riassunto vii
Table of Contents ix
List of Figures xi
List of Equation xiii
List of Abbreviations xv
Thesis structure xix
Chapter 1 SCNPs: chemistry and application 1
1.1 Polymer Chain 2
1.2 From a chain to a particle 6
1.3 Single-chain technology 8
1.4 Applications in drug delivery 11
1.5 Reference 14
Chapter 2 SCNPs: topology and characterization 19
2.1 Topology 20
2.2 Characterization 27
2.3 Summary 39
2.4 Reference 40
Chapter 3 Cellular uptake 45
3.1 Why nano? 46
3.2 En route to the cytosol 47
3.3 Cellular uptake of SCNPs 54
3.4 Summary 57
3.5 Reference 58
Chapter 4 Control and Characterization of SCNP Topology 63
4.1 Abstract 64
4.2 Introduction 64
4.3 Results and Discussion 68
4.4 Summary 76
4.5 Supplmentary Information 78
4.6 Reference 89
Chapter 5 Cellular Uptake Discriminates SCNP Topological Isomers 95
5.1 Abstract 96

5.2 Introduction 96
5.3 Scheme and Characterization 98
5.4 Cell penetration observed with CLSM 100
5.5 Endocytoci Inhibitor Assay 101
5.6 Solvent-guided reshuffle 102
5.7 GIGT: cytosol-accessing ability 105
5.8 Summary 106
5.9 Supplementary Information 107
5.10 Reference 116
Chapter 6 Summary and Outlook 119
6.1 Contributions of this thesis 119
6.2 Outstanding questions 119
Curriculum Vitae 123

List of Figures

Figure 1.1 Basic concepts in polymer science..2
Figure 1.2 Schematic illustration of a polymer chain occupying the space of approximately a sphere of its gyration radius 3
Figure 1.3 Concentration regimes of polymer solutions 4
Figure 1.4 Polymer-solvent mixing, Flory-Huggins parameter and polymer chain conformation in solution. 5
Figure 1.5 Polymeric nanoparticles 7
Figure 1.6 Protein folding..8
Figure 1.7 Three general modes of single-chain compaction......................................9
Figure 1.8 The evolution of single-chain technology...10
Figure 1.9 Peptide delivery with SCNPs...12
Figure 2.1 A mug and a donut. 20
Figure 2.2 Loops as one of the topological features in polymer networks................21
Figure 2.3 Loops are characterized both by the individual geometry and the collective topology. 23
Figure 2.4 Schematic illustration of two main types of single-chain cross-linking strategies and the corresponding topological defects 24
Figure 2.5 Illustration of two distinct topologies (sparse and compact) of SCNPs....25
Figure 2.6 Viscometry. 28
Figure 2.7 Size exclusion chromatography 29
Figure 2.8 Atomic force microscopy 30
Figure 2.9 Small angle neuron scattering 32
Figure 2.10 Diffusion ordered spectroscopy NMR 33
Figure 2.11 NMR relaxation..34
Figure 2.12 AUC: instrumentation, force analysis, and data acquisition 36
Figure 3.1 Size of nanoparticles affect their biological distribution 47
Figure 3.2 Main endocytic pathways...47
Figure 3.3 The cellular uptake pathway is size/shape dependent...............................49
Figure 3.4 Different endosomal escape mechanisms. 50
Figure 3.5 Using the fluorescent pattern to judge cytosolic localization of nanoparticles...52
Figure 3.6 The mechanism of GIGT assay..53
Figure 3.7 SCNPs' interacting modes with cells as an interplay between rigidity and hydrophobicity...54

Figure 3.8 Cytosolic delivery of SCNPs highly depends on their surface charge......55
Figure 4.1 PALA SCNPs crosslinked with dicarboxylic acids. 69
Figure 4.2 Plots of diffusion coefficients (panels in the upper row) determined from DOSY-NMR. 71
Figure 4.3 Viscosity-concentration plots for SCNP solutions...................................72
Figure 4.4 Contour plots of sedimentation coefficients vs frictional ratio for SCNPs.73
Figure 4.5 NMR relaxation of PALA SCNPs. 75
Figure 4.6 Topology-cytotoxicity relationship. 76
Figure 5.1 Control and characterization of the topology of SCNPs. 98
Figure 5.2 Cell penetration assay observed with CLSM. 100
Figure 5.3 Endodocytic inhibitor assay. 101
Figure 5.4 Solvent-guided topological reshuffle. 102
Figure 5.5 Distribution of sedimentation coefficients of all samples. 104
Figure 5.6 Schematic illustration and result of GIGT assay....................................105

List of Equation

Eqn. 1-1 Estimation the overlap concentration 4
Eqn. 1-2 Overlap concentration and intrinsic viscosity 4
Eqn. 1-3 Flory-Huggins χ parameter 5
Eqn. 2-1 Mark-Houwink equation 27
Eqn. 2-2 Flory-Huggins equation 28
Eqn. 2-3 Stokes-Einstein relationship 31
Eqn. 2-4 Stejskal Tanner equation 33
Eqn. 2-5 Mono-exponential decay in NMR transverse relaxation 33
Eqn. 2-6 Svedberg equation 36
Eqn. 2-7 Lamm equation 37
Eqn. 2-8 The six relationships among key hydrodynamic parameters in SV-AUC ... 37

List of Abbreviations

AF647	Alexa Flour 647
AFM	atomic force microscopy
ATP	adenosine triphosphate
AUC	Analytical Ultracentrifugation
BBB	blood brain barrier
BTA	Benzene-1,3,5-tricarboxamide
CLSM	confocal laser scanning microscopy
CME	clathrin-mediated endocytosis
CPZ	chlorpromazine
DEX	dexamethasone acid
DLS	dynamic light scattering
DMEM	Dulbecco's modified Eagle medium
DNA	deoxyribonucleic acid
DOSY	diffusion-ordered spectroscopy
DTT	dithiothreitol
Dyn	dynasore
EDC	N-(3-Dimethylaminopropyl)-N -ethylcarbodiimide hydrochloride
EIPA	5-(N-Ethyl-N-isopropyl)amiloride
EPR	enhanced permeability and retention
ESI-MS	electrospray ionization mass spectrometry
FACS	fluorescence-activated cell sorting
FBS	fetal bovine serum
GFP	green fluorescence protein

GIGT	Glucocorticoid receptor Induced GFP Translocation
GR	glucocorticoid receptor
MALLS	multiple angle laser light scattering
MCNP	multi-chain nanoparticle
MD	molecular dynamics
MFI	mean fluorescence intensity
MW	molecular weight
MβCD	methyl-β-cyclodextrin
NHS	N-Hydroxysuccinimide
NMR	nuclear magnetic resonance
Nys	nystatin
OD	optical density
PALA	polyallylamine
PAMAM	poly(amidoamine)
PBS	phophate-buffered saline
PDI	polydispersity index
PGSE	pulsed gradient spin echo
PMMA	polymethyl methacrylate
RNA	ribonucleic acid
SANS	small angle neutron scattering
SAXS	small angle x-ray scattering
SCNP	single-chain nanoparticles
SD	standard deviation
SEC	size exclusion chromatography
SEM	scanning electron microscopy
siRNA	small interfering RNA

SLS	static light scattering
SV-AUC	sedimentation velocity-analytical ultracentrifugation
TEM	transmission electron microscopy
Upy	2-ureido-pyrimidinone
Wort	wortmannin

Thesis structure

Chapter 1 gives an overall review to the state of the art on SCNPs. The discussion unfolds with the fundamentals about polymer and dilute polymer solutions, where the interaction between solvent molecules and single polymer chains are discussed. The section "single-chain technology" will briefly discuss the synthetic strategies to construct SCNPs. SCNPs' applications, especially as drug delivery vehicles, are summarized.

Chapter 2 gives some topological perspective on SCNPs. Crosslinking is regarded as an event to introduce loops to polymeric networks. The local collective topologies of loops have fundamental effect on the global topology of SCNPs. Common analytical techniques to characterize single-chain crosslinking are summarized in this chapter as well.

Chapter 3 discusses the considerations when constructing a drug delivery vehicle. The challenges on crossing biological barriers of all levels are mentioned with the focus on how nanoparticles interact with cellular membranes and escape from endolysosomal compartments.

Chapter 4 is restructured from a published work entitled *Control and characterization of the compactness of SCNPs*. This work/chapter discusses how the compactness of SCNPs are mediated by two important factors (the length of cross-linkers and solvent quality). Novel characterization tools are introduced to probe the compactness. Such compactness was shown to have correlation with the cytotoxicity and the compaction strategy provided in this work could be applied to mitigate the cytotoxicity of cationic polymers.

Chapter 5 studies how the topology of SCNPs affects their cellular uptake pathway. Two of the samples from the work presented in Chapter 4 with the similar molecular formula but only differ in compactness were applied to study their cellular uptake profiles by either varying the incubation temperature or via the application of endocytic inhibitors. The permanent covalent bonds were then replaced with a type of disulfide cross-linker. The dynamic nature of disulfide bonds enables us to reshuffle (in a more refined manner through their interaction with solvent molecules) from the same batch of SCNPs into isomers only differ in compactness, as evidenced by SV-AUC. The cytosol-accessing ability of SCNPs with distinct compactness was then evaluated with GIGT assay.

Chapter 6 summarizes all the investigations from this thesis and points out future directions.

Chapter 1 SCNPs: chemistry and application

Single-chain polymeric nanoparticles (SCNPs) are a type of polymeric particles formed by the self-crosslinking of single polymer chains. Compared to conventional polymeric nanoparticles, they are ultrasmall within the size range of sub 20 nm. This chapter briefs the reader about the basics of polymer science, the rationales of single-chain compaction, the single-chain technology, and the applications of SCNPs.

1.1 POLYMER CHAIN

1.1.1 Basics

The concept of “polymer”, as derived from the Greek word πολὺς (polus, meaning “many”) and μέρος (meros, meaning “part”), refers to the substance composed of many parts. “One part” makes it a monomer; “two parts” makes it a dimer; “three parts” makes it a trimer; “a few parts” is an oligomer. A polymer is made by polymerizing *n* units of the monomers. On the polymer chains, monomers form units that repeatedly appear, termed as repeating units.

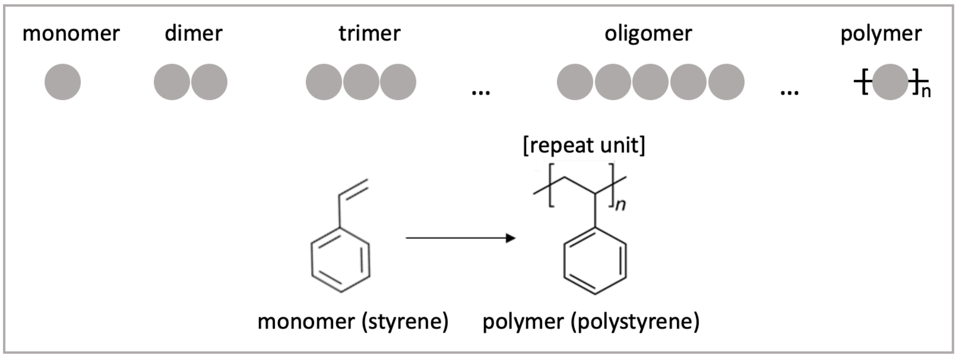

Figure 1.1 Basic concepts in polymer science

The synthetic process to produce polymers is called **polymerization**. The conventional polymerization method is called free radical polymerization (FRP). During FRP, one has limited control on the chain growth, thus the product is heterogenous in chain lengths. Such heterogeneity of chain lengths is quantified as dispersity *Đ*, the quotient of the weight average molecular weight (Mw) to the number average molecular weight (Mn). Controlled radical polymerization (CRP), in contrast to FRP, has been developed to afford polymeric products with more uniform length, architecture, and end groups. Two popular methodologies of CRP are atom transfer radical polymerization (ATRP) and reversible addition-fragmentation chain-transfer (RAFT) polymerization. Mechanism of polymerization, especially the comparison between ATRP and RAFT was elucidated in a recent perspective article[1] by Anastasaki and coworkers.

Some popular classifications of polymeric materials are based on, the structure (linear, branched, or network), the thermo-response (plastics, rubbers, or thermosets), the monomer (homopolymer or copolymer), the polymerizing mode (addition or condensation), the tacticity (isotactic, atactic or syndiotactic), and the origin (natural or synthetic polymer).

1.1.2 Polymer solution

The single-chain folding reaction requires well separation of the polymer into single-chain state. This is usually achieved by dissolving the polymer as solution below the overlap concentration.

Concentration regimes

A single polymer chain roughly occupies the space of a sphere of a linear dimension of its own gyration radius R_g, as illustrated in Figure 1.2.

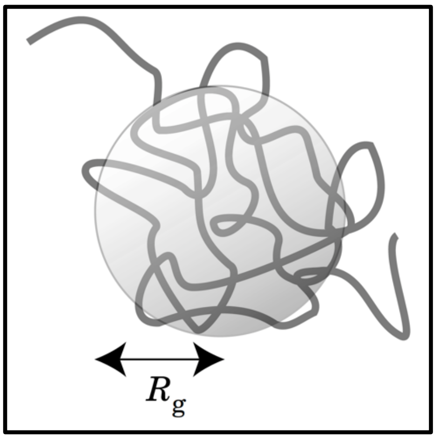

Figure 1.2 Schematic illustration of a polymer chain occupying the space of approximately a sphere of its gyration radius
(Reproduced with permission of the Wiley and Sons)[2]

At a sufficiently low concentration, polymer chains are well separated from each other. As the concentration increases to a critical value, c^*, one starts to observe inter-chain entanglement (Figure 1.3). This critical concentration is called **overlap concentration**, below which, the polymer solution is considered to be dilute. Most of the single-chain cross-linking reactions are conducted in dilute solution to avoid chain entanglement and interact primarily with solvent molecules.

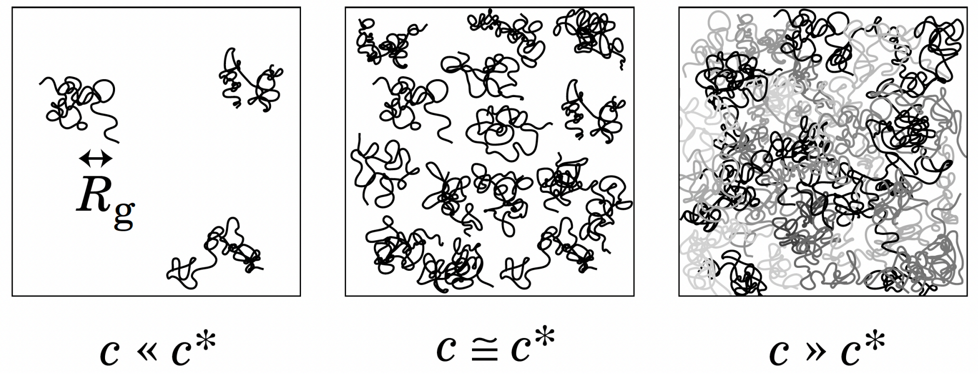

Figure 1.3 Concentration regimes of polymer solutions

(Reproduced with permission of the Wiley and Sons)[2]

Estimation of the overlap concentration (for instance, expressed as mass concentration) can be calculated by Eqn. 1-1, where M/N_A stands for the mass of an individual polymer chain. (M: molecular weight of the polymer; N_A: Avogadro's number)

Eqn. 1-1 Estimation of the overlap concentration

$$c^*\left(\frac{4\pi}{3}R_g{}^3\right) = \frac{M}{N_A}$$

In practice, overlap concentration c^* can be experimentally measured as the inverse of the intrinsic viscosity $[\eta]$. Discussion regarding viscometry can be found in the section Viscometry.

Eqn. 1-2 Overlap concentration and intrinsic viscosity

$$c^*[\eta] = 1$$

Solvent qualities

Some solvents can dissolve certain polymers well and they are termed as "good solvents", otherwise they are considered "bad solvents" or "poor solvents". Solvation of the polymer into its good solvents lowers the free energy. Although the free energy is co-determined by the enthalpy term and the entropy term, the latter is negligible for polymer-solvent systems, especially when the concentration is low. Thus, the enthalpy of mixing will, to a large extent, determine the miscibility.

When the polymer is dissolved below the overlap concentration as single polymer chains, the enthalpic interplay between the polymer and the solvent molecules determines the conformation of the polymer chains. This can be understood by the lattice fluid model where the interactions are considered between nearest neighbors. We use ε_{ss}, ε_{pp}, and ε_{ps} to denote the interaction between solvent-solvent contacts, polymer-polymer contacts, and polymer-solvent contacts, respectively.

Mixing the polymer and the solvents is a process where the contacts are rearranged, as shown in Figure 1.4A. One theoretical parameter to characterize the solvent quality is the Flory-Huggins χ parameter, as defined by Eqn. 1-3, as the product of the lattice coordinate Z and the energy change reduced by k_BT.

Eqn. 1-3 Flory-Huggins χ parameter

$$\chi = Z[\varepsilon_{PS} - (\varepsilon_{PP} + \varepsilon_{SS})/2]/k_BT$$

Positive χ values indicate that polymer-solvent contacts are less favored than polymer-polymer contacts and solvent-solvent contacts, and *vice versa*. Depending on their interaction with the solvent, the polymer chains in dilute solutions present extended coil conformation in good solvents, or contracted globule conformation (sometimes even aggregates) in poor solvents (Figure 1.4C).

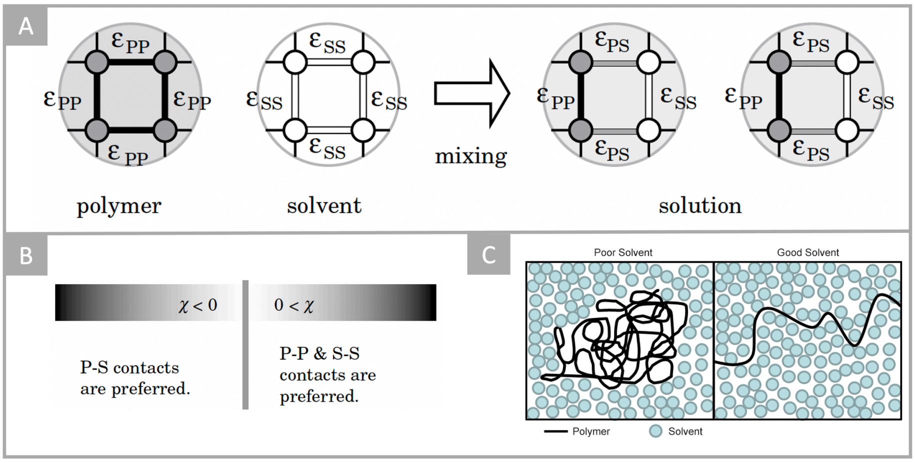
A
ε_PP
ε_PP
ε_PP
ε_PP
ε_SS
ε_SS
ε_SS
ε_SS
mixing
ε_PS
ε_PP
ε_SS
ε_PS
ε_PS
ε_PP
ε_SS
ε_PS
polymer
solvent
solution
B
χ < 0
0 < χ
P-S contacts are preferred.
P-P & S-S contacts are preferred.
C
Poor Solvent
Good Solvent
Polymer
Solvent

Figure 1.4 Polymer-solvent mixing, Flory-Huggins parameter and polymer chain conformation in solution.

A) The lattice fluid model to study the interaction between the polymer and the solvent; B) Flory-Huggins parameter χ as an indicator for solvent quality; C) Polymer chain conformation under different solvent conditions. (Reproduced with permission of the Wiley and Sons)[2]

1.2 FROM A CHAIN TO A PARTICLE

1.2.1 Nanoparticles

The term “nano” comes from ancient Greek “nános”, meaning dwarf. When used as a prefix, “nano” denotes 10^{-9}. The term “particle” usually refers to a spherical, or close to spherical object. As the discussion expands in the latter sections of the thesis, you will find that SCNPs don’t necessarily possess a spherical geometry. But as the convention, we keep using the term.

The history of nanoparticles can be traced back to the fourth century by the Roman with the Lycurgus Cup[3] where the presence of silver-gold alloy with 50 -100 nm in diameter creates the phenomenon of dichroism. The modern concept of nanotechnology was introduced in 1959 by Richard Feynman[4] in his lecture entitled “There’s Plenty of Room at the Bottom” at Caltech. In 2011, the EU Commission[5] defines a nanomaterial as “a natural, incidental or manufactured material containing particles, in an unbound state or as an aggregate or as an agglomerate and where, for 50% or more of the particles in the number size distribution, one or more external dimensions is in the size range 1 - 100 nm.”

Decades of intense research have enabled us to construct inorganic nanoparticles from an array of materials,[6] of different sizes,[7,8] with a variety of surface[9], and with defined shapes[10].

Polymeric materials have the potential advantages over inorganic materials, such as biodegradability, easy elimination, biocompatibility, nontoxicity, and their capability of packaging and delivering cargos,[11] thus receiving great research interest, especially in biomedicine.

Under the context of biomedicine, convectional **polymeric nanoparticles** (PNP) are usually formed upon drug formulation. They are characterized with an average size between 10 and 100 nm.[12] Depending on the morphological structure, PNPs can be classified into two categories, nanocapsule, and nanosphere,[13,14] as illustrated in Figure 1.5. The nanocapsule approach forms a clear reservoir system where the drug molecules can be loaded in the core region; the nanosphere approach forms a matrix system where the drug molecules are entrapped in the network.

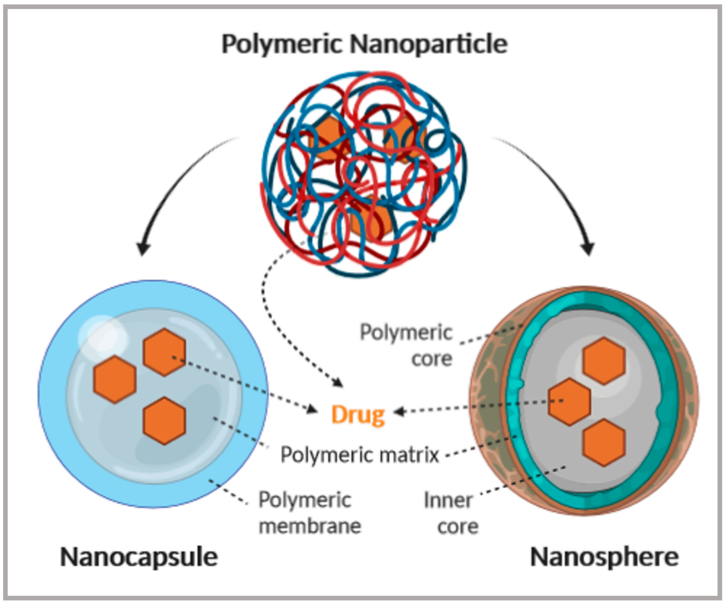

Figure 1.5 Polymeric nanoparticles

(Reproduced from ref[14])

1.2.2 Why fold a polymer chain?

Plenty of room deep inside

If we rephrase the famous quote from Feynman under the context of nanomedicine, we can safely say that there's still plenty of room deep inside. To navigate drug molecules across some biological barriers requires ultrasmall sizes. Conventional polymeric nanoparticles as large (mostly >50 nm) aggregates of polymer chains are no longer the best candidates. Instead, forming polymeric nanoparticles from single chains fills the blank of <10 nm.

Inspiration from proteins

Biopolymers are not readily endowed with certain functions as soon as the polymerization is done. They need to go through a rather delicate process where they self-interact to evolve into a higher order structure. We take protein as example. Putting the ribosome's translation of mRNA in synthetic terms, the monomers (amino acids) are first polymerized in a certain order into polypeptide chains via condensation. The resulting polypeptides are mono-disperse polymer chains with defined sequences, serving as the precursor for protein folding. While the folding pathway and the mechanism is still not clear, it's widely accepted that the sequence of amino acids dictates the proteins' final higher order structure, as shown in Figure 1.6. Folding synthetic polymer chains into SCNPs has been partly inspired by protein folding to gain more complex structures and in turn certain functions.

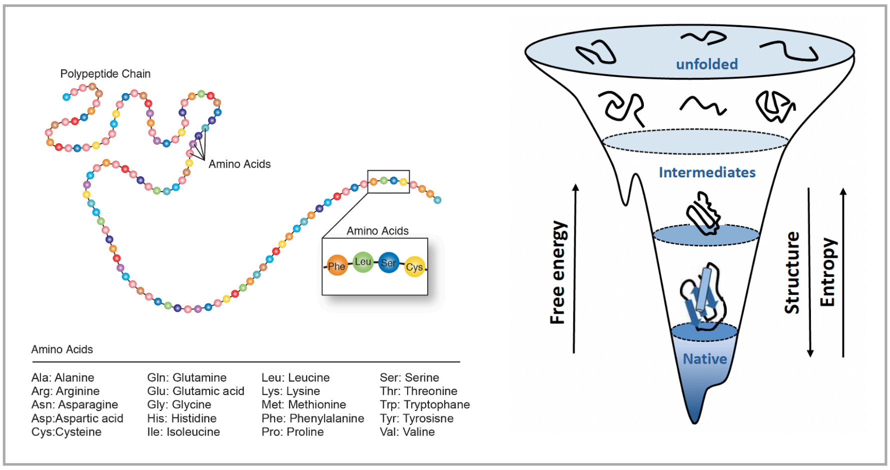
Polypeptide Chain
Amino Acids
Amino Acids
Phe
Leu
Ser
Cys
Amino Acids
Ala: Alanine
Arg: Arginine
Asn: Asparagine
Asp:Aspartic acid
Cys:Cysteine
Gln: Glutamine
Glu: Glutamic acid
Gly: Glycine
His: Histidine
Ile: Isoleucine
Leu: Leucine
Lys: Lysine
Met: Methionine
Phe: Phenylalanine
Pro: Proline
Ser: Serine
Thr: Threonine
Trp: Tryptophane
Tyr: Tyrosisne
Val: Valine
unfolded
Intermediates
Native
Free energy
Structure
Entropy

Figure 1.6 Protein folding

1.3 SINGLE-CHAIN TECHNOLOGY

While the IUPAC gold book[15] defines crosslinking as an inter-molecular event, putting this term under the context of SCNPs, the crosslinking generates intra-molecular linkage to induce chain collapse. The intra-molecular crosslinking strategies are summarized as single-chain technology.

1.3.1 Mode of crosslinking

One popular way to classify single-chain technologies is through the modes of crosslinking as shown in Figure 1.7. In homo-functional chain-collapse, the polymer chain is functionalized with self-complementary A groups (e.g., thiols or olefin). In hetero-functional chain-collapse, instead of having one type of functional group, two types of complementary moieties, A and B, are required to exist simultaneously on the same backbone. The third strategy is to mediate chain collapse via external cross-linkers. The collapse of A-decorating polymer chains is induced by reacting with the two B-end groups of the cross-linkers.

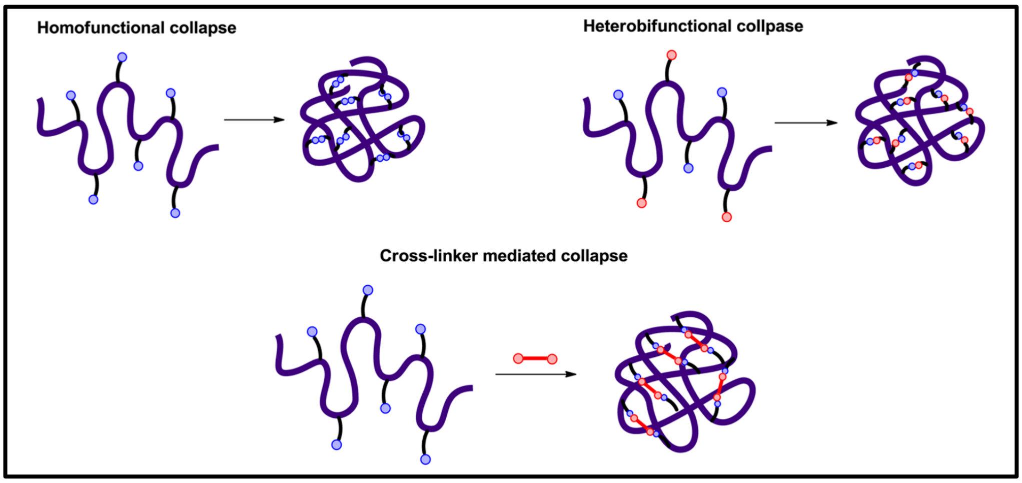

Figure 1.7 Three general modes of single-chain compaction.
Homofunctional collapse; heterofunctional collapse; cross-linker mediated collapse.
(Reproduced from ref[16])

While most of the works from the community of SCNPs can be covered by one of the three types of cross-linking modes, there are some exceptions. For instance, the polymer chains could be diblock or triblock copolymers so that the final SCNPs can exhibit tadpole-like[17], Janus[18] or dumbbell-like[19] morphology; in the case of hetero-internal-crosslinking, more than two types of complementary moieties can reside on the polymer chain to support orthogonal[4], or step-wise folding[20,21], not to mention the huge potential behind the advancement of sequence-defined synthetic polymer; the architecture of the external cross-linkers can be bidentate, tridentate and so on. For the interest of reading about cross-linking chemistry, the reader can be directed to the review by Lemcoff et al.[16]

1.3.2 Types of interaction

Another fashion of classifying single-chain technologies is by the nature of crosslinking bonds to be permanent or dynamic. As shown in Figure 1.8, permanent SCNPs are formed with covalent bonds; dynamic SCNPs can be formed via non-covalent/ supramolecular interactions (H bonds, pi stacking, metal coordination, hydrophobic interaction *et cetera*) or dynamic covalent bonds (disulfide bonds, Coumarin dimerization *et cetera*).

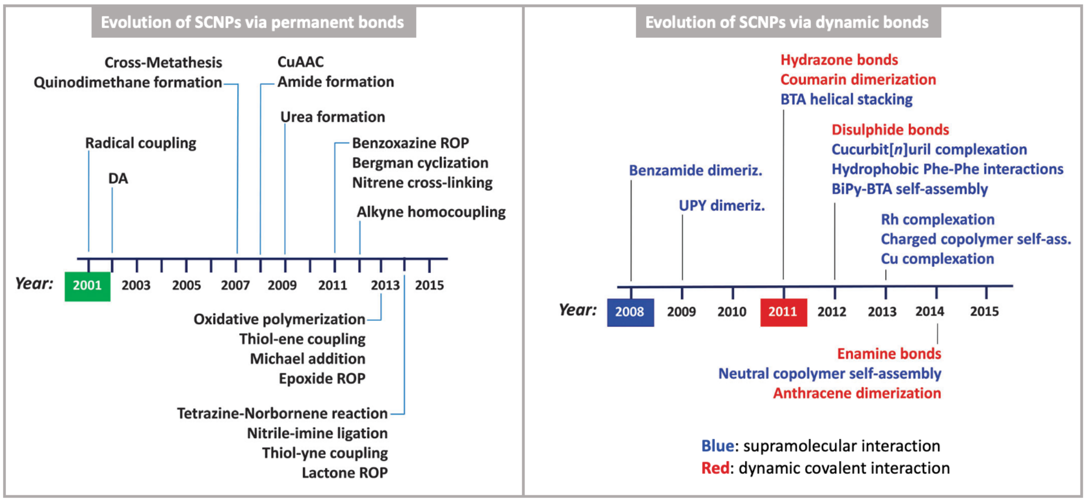
Evolution of SCNPs via permanent bonds
Cross-Metathesis
Quinodimethane formation
CuAAC
Amide formation
Urea formation
Radical coupling
DA
Benzoxazine ROP
Bergman cyclization
Nitrene cross-linking
Alkyne homocoupling
Year:
2001
2003
2005
2007
2009
2011
2013
2015
Oxidative polymerization
Thiol-ene coupling
Michael addition
Epoxide ROP
Tetrazine-Norbornene reaction
Nitrile-imine ligation
Thiol-yne coupling
Lactone ROP
Evolution of SCNPs via dynamic bonds
Hydrazone bonds
Coumarin dimerization
BTA helical stacking
Disulphide bonds
Cucurbit[n]uril complexation
Hydrophobic Phe-Phe interactions
BiPy-BTA self-assembly
Benzamide dimeriz.
UPY dimeriz.
Rh complexation
Charged copolymer self-ass.
Cu complexation
Year:
2008
2009
2010
2011
2012
2013
2014
2015
Enamine bonds
Neutral copolymer self-assembly
Anthracene dimerization
Blue: supramolecular interaction
Red: dynamic covalent interaction

Figure 1.8 The evolution of single-chain technology.
(Adapted from ref[22])

Over the past decades, researchers from the field of SCNPs have been continuously updating the progress of single-chain technology. Herein, instead of making redundant efforts, this section summarizes some noteworthy reviews on the chemistry of SCNPs for interested readers to extend their reading.

The Berda group published a user's guide[23,24] and a perspective article on SCNPs in 2015 outlining various aspects of SCNPs from synthesis, characterization to applications. Some review articles from Barner-Kowollik and coworkers critically explore the hurdles and challenges in the field of polymer chemistry limiting SCNP design[25,26,27]. The review by Chen and Berda[28] summarized the progress in SCNP of complex architectures and highlight unresolved issues in the field, such as scalability and topological purity of SCNP. Becer and coworkers' 2021 review[29] updated the readership on the recent developments in SCNPs according to their synthetic approaches via either **selective point folding** methods or repeat unit folding routes. The perspective article by Lutz, Sawamoto and coworkers[30] described in detail advances in macromolecular science and emphasize the possible emergence of technologies based on single-chain devices. Meijer, Palman and coworkers[31] highlighted the potential of SCNPs for catalysis in water and sensing, functions that all arise as a result of the well-defined conformations that are attained by directional **non-covalent** interactions. Single-chain technology in constructing different nanoscale architectures was reviewed by Pomposo and coworkers[22]; and also the same group[32] summarized recent research about **multi-orthogonally** folded SCNPs prepared through both reversible and permanent bonds. The review[33] by Meijer and coworkers focuses on the folding of single polymer chains into well-defined nanoparticles using **supramolecular** interactions and their possible use as enzyme mimics. The Pomposo group[34] highlighted the usage of **click chemistry** in constructing SCNPs.

1.4 APPLICATIONS IN DRUG DELIVERY

SCNPs have found applications in three major areas, nanomedicine, catalysis, sensing, together with some other developments. This thesis strives for SCNPs' applications for drug delivery. Thus, the section will make a literature review in this regard. For other applications to the interested readership, I make a summary about related reviews and research articles. Zimmerman and coworkers discussed the intra-chain reactions, physical properties and enzyme mimicking.[35] De-La-Cuesta et al. reviewed the methods to generate fluorescent SCNPs and their potential in cell biology and nanomedicine.[36] Latorre-Sánchez and Pomposo summarized SCNPs' bioinspired applications, such as protein mimics and biosensing.[37] Pomposo and coworkers discussed the opportunities in the confinement effect of SCNPs, such as improving the catalytic performance, drug loading and transportation, and bioimaging.[38] Endowed with the ultrasmall size, SCNPs exhibit unique biodistribution profiles. Loinaz and coworkers demonstrated their application as image contrast agents for pancreatic tumor diagnosis[39] and deep penetration of lung[40]. Liang et al.[41] crosslinked single polyacrylamide chains with diamines into SCNPs as the mimics of β-crystallins, one of the most abundant globular proteins of the human lens. Their SCNPs match the hydrodynamic radius, refractive index, size, density, and intrinsic and dynamic viscosities with β-crystallins while showing good biocompatibility with relevant cells, thus holding promise for the treatment of presbyopia and cataracts.

Some recent works have demonstrated the potential of SCNPs' usage as drug delivery vehicles[42] for small molecules, peptides, and proteins.

Pomposo and coworkers[43,44] showed that vitamin B9 and hinokitiol, two dermal bioactive cargos could be successfully loaded into sparse SCNPs, for potential dermal supply. Huang and coworkers[45] explored the strategy to load 5-fluorouracil, a type of anticancer drug, into SCNPs crosslinked with hydrogen bonds. Thayumanavan and coworkers[46] synthesized SCNPs exhibiting host–guest properties to stably encapsulate hydrophobic guests (fluorescent dyes and doxorubicin) to be released upon redox triggering. Appel and coworkers[47] utilized controlled radical polymerization techniques to prepare amphiphilic comb copolymers that self-assemble into unimolecular “micelle-like” nanocarriers of predictable size and demonstrated their potential for drug delivery with hydrophobic fluorescent dyes. Gracia et al.[48] report on the conjugation of a synthetic Tn-antigen mimetic to biocompatible and water-dispersible dextran-based SCNPs.

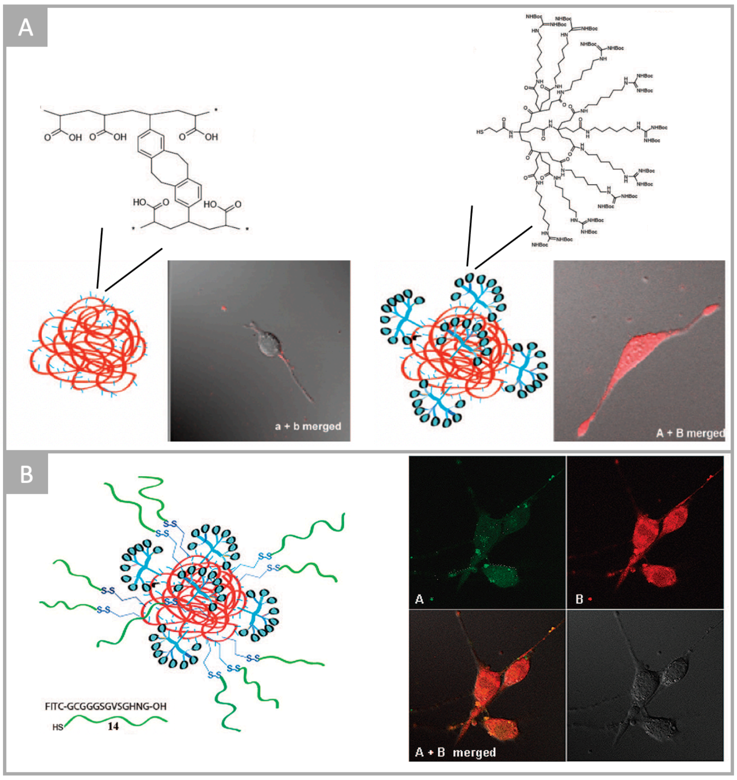

Figure 1.9 Peptide delivery with SCNPs.

A) the dendritic decorating units boost the cell penetrating ability; B) Model peptides labelled with FITC were conjugated to the SCNPs via disulfide bonds. Confocal imaging showed uniform distribution of FITC signal indicating cytosolic delivery of the peptides. (Adapted from ref[49])

To develop SCNPs as a platform for peptide delivery, Hamilton and Harth[49] conjugated a type of dendritic molecular transporter units onto SCNPs to improve their cell penetrating profile, as shown in Figure 1.9A. The model FITC-labelled peptides were loaded onto the SCNPs via disulfide bonds to be successfully delivered into NIH 3T3 cells (Figure 1.9B).

SCNPs also hold potential for fulfilling the delivery task of biomacromolecules such as proteins. Sawamoto, Maynard and coworkers[50,51] amphiphilic/fluorous random copolymers bearing poly(ethylene glycol) (PEG) chains and perfluorinated alkane pendants were developed as precursor polymers for protein loading via disulfide conjugation or encapsulation.

1.5 REFERENCE

(1) Truong, N. P.; Jones, G. R.; Bradford, K. G. E.; Konkolewicz, D.; Anastasaki, A. A Comparison of RAFT and ATRP Methods for Controlled Radical Polymerization. *Nat Rev Chem* **2021**, *5* (12), 859–869. https://doi.org/10.1038/s41570-021-00328-8.

(2) Polymer Solutions: An Introduction to Physical Properties | Wiley https://www.wiley.com/en-us/Polymer+Solutions%3A+An+Introduction+to+Physical+Properties-p-9780471389293.

(3) Lycurgus Cup. *Wikipedia*; 2021.

(4) Feynman, R. P. Plenty of Room at the Bottom. 7.

(5) Union, P. O. of the E. Commission Recommendation of 18 October 2011 on the definition of nanomaterial Text with EEA relevance, CELEX1 http://op.europa.eu/en/publication-detail/-/publication/17af73d9-da70-4a46-a421-c62e3d1df6ce/language-en.

(6) Heiligtag, F. J.; Niederberger, M. The Fascinating World of Nanoparticle Research. *Materials Today* **2013**, *16* (7), 262–271. https://doi.org/10.1016/j.mattod.2013.07.004.

(7) Zheng, N.; Fan, J.; Stucky, G. D. One-Step One-Phase Synthesis of Monodisperse Noble-Metallic Nanoparticles and Their Colloidal Crystals. *J. Am. Chem. Soc.* **2006**, *128* (20), 6550–6551. https://doi.org/10.1021/ja0604717.

(8) Piella, J.; Bastús, N. G.; Puntes, V. Size-Controlled Synthesis of Sub-10-Nanometer Citrate-Stabilized Gold Nanoparticles and Related Optical Properties. *Chem. Mater.* **2016**, *28* (4), 1066–1075. https://doi.org/10.1021/acs.chemmater.5b04406.

(9) Verma, A.; Stellacci, F. Effect of Surface Properties on Nanoparticle–Cell Interactions. *Small* **2010**, *6* (1), 12–21. https://doi.org/10.1002/smll.200901158.

(10) Khodashenas, B.; Ghorbani, H. R. Synthesis of Silver Nanoparticles with Different Shapes. *Arabian Journal of Chemistry* **2019**, *12* (8), 1823–1838. https://doi.org/10.1016/j.arabjc.2014.12.014.

(11) Elsabahy, M.; L. Wooley, K. Design of Polymeric Nanoparticles for Biomedical Delivery Applications. *Chemical Society Reviews* **2012**, *41* (7), 2545–2561. https://doi.org/10.1039/C2CS15327K.

(12) Cano, A.; Sánchez-López, E.; Ettcheto, M.; López-Machado, A.; Espina, M.; Souto, E. B.; Galindo, R.; Camins, A.; García, M. L.; Turowski, P. Current Advances in the Development of Novel Polymeric Nanoparticles for the Treatment of Neurodegenerative Diseases. *Nanomedicine* **2020**, *15* (12), 1239–1261. https://doi.org/10.2217/nnm-2019-0443.

(13) Kumari, A.; Yadav, S. K.; Yadav, S. C. Biodegradable Polymeric Nanoparticles Based Drug Delivery Systems. *Colloids and Surfaces B: Biointerfaces* **2010**, *75* (1), 1–18. https://doi.org/10.1016/j.colsurfb.2009.09.001.

(14) Zielińska, A.; Carreiró, F.; Oliveira, A. M.; Neves, A.; Pires, B.; Venkatesh, D. N.; Durazzo, A.; Lucarini, M.; Eder, P.; Silva, A. M.; Santini, A.; Souto, E. B. Polymeric Nanoparticles: Production,

Characterization, Toxicology and Ecotoxicology. *Molecules* **2020**, *25* (16), 3731. https://doi.org/10.3390/molecules25163731.

(15) Chemistry (IUPAC), T. I. U. of P. and A. IUPAC - crosslink (C01409) https://goldbook.iupac.org/terms/view/C01409.

(16) Mavila, S.; Eivgi, O.; Berkovich, I.; Lemcoff, N. G. Intramolecular Cross-Linking Methodologies for the Synthesis of Polymer Nanoparticles. *Chem. Rev.* **2016**, *116* (3), 878–961. https://doi.org/10.1021/acs.chemrev.5b00290.

(17) Asenjo-Sanz, I.; Verde-Sesto, E.; Pomposo, J. A. Valuable Structure-Size Relationships for Tadpole-Shaped Single-Chain Nanoparticles with Long and Short Flexible Tails Unveiled. *Phys. Chem. Chem. Phys.* **2019**, *21* (21), 10884–10887. https://doi.org/10.1039/C9CP01318K.

(18) Jiang, L.; Xie, M.; Dou, J.; Li, H.; Huang, X.; Chen, D. Efficient Fabrication of Pure, Single-Chain Janus Particles through Their Exclusive Self-Assembly in Mixtures with Their Analogues. *ACS Macro Lett.* **2018**, *7* (11), 1278–1282. https://doi.org/10.1021/acsmacrolett.8b00503.

(19) Cui, Z.; Huang, L.; Ding, Y.; Zhu, X.; Lu, X.; Cai, Y. Compartmentalization and Unidirectional Cross-Domain Molecule Shuttling of Organometallic Single-Chain Nanoparticles. *ACS Macro Lett.* **2018**, *7* (5), 572–575. https://doi.org/10.1021/acsmacrolett.8b00199.

(20) Verso, F. L.; A. Pomposo, J.; Colmenero, J.; J. Moreno, A. Multi-Orthogonal Folding of Single Polymer Chains into Soft Nanoparticles. *Soft Matter* **2014**, *10* (27), 4813–4821. https://doi.org/10.1039/C4SM00459K.

(21) Chao, D.; Jia, X.; Tuten, B.; Wang, C.; Berda, E. B. Controlled Folding of a Novel Electroactive Polyolefin via Multiple Sequential Orthogonal Intra-Chain Interactions. *Chem. Commun.* **2013**, *49* (39), 4178–4180. https://doi.org/10.1039/C2CC37157J.

(22) Gonzalez-Burgos, M.; Latorre-Sanchez, A.; Pomposo, J. A. Advances in Single Chain Technology. *Chem. Soc. Rev.* **2015**, *44* (17), 6122–6142. https://doi.org/10.1039/C5CS00209E.

(23) Lyon, C. K.; Prasher, A.; Hanlon, A. M.; Tuten, B. T.; Tooley, C. A.; Frank, P. G.; Berda, E. B. A Brief User's Guide to Single-Chain Nanoparticles. *Polym. Chem.* **2014**, *6* (2), 181–197. https://doi.org/10.1039/C4PY01217H.

(24) Hanlon, A. M.; Lyon, C. K.; Berda, E. B. What Is Next in Single-Chain Nanoparticles? *Macromolecules* **2016**, *49* (1), 2–14. https://doi.org/10.1021/acs.macromol.5b01456.

(25) Frisch, H.; Tuten, B. T.; Barner-Kowollik, C. Macromolecular Superstructures: A Future Beyond Single Chain Nanoparticles. *Israel Journal of Chemistry* **2020**, *60* (1–2), 86–99. https://doi.org/10.1002/ijch.201900145.

(26) Altintas, O.; Barner-Kowollik, C. Single Chain Folding of Synthetic Polymers by Covalent and Non-Covalent Interactions: Current Status and Future Perspectives. *Macromolecular Rapid Communications* **2012**, *33* (11), 958–971. https://doi.org/10.1002/marc.201200049.

(27) Altintas, O.; Barner-Kowollik, C. Single-Chain Folding of Synthetic Polymers: A Critical Update. *Macromolecular Rapid Communications* **2016**, *37* (1), 29–46. https://doi.org/10.1002/marc.201500547.

(28) Chen, R.; Berda, E. B. 100th Anniversary of Macromolecular Science Viewpoint: Re-Examining Single-Chain Nanoparticles. *ACS Macro Lett.* **2020**, *9* (12), 1836–1843. https://doi.org/10.1021/acsmacrolett.0c00774.

(29) Alqarni, M. A. M.; Waldron, C.; Yilmaz, G.; Becer, C. R. Synthetic Routes to Single Chain Polymer Nanoparticles (SCNPs): Current Status and Perspectives. *Macromolecular Rapid Communications* **2021**, *42* (11), 2100035. https://doi.org/10.1002/marc.202100035.

(30) Ouchi, M.; Badi, N.; Lutz, J.-F.; Sawamoto, M. Single-Chain Technology Using Discrete Synthetic Macromolecules. *Nature Chemistry* **2011**, *3* (12), 917–924. https://doi.org/10.1038/nchem.1175.

(31) Artar, M.; Huerta, E.; Meijer, E. W.; Palmans, A. R. A. Dynamic Single Chain Polymeric Nanoparticles: From Structure to Function. In *Sequence-Controlled Polymers: Synthesis, Self-Assembly, and Properties*; Lutz, J.-F., Meyer, T. Y., Ouchi, M., Sawamoto, M., Eds.; American Chemical Society, Series Ed.; ACS Symposium Series; American Chemical Society: Washington, DC, 2014; Vol. 1170, pp 313–325. https://doi.org/10.1021/bk-2014-1170.ch021.

(32) Blazquez-Martín, A.; Verde-Sesto, E.; Moreno, A. J.; Arbe, A.; Colmenero, J.; Pomposo, J. A. Advances in the Multi-Orthogonal Folding of Single Polymer Chains into Single-Chain Nanoparticles. *Polymers* **2021**, *13* (2), 293. https://doi.org/10.3390/polym13020293.

(33) Huurne, G. M. ter; Palmans, A. R. A.; Meijer, E. W. Supramolecular Single-Chain Polymeric Nanoparticles. *CCS Chem* **2019**, 64–82. https://doi.org/10.31635/ccschem.019.20180036.

(34) Sanchez-Sanchez, A.; Pérez-Baena, I.; Pomposo, J. A. Advances in Click Chemistry for Single-Chain Nanoparticle Construction. *Molecules* **2013**, *18* (3), 3339–3355. https://doi.org/10.3390/molecules18033339.

(35) Chen, J.; Garcia, E. S.; Zimmerman, S. C. Intramolecularly Cross-Linked Polymers: From Structure to Function with Applications as Artificial Antibodies and Artificial Enzymes. *Acc. Chem. Res.* **2020**, *53* (6), 1244–1256. https://doi.org/10.1021/acs.accounts.0c00178.

(36) De-La-Cuesta, J.; González, E.; Pomposo, J. A. Advances in Fluorescent Single-Chain Nanoparticles. *Molecules* **2017**, *22* (11), 1819. https://doi.org/10.3390/molecules22111819.

(37) Latorre-Sánchez, A.; Pomposo, J. A. Recent Bioinspired Applications of Single-Chain Nanoparticles. *Polymer International* **2016**, *65* (8), 855–860. https://doi.org/10.1002/pi.5078.

(38) Verde-Sesto, E.; Arbe, A.; Moreno, A. J.; Cangialosi, D.; Alegría, A.; Colmenero, J.; Pomposo, J. A. Single-Chain Nanoparticles: Opportunities Provided by Internal and External Confinement. *Mater. Horiz.* **2020**, *7* (9), 2292–2313. https://doi.org/10.1039/D0MH00846J.

(39) Benito, A. B.; Aiertza, M. K.; Marradi, M.; Gil-Iceta, L.; Shekhter Zahavi, T.; Szczupak, B.; Jiménez-González, M.; Reese, T.; Scanziani, E.; Passoni, L.; Matteoli, M.; De Maglie, M.; Orenstein, A.; Oron-Herman, M.; Kostenich, G.; Buzhansky, L.; Gazit, E.; Grande, H.-J.; Gómez-Vallejo, V.; Llop, J.; Loinaz, I. Functional Single-Chain Polymer Nanoparticles: Targeting and Imaging Pancreatic Tumors *in Vivo*. *Biomacromolecules* **2016**, *17* (10), 3213–3221. https://doi.org/10.1021/acs.biomac.6b00941.

(40) Gracia, R.; Marradi, M.; Cossío, U.; Benito, A.; Vicente, A. P.-S.; Gómez-Vallejo, V.; Grande, H.-J.; Llop, J.; Loinaz, I. Synthesis and Functionalization of Dextran-Based Single-Chain Nanoparticles in Aqueous Media. *J. Mater. Chem. B* **2017**, *5* (6), 1143–1147. https://doi.org/10.1039/C6TB02773C.

(41) Liang, J.; Struckhoff, J. J.; Hamilton, P. D.; Ravi, N. Preparation and Characterization of Biomimetic β-Lens Crystallins Using Single-Chain Polymeric Nanoparticles. *Langmuir* **2017**, *33* (31), 7660–7668. https://doi.org/10.1021/acs.langmuir.7b01290.

(42) Kröger, A. P. P.; Paulusse, J. M. J. Single-Chain Polymer Nanoparticles in Controlled Drug Delivery and Targeted Imaging. *Journal of Controlled Release* **2018**, *286*, 326–347. https://doi.org/10.1016/j.jconrel.2018.07.041.

(43) Sanchez-Sanchez, A.; Akbari, S.; Etxeberria, A.; Arbe, A.; Gasser, U.; Moreno, A. J.; Colmenero, J.; Pomposo, J. A. “Michael” Nanocarriers Mimicking Transient-Binding Disordered Proteins. *ACS Macro Lett.* **2013**, *2* (6), 491–495. https://doi.org/10.1021/mz400173c.

(44) Sanchez-Sanchez, A.; Akbari, S.; Moreno, A. J.; Verso, F. L.; Arbe, A.; Colmenero, J.; Pomposo, J. A. Design and Preparation of Single-Chain Nanocarriers Mimicking Disordered Proteins for Combined Delivery of Dermal Bioactive Cargos. *Macromolecular Rapid Communications* **2013**, *34* (21), 1681–1686. https://doi.org/10.1002/marc.201300562.

(45) Cheng, C.-C.; Lee, D.-J.; Liao, Z.-S.; Huang, J.-J. Stimuli-Responsive Single-Chain Polymeric Nanoparticles towards the Development of Efficient Drug Delivery Systems. *Polym. Chem.* **2016**, *7* (40), 6164–6169. https://doi.org/10.1039/C6PY01623E.

(46) Ryu, J.-H.; Chacko, R. T.; Jiwpanich, S.; Bickerton, S.; Babu, R. P.; Thayumanavan, S. Self-Cross-Linked Polymer Nanogels: A Versatile Nanoscopic Drug Delivery Platform. *J. Am. Chem. Soc.* **2010**, *132* (48), 17227–17235. https://doi.org/10.1021/ja1069932.

(47) Chan, D.; Yu, A. C.; Appel, E. A. Single-Chain Polymeric Nanocarriers: A Platform for Determining Structure–Function Correlations in the Delivery of Molecular Cargo. *Biomacromolecules* **2017**, *18* (4), 1434–1439. https://doi.org/10.1021/acs.biomac.7b00249.

(48) Gracia, R.; Marradi, M.; Salerno, G.; Pérez-Nicado, R.; Pérez-San Vicente, A.; Dupin, D.; Rodriguez, J.; Loinaz, I.; Chiodo, F.; Nativi, C. Biocompatible Single-Chain Polymer Nanoparticles Loaded with an Antigen Mimetic as Potential Anticancer Vaccine. *ACS Macro Lett.* **2018**, *7* (2), 196–200. https://doi.org/10.1021/acsmacrolett.8b00052.

(49) Hamilton, S. K.; Harth, E. Molecular Dendritic Transporter Nanoparticle Vectors Provide Efficient Intracellular Delivery of Peptides. *ACS Nano* **2009**, *3* (2), 402–410. https://doi.org/10.1021/nn800679z.

(50) Koda, Y.; Terashima, T.; Sawamoto, M.; Maynard, H. D. Amphiphilic/Fluorous Random Copolymers as a New Class of Non-Cytotoxic Polymeric Materials for Protein Conjugation. *Polym. Chem.* **2014**, *6* (2), 240–247. https://doi.org/10.1039/C4PY01346H.

(51) Koda, Y.; Terashima, T.; Maynard, H. D.; Sawamoto, M. Protein Storage with Perfluorinated PEG Compartments in a Hydrofluorocarbon Solvent. *Polym. Chem.* **2016**, *7* (44), 6694–6698. https://doi.org/10.1039/C6PY01333C.

Chapter 2 SCNPs: topology and characterization

Due to the softness of their polymeric nature, SCNPs should be described with topological, instead of geometrical terms. This chapter provides topological perspectives on the formation of SCNPs and their overall structure. Typical characterizing methods are summarized. The working principle of analytical ultracentrifugation is introduced to the reader.

2.1 TOPOLOGY

Due to the dominant position of rigid objects, a traditional paradigm of "geometry-property-functionality" has been built. Soft objects can deform in response to external perturbations. For instance, as mentioned in Figure 1.4C, a polymer chain exhibits as an extended-coil geometry in good solvents while collapsed into globule-like geometry in poor solvents. Describing soft objects with geometrical terms lacks robustness. Thus, we wonder if there is a "topology-property-functionality" paradigm that's worth exploring?

2.1.1 Topology v.s. Geometry

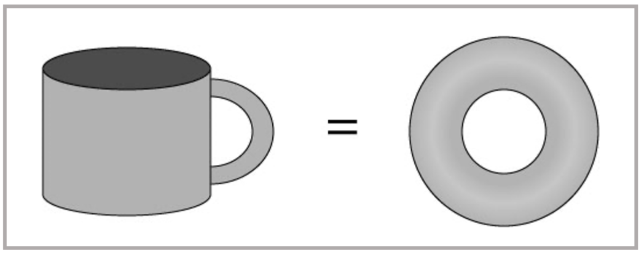

Figure 2.1 A mug and a donut.

The two objects are geometrically distinct but topologically equivalent

Topology is a field that studies the invariance of certain properties under continuous deformation, such as stretching, twisting, crumpling, and bending, of the underlying object; Geometry is a field that studies the properties of space that are related to distance, size, and shape. When being used to describe objects, topology refers to connectivity while geometry refers to spatial arrangement. A classical example is shown in Figure 2.1, where two objects, a mug and a donut, with distinct geometries, are topologically equivalent.

First, let's define the topological features due to crosslinking.

2.1.2 Local topology

To be simple, we define crosslinking as the event where two sites on the same chain/two different chains form one contact. A loop is the chain segment between the two crosslinking sites. A fundamental understanding of the loop formation and classification can provide us with better comprehension of the topological features in SCNPs. The rest of the section is concerned with the possible topological outcomes due to crosslinking events in either polymer network or SCNPs.

Crosslinking…

…multiple chains

Crosslinking multiple chains forms a network. Johnson and coworkers[1,2] revisited the structure-property relationship in polymer network from the topological perspective from different length scales: < 1 nm, 1–10 nm, 10–100 nm.

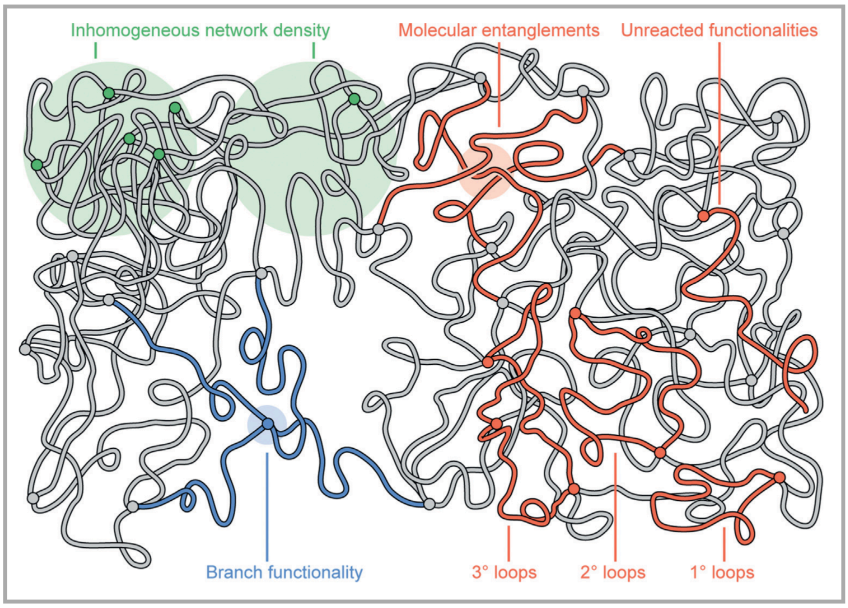
Inhomogeneous network density
Molecular entanglements
Unreacted functionalities
Branch functionality
3° loops
2° loops
1° loops

Figure 2.2 Loops as one of the topological features in polymer networks (Reproduced from ref[2])

Below 1nm (blue in Figure 2.2), the main topological feature is the branch functionality, describing the maximum number of strands connected to a network junction.

In 1-10 nm (red in Figure 2.2), loops of various orders are the main topological feature, together with dangling chains and entanglements. The loop order describes the number of polymer chains involved. For instance, a primary loop (1° loop) is formed by self-crosslinking of a polymer chain; a secondary loop (2° loop) crosslinks two polymer chains and so on.

At 10–100 nm length scale (green in Figure 2.2), inhomogeneity in the distribution of network junctions is the main topological feature.

…a single chain

Apparently, when dealing with the self-crosslinking of a single chain, loops are the dominant topological feature. A collection of self-crosslinking events transforms a single polymer chain into a particle whose size is within the nanoscale. In another word, an SCNP is topologically equivalent to “loops on a chain”. Thus, understanding the loop and their interplay can help us understand and control the formation of SCNPs.

Real loops are characterized both by their individual geometries and collective topologies. The geometry of a loop is the contour length of the chain segment defined by the two crosslinking sites. Depending on the arrangement of the crosslinking sites, we can define three types of loop topologies: Parallel, Cross, and Series, as illustrated in Figure 2.3A. Depending on the fractions of the three topologies, a SCNP can be represented as a point in the ternary plot of Figure 2.3B.

Loops’ geometry and topology are convoluted. Big loops statistically favor the Cross topology while small loops are more likely to form the Series topology. Such realization opens the door for facile and versatile approaches to control the global topology of SCNPs.

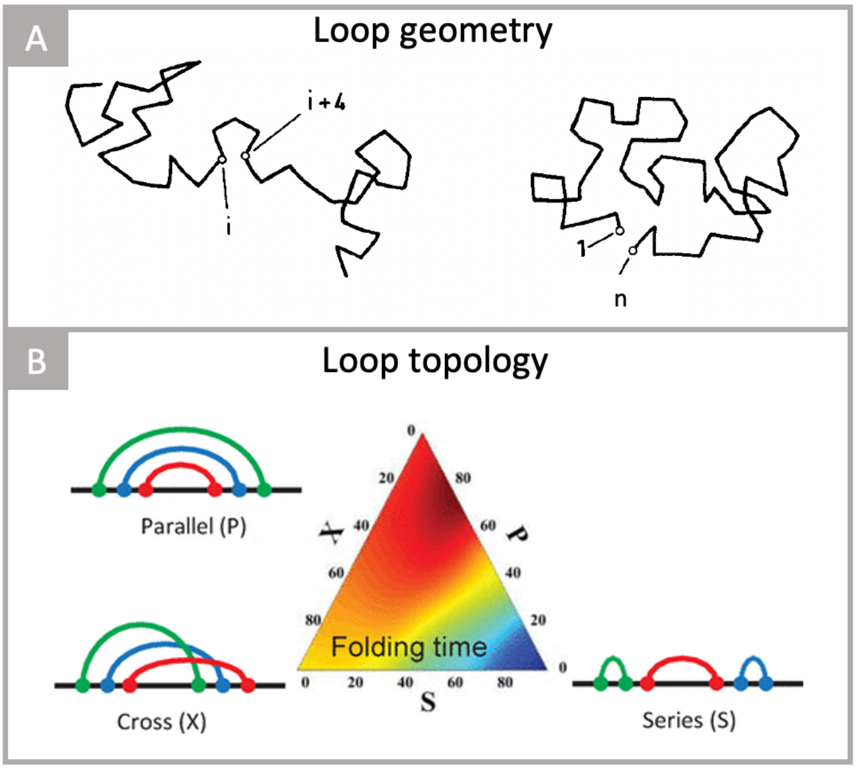

Figure 2.3 Loops are characterized both by the individual geometry and the collective topology.

61) Loop geometry is the contour length defined by the crosslinking sites; (Reproduced from ref [3]); B) Parallel, Cross, and Series are three types of single-chain loop topologies depending on interplay among the loops (Reproduced from ref [4]).

...can fail

The deviations from the given/intended local topological structures are called topological defects. Their presence can sometimes substantially alter materials' global structure, properties, and functionalities. For instance, the heptagons in the hexagonal network can transform the graphene into carbon nanotubes; dislocation and disclination can affect the crystals' mechanical properties; even ppb level concentration of defects can endow semiconductors with novel electronic structures. Thus, it's important to define, assess and exploit the topological defects in SCNP

When single-chain crosslinking attempts fail, instead of forming the intended loops, dangling chains are generated as topological defects. As SCNPs can be formed via external cross-linkers or internal cross-linkers (Figure 1.7), we can classify two types of SCNP topological defects, as shown in Figure 2.4.

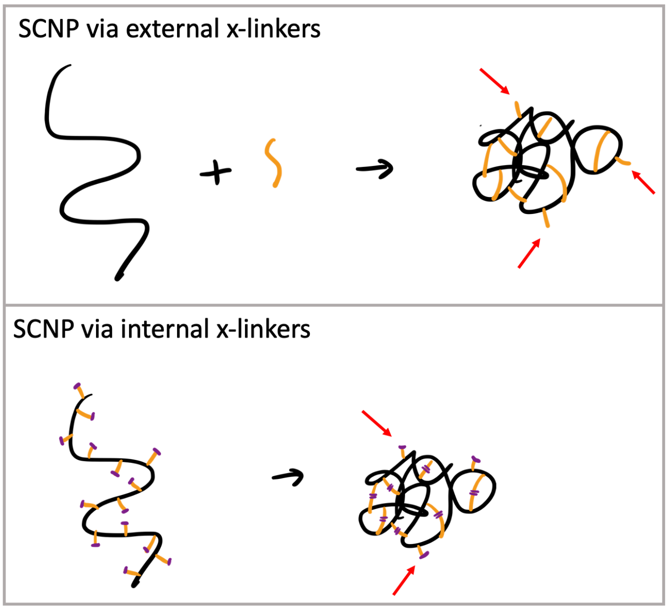

Figure 2.4 Schematic illustration of two main types of single-chain cross-linking strategies and the corresponding topological defects

2.1.3 Global topology

The looping system of SCNPs has many possibilities. A polymer chain with 100 crosslinking sites, of which if 30% contributes to crosslinking, assuming no topological defects, generating 15 loops. The combination of the three loop topologies among the 15 loops gives rise to the topological polydispersity (in pure mathematical sense) of the SCNPs.

Apart from the lack of pure mathematical description of SCNP topology, the experimental validation is nevertheless a handy task, if not a mission impossible. We list a few of the challenges in practical experimental investigation. MW-monodisperse polymer chains should be synthesized as the precursor; it's impossible for the crosslinked SCNPs to be topologically monodisperse but rather with a distribution of topologies; How can we ensure the SCNPs are pure from topological defects? Finally, is there an effective analytical approach to characterize the topology?

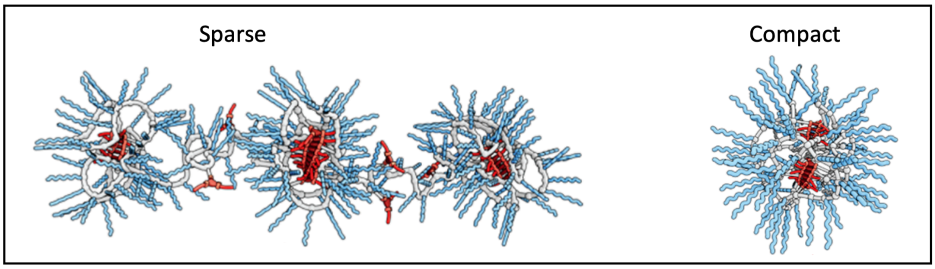

Figure 2.5 Illustration of two distinct topologies (sparse and compact) of SCNPs. (Reproduced from ref[5])

We decide to use the term, topology, to describe the structure of SCNPs, in a more practical manner. Depending on the fraction of the three types of loop topologies and their contour lengths, the SCNPs presents different global topologies. When small loops and/or the Series topology dominate, the single-chain crosslinking creates local blebs and the SCNPs' morphology can be described as "beads on a string", defined as the sparse topology. Whereases, when large loops and/or the Cross/Parallel topology dominate, the single-chain crosslinking achieves global compaction and the SCNPs' morphology is more "globule-like", defined as the compact topology as shown in Figure 2.5.

The phenomenon that single-chain crosslinking does not necessarily produce compact topology gains notice from early days and reiterates till today. Longi et al.[6], in 1968, tried to intramolecularly cross-link α-olefin/allylsilane copolymer via the formation of Si-O-Si bridges but they did not observe noticeable change in the intrinsic viscosity although the formation of siloxane cross-links was confirmed. In 1983, Martin and Eichinger carried out Friedel-Crafts-mediated cross-linking of polystyrene under θ conditions but only found slight size reduction.[7,8] In 1988, Antonietti et al. cross-linked linear polystyrene in good solvent and surprisingly found small reduction of the radius of gyration and hydrodynamic radius even for high cross-linking density.[9] In 1991, Frank and Burchard cross-linked water-soluble poly(allylamine) with 1,4-dimethoxybutane-1,4-diimine dihydrochloride to form single-chain microgels but found it difficult to evidence single-chain compaction due to the weakly pronounced differences in the dimension before and after the reaction.[10] In around 2014, the observations based on SANS and SAXS results, together with MD simulations led Colmenero et al. to investigate into the question, *How Far Are Single-Chain Polymer Nanoparticles in Solution from the Globular State?*[11] In the viewpoint paper, they summarized hydrodynamic size data for poly(styrene) SCNPs in solution synthesized from 30 different precursors and 11 different crosslinking chemistries. They first estimated the hydrodynamic radius R_{H} of the linear PS precursors from their molecular weight Mw by SEC; for SCNPs, the same operation was done but with the apparent SEC Mw for R_H; the R_H for ideal spheres was calculated based on the mass density assumption and Mw. The comparison indicated some size reduction due to single-chain crosslinking but there is still room for further compaction to be ideal globules.

2.2 CHARACTERIZATION

Rigid inorganic nanoparticles can be well represented by their geometrical identity, i.e., size and shape. SCNPs are soft objects with dynamic and interactive nature, thus extra cares should be taken to ensure sound characterization. For instance, SCNPs with sparse topology can be disguised as compact ones when being placed in poor solvents thus obscuring the interpretation; due to the same reason, SCNPs with compact topology can present different sizes depending on their swelling behavior. Thus, for robust characterization of the SCNP global topology, one should dissolve the SCNPs in good solvents while be careful with other conditions, such as pH and ionic strengths etc. This section summarizes some of the common analytical techniques on the characterization of SCNPs. The final part of this section introduces a classical biophysical analytical tool, Analytical Ultracentrifugation, to resolve the nuance in SCNP topology.

2.2.1 Viscometry

One of the most conventional approaches to study single-chain compaction is via solution viscometry. When inter-chain events create network among polymer chains, the solution viscometry increases, whereas intra-chain events reduce the hydrodynamic dimension of polymer chains, thus leading to lower solution viscosity. As mentioned above, the overlap concentration $c*$ can be calculated as the inverse of $[\eta]$, the intrinsic viscosity, which characterizes the solute's contribution to the solution viscosity. The intrinsic viscosity is related to the solute's molar mass M via the Mark-Houwink equation, where a depends on the interaction between the solute and the solvent system.

Eqn. 2-1 Mark-Houwink equation

$$[\eta] = \mathrm{KM}^{\mathrm{a}}$$

One example of using viscometry to probe single-chain compaction was demonstrated by Hawker et al.[12] They first prepared random copolymers with isocyanate functionalities to react with external diamine cross-linkers. To confirm the single-chain collapsing, the reduced viscosities[13] of the solutions of both the precursor polymer and the collapse SCNPs were mapped against a series of concentrations, as shown in Figure 2.6. And the intrinsic viscosities can be directly read as the y-intercept, as indicated by the equation below.

Eqn. 2-2 Flory-Huggins equation

$$\eta_{\mathrm{red}} \equiv \eta_{\mathrm{sp}}/c = \frac{\eta - \eta_{\mathrm{s}}}{\eta_{\mathrm{s}} c} = [\eta] + K_{\mathrm{v}} c + \cdots \quad \text{reduced viscosity}$$

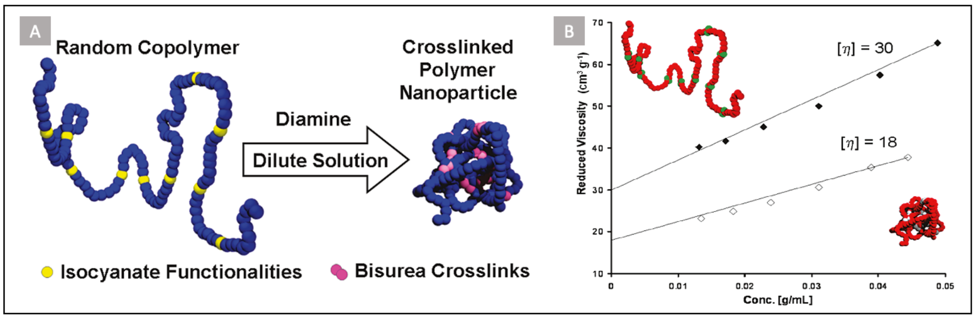

Figure 2.6 Viscometry.

A) The precursor polymer chain bearing isocyanate moieties is crosslinked with diamine to form SCNPs. B) the sing-chain reaction was confirmed with the reduction in intrinsic viscosity, $[\eta]$ (Reproduced from Ref [12])

The reader can be directed to the review[14] by Harding et al. for more information about the instrumentation, mathematics, interpretation etc.

2.2.2 SEC

SEC is a type of liquid chromatography tool where the solutes are separated by their hydrodynamic dimension.[15] A SEC column is usually packed with particles to create a porous structure. When being forced through such a column, smaller solutes' ability to penetrate the pore complicates their travelling trajectory and prolongs their retention time in the column.

An excellent example was demonstrated by Satoh et al.[16] where they synthesized olefin-bearing polymer precursor for single-chain compaction via metathesis. The retention time via SEC evidenced that the degree of compaction can be tune via the cross-linking density.

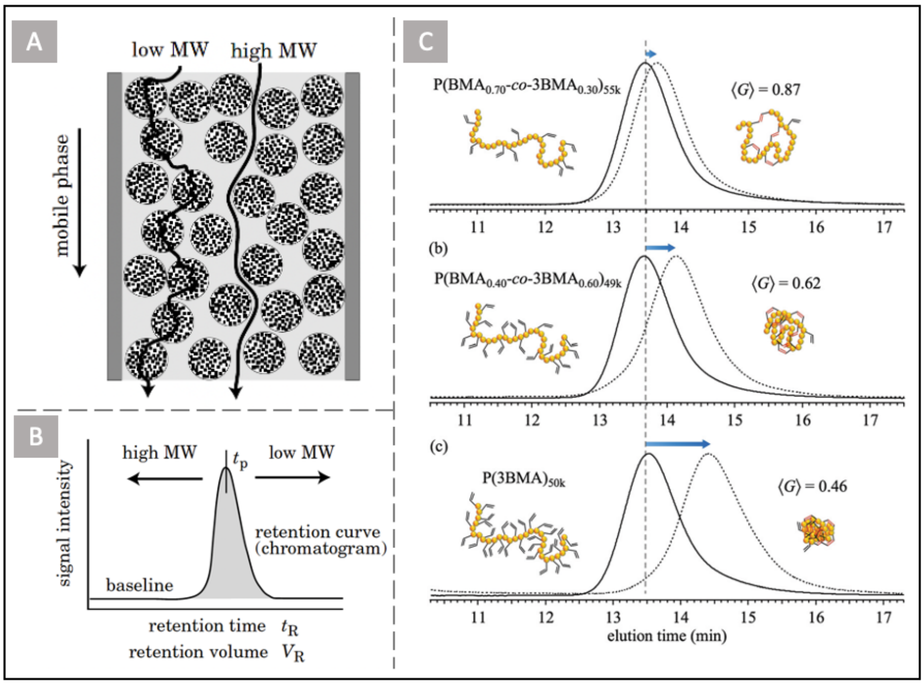
A
low MW
high MW
mobile phase
B
high MW
t_p
low MW
signal intensity
retention curve (chromatogram)
baseline
retention time t_R
retention volume V_R
C
P(BMA$_{0.70}$-co-3BMA$_{0.30}$)$_{55k}$
⟨G⟩ = 0.87
11 12 13 14 15 16 17
(b)
P(BMA$_{0.40}$-co-3BMA$_{0.60}$)$_{49k}$
⟨G⟩ = 0.62
11 12 13 14 15 16 17
(c)
P(3BMA)$_{50k}$
⟨G⟩ = 0.46
11 12 13 14 15 16 17
elution time (min)

Figure 2.7 Size exclusion chromatography

A) An SEC column distinguishes polymer of various MWs by their interaction with the porous stationary phase; B) The polymer's MW/gyration radius can be described by their retention time; C) The final SCNPs size can be tuned by the cross-linking density and characterized via SEC. (Reproduced from ref[17] and ref[16])

Conventionally, SEC is usually coupled with a certain type of concentration-sensitive detector, such as absorbance and RI.

SEC by itself as a fractionation tool, in principle, can be hyphenated with any other analytical tools. Here we decide not to expand the discussion but just to list a few recent works for the interest to the readership. Berda et al. used SEC-MALS to showcase its capability to resolve multi-chain aggregates.[15] Barner-Kowollik et al. coupled SEC with high resolution ESI-MS (electrospray ionization mass spectrometry) to monitor the elimination of nitrogen molecules to assess the chain collapsing.[18,19] Pomposo et al. discussed the potential of conventional SEC to reveal that the reduction of PDI can be detected upon single-chain compaction.[20,21]

Despite that SEC is one of the most commonly use tools in polymer research under both industry and academia settings, one should be careful with the interpretation of its results, as the statistics of the size and shape of polymer is the result of its interaction with the SEC buffer and the column. The reviews by Engelke and co-workers can provide some insight for some critical thinking on SEC.[22,23]

Eichiger discussed which solvent condition should use to not to complicate the data interpretation.[7]

2.2.3 Microscopy

Direct imaging techniques including AFM[24–35] and TEM[36–41] doubtlessly produce the one of the most intuitive results comparing to other tools.

In the work by Meijr et al.,[42] a type of o-nitrobenzyl-protected 2-ureidopyrimidinone (UPy) pendant moiety is clicked onto PMMA backbone. The UV irradiation removes the o-nitrobenzy protection group to the pendant UPy moieties, which induce single-chain compaction via H-bond formation. The AFM performed under different modes (height, amplitude and phase) all indicated phase separation between the core and the periphery.

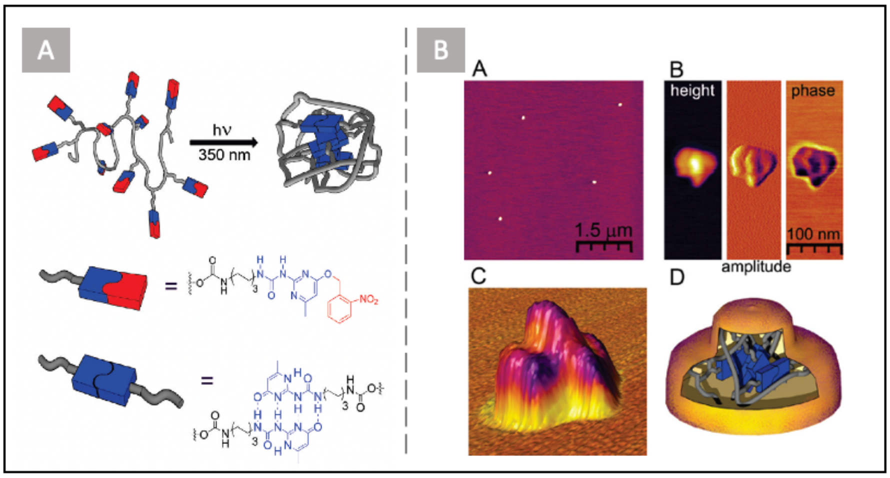

Figure 2.8 Atomic force microscopy

A) SCNP formation was induced by UV irradiation to expose the UPy-urethane side groups; B) High-resolution AFM revealing the complex geometry and one possible explanation was the UPy-urethane rich core. (Reproduced from ref[42])

The typical TEM sample preparation usually drop-casts dilute SCNP solution onto a conductive surface. The sample is resolved due to their ability to scatter the electron beam. However, rendering carbon-based polymeric nanoparticle with ability to scatter electrons usually requires contrasting agent, such as ruthenium oxide, uranyl acetate etc. Such counterion additives might introduce unwanted ionic interaction to obscure the characterization, not to mention the potential artefacts during the drying process. This might explain why most of the publications found spherical morphology, which is not indicated by theory and in-solution characterization.

2.2.4 Scattering

Scattering methods usually collectively including DLS (dynamic light scattering), SLS (static light scattering), SAXS (small angle x-ray scattering) and SANS (small angle neutron scattering), are widely used to characterize colloidal systems. The scattering pattern resulting from the interaction between the probe (laser, neutron, or x-ray) and the analyte provide information on the size and shape etc. Although they share similar working principles, due to the difference in the nature of the radiation, these techniques probe the samples' features from different length scales, thus they are complementary.

Due to the particles' Brownian motion, the intensity of the scattered light fluctuates. DLS monitor such intensity fluctuation at a certain angle as a function of time to fit for the translational mutual diffusion coefficient D of the particles. Under the spherical-particle assumption, D is directly related to the hydrodynamic radius r_s by the Stokes-Einstein relationship.

Eqn. 2-3 Stokes-Einstein relationship

$$D = \frac{kT}{(6\pi\eta r_s)}$$

SLS records the angular dependence of the intensity of the scattered light to allow for the calculation of gyration radius and molecular weight. Simultaneous measurement at several angles can be implemented. Such detector is known as MALLS (multi-angle laser light scattering), which can be coupled to SEC in some applications.

SANS and SAXS both belong to small angle scattering and share the same basic equations and laws (Guinier, Zimm, Kratky and Porod) but differ in the way they interact with the analyte. Neutrons beams are scattered by the atomic nucleus while in SAXS, the electromagnetic irradiation interacts with electrons to create contrast.

In one example, Mureno et al.[43] employed SANS to characterize SCNPs' conformation dependency on the concentration of the solution to validate their computational simulation. Using deuterated solvents to create contrast with the analyte, the form factor resolved by SANS reveals the crowding effect on the morphology of SCNPs.

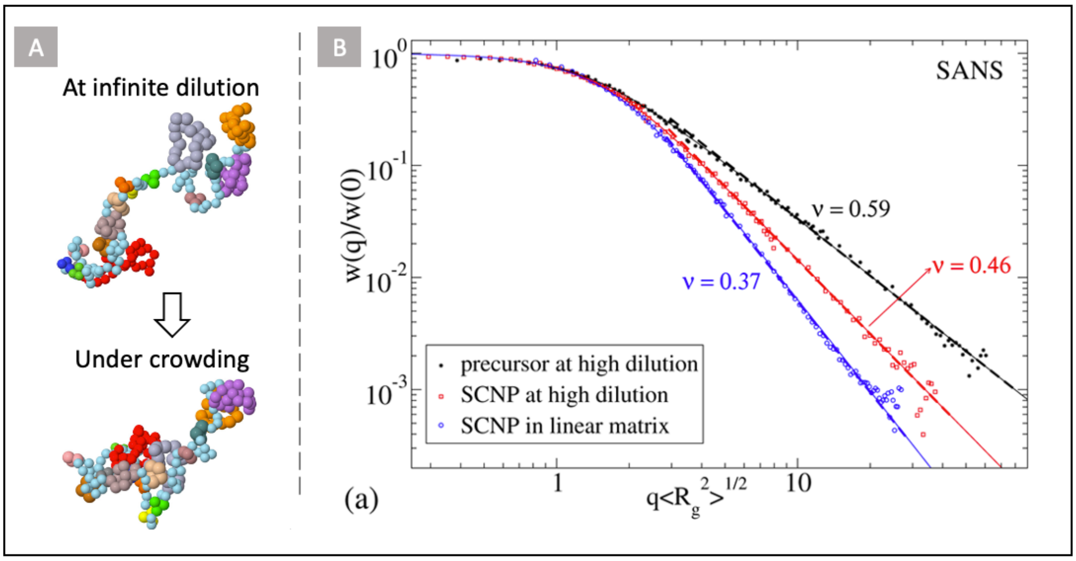

Figure 2.9 Small angle neuron scattering

A) The SCNPs at infinite dilution present sparse conformation while compact itself under crowded surrounding molecular environment, resembling the case of intrinsic disorder proteins in cell environments; B) Such effect was observed with SANS where dPEO was applied as the crowding molecules. (Reproduced from ref[43])

2.2.5 NMR

NMR comprises a big arsenal for structural elucidation. Apparently, 1D NMR is generally performed as the first handy tool to validate the reaction and followed with are 2D NMR spectra to resolve the molecular structures. Herein, we make a brief introduction to DOSY (Diffusion Ordered Spectroscopy) NMR and NMR relaxation experiment, as they are relevant in terms of probing single-chain compaction.

DOSY

DOSY NMR resolves mixtures spectroscopically based on their difference in self-diffusion. It's also sometimes referred as PGSE (pulsed gradient spin echo) NMR to reveal its actual mechanism. Briefly, it applies a gradient of field strength to spatially label the analytes depending on their position in the NMR tube; then a given duration is given to allow the analytes to diffuse to a new location, which can be decoded by a second gradient. Due to the Brownian motion, the signal is expected to take the form of mono-exponential decay, called Stejskal-Tanner equation (equation below, I is the observed intensity, I0 he unattenuated signal, D the diffusion coefficient, γ the gyromagnetic ratio of the interested nucleus, g the gradient strength, δ the length of the gradient, and Δ the diffusion duration). A more detailed technical explanation can be found by Johnson.[44]

Eqn. 2-4 Stejskal Tanner equation

$$I = I_0 \, e^{-D\gamma^2 g^2 \delta^2 (\Delta - \delta/3)}$$

The size reduction due to single-chain compaction leads to faster Brownian motion and larger diffusion coefficient. DOSY has been widely employed by the single-chain community.[18,24,35,45–50] In the example demonstrated by Loinaz et al.[35], the SCNPs (in black) show larger diffusion coefficient than their parent polymers (in blue).

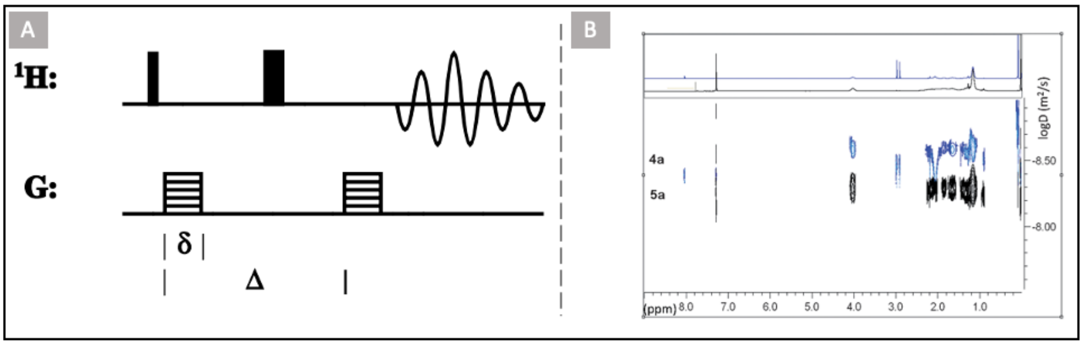

Figure 2.10 Diffusion ordered spectroscopy NMR

A) the spin echo pulse sequence as described by Stejskal and Tanner in 1965; B) SCNPs (blue trace) exhibit large diffusion coefficient and their precursor polymer (black trace) (Reproduced from the work by Loinaz et al.[35])

Relaxation

NMR relaxation is recognized as facile yet versatile tool to probe sub-molecular dynamics through longitudinal (T_1) and transverse (T_2) relaxation behavior and nuclear Overhauser effects. To perform a transverse relaxation experiment, after a 90° pulse, the spin system under nonequilibrium condition will immediately return to equilibrium. The transverse component of the magnetization I_{xy} decays to zero in an exponential manner, as indicated in Equation below, where I_0 is the intensity at t=0.

Eqn. 2-5 Mono-exponential decay in NMR transverse relaxation

$$I_{xy} = I_0 \exp\left(-t/T_2 \right)$$

The example in Figure 2.11 featured the work by Barner-Kowollik et al.[51] The SCNPs were constructed by introducing palladium (II) coordination to the precursor polymer chain. Such intra-molecular cross-linking restricts the segment mobility so that the SCNPs have smaller T_2 (70 ms) than the precursor (147 ms). To date, NMR relaxation is not a commonly used in this field[36] although it provides another viewpoint to inspect single-chain compaction.

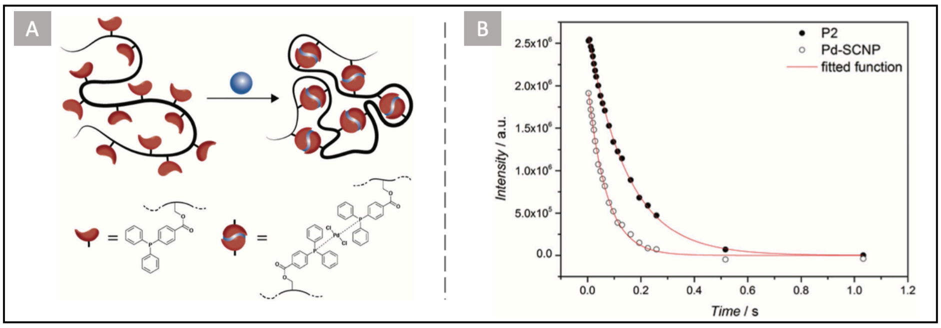

Figure 2.11 NMR relaxation

A) The SCNPs were constructed by introducing palladium coordination; B) Single-chain cross-linking reduces segment mobility so that SCNPs have a smaller T_2 than their precursors.

2.2.6 Analytical Ultracentrifugation

The characterization of SCNPs has been mostly inspired by the field of polymer science. Moreover, from the viewpoint of protein mimicking, we could also translate the tools from structural biology. Over the past 100 years since the development of AUC to characterize biomacromolecules by Theodor Svedberg and his colleagues in the 1920s, AUC has been widely used to determine the molecular weight and hydrodynamic and thermodynamic properties of macromolecules, including proteins, RNA/DNA and a variety of inorganic nanoparticles. Here, I briefly describe the working principles of one type of AUC approaches, called SV-AUC (sedimentation velocity). Works in this thesis are the first to introduce SV-AUC into the field of SCNPs. More thorough explanation and tutorial can be found in the following books. *Introduction to Analytical Ultracentrifugation* by Greg Ralston is a good starting point for whoever wants to have an overview.[52] *BASIC PRINCIPLES of ANALYTICAL ULTRACENTRIFUGATION* by Schuck et al.[53] covers many details in AUC experimental design and data interpretation. *Analytical Ultracentrifugation of Polymers and Nanoparticles* by Börger et al.[54] explains the three main types of AUC experiments, sedimentation velocity, sedimentation equilibrium and density gradient, with more focus on polymer and nanoparticle systems. Another noteworthy book is *Analytical Ultracentrifugation: Techniques and Methods*,[55] compiled by many experts on AUC to deliver thoughts on simulation, software, interaction between biomacromolecules, application in colloidal systems etc.

Working principle

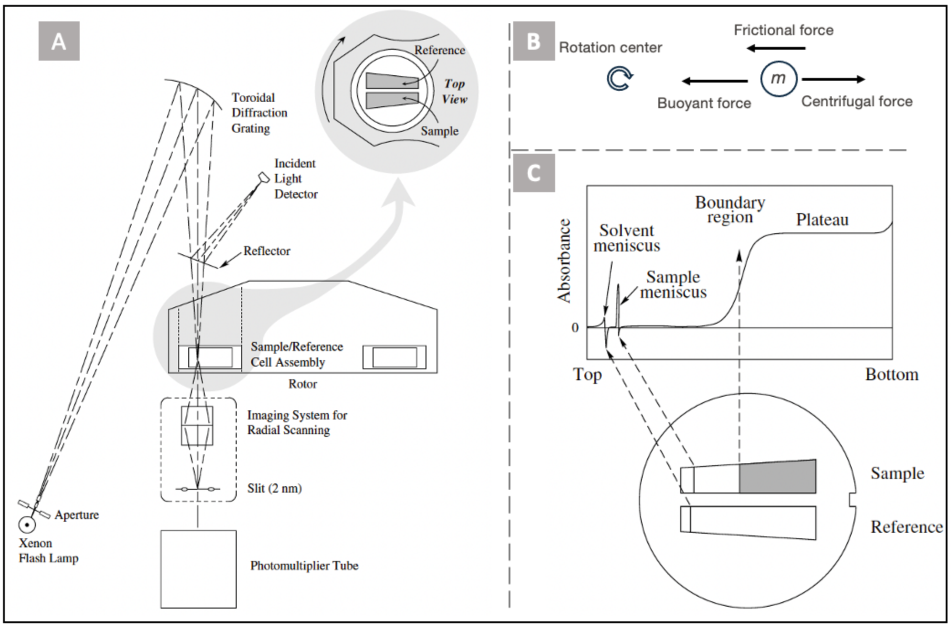
A
Toroidal Diffraction Grating
Reference
Top View
Sample
Incident Light Detector
Reflector
Sample/Reference Cell Assembly
Rotor
Imaging System for Radial Scanning
Slit (2 nm)
Aperture
Xenon Flash Lamp
Photomultiplier Tube
B
Rotation center
Frictional force
m
Buoyant force
Centrifugal force
C
Absorbance
0
Solvent meniscus
Boundary region
Plateau
Sample meniscus
Top
Bottom
Sample
Reference

Figure 2.12 AUC: instrumentation, force analysis, and data acquisition

A) Instrumentation; B) Force analysis during the centrifugation of nanoparticles; C) The samples' sedimentation is recorded as radial distribution over time. This example uses absorbance detector and shows one curve during the sedimentation. (Reproduced from ref[52])

In brief, AUC is a centrifugation system with analytical capabilities. A large centrifugal force (up to 250000g) can be generated to sediment nanoparticles or macromolecules in the chosen buffer. The sedimentation of analytes creates a concentration gradient (boundary as in Figure 2.12C) which drive the diffusion flux. AUC's detector (absorbance, interference, or fluorescence) observes the radial distribution of the analytes overtime to record the diffusion and the sedimentation process. One typical scanning curve is demonstrated in Figure 2.12C. In a centrifugal field, the particles' terminal velocity is a balanced result of three forces, centrifugal, buoyant, and frictional forces (Figure 2.12B). Balancing the three forces, one can yield the Svedberg equation (M: molecular mass; s: sedimentation coefficient; R: ideal gas constant; T: absolute temperature; D: diffusion coefficient; ρ_0: solvent density; v: partial specific volume of the particle).

Eqn. 2-6 Svedberg equation

$$M = \frac{RTs}{\left(1 - v\rho_0\right)D}$$

The boundary movement (due to sedimentation) and broadening (due to diffusion) are described by the Lamm equation (C: concentration; r: radius; t: time; ω: angular velocity).

Eqn. 2-7 Lamm equation

$$\frac{\partial C}{\partial t} = \frac{1}{r}\frac{\partial}{\partial r}\left(s\omega^2 rC - Dr\frac{\partial C}{\partial r}\right)$$

Solving the Lamm equation takes the approach of finite element method, where the grid of s and D pairs is constructed to represent all possible solutions. And the final solution takes such form as the concentration function of s and D, $C(s_{i,j}, D_{i,j})$. In practice, one can use established software, such as SEDFIT[56] and UltraScan[57] for such purpose. As shown by the Svedberg equation, the solution of the Lamm equation, s and D are related to a set of hydrodynamic properties of the analyte. Shown below are equations[58] that we will use to study the anisotropy of the analytes:

Eqn. 2-8 The six relationships among key hydrodynamic parameters in SV-AUC

$$V = \frac{M\bar{\nu}}{N} \quad (1)$$

$$r_0 = \left(\frac{3V}{4\pi}\right)^{1/3} \quad (2)$$

$$f_0 = 6\pi\eta r_0 \quad (3)$$

$$f = \varphi f_0 \quad (4)$$

$$s = \frac{M(1 - \bar{\nu}\rho)}{Nf} \quad (5)$$

$$D = \frac{RT}{Nf} \quad (6)$$

Anisotropy analysis

Absolute approach

The absolute parameter to describe the analytes' anisotropy is the frictional ratio, φ. As shown by eq 4, it's the ratio of the frictional coefficient of the analyte f to the frictional coefficient of a sphere f_0 which has the same volume as the analyte. While the frictional coefficient of the analyte f is related to the diffusion coefficient D (eq 6), solving f_0 requires prior knowledge/assumption of the analytes' density. Combing eq 5 and eq 6, knowing the density or partial specific volume $\bar{\nu}$, the molecular weight M

is obtained. With eq 1, eq 2 and eq 3, one gets f_0. Since the spherical shape induces the minimal friction, the frictional ratio φ is always large than 1 and the extent to which φ departs from 1 describes the analytes' anisotropy. For biomacromolecules, the density can be predicted from their sequence. The experimental approach for density measurement can be found in the work from Minton and co-workers.[59]

Relative approach

The absolute approach suffers from some limitations. Measuring the density and using one constant to represent all samples is not ideal especially when the analytes are polydisperse synthetic polymers. Erroneous results may come from the problematic results from the fitting of diffusion coefficient. One reason is that SV-AUC's tracking on the diffusion process is not sensitive. Besides, the data fitting should be treated with care and specialist knowledge to ensure the numerical methods to solve the partial differential Lamm equation is carried out correctly.

The SV-AUC was primarily developed in 1920s by Theodor Svedberg to sensitively track the boundary movement, thus the sedimentation process. The calculation of sedimentation coefficient does not rely on computational fitting. Thus, the sedimentation coefficient is far more sensitive and robust than the diffusion coefficient. As shown by the Svedberg equation (eq 5), when M and $\bar{v}$ are constants (so is f_0), f (and in turn f/f_0) is related to s in an inversely proportional manner. The 1D distribution of sedimentation coefficient can be treated as the spectrum of the compactness of SCNPs should the samples agree with the assumption of constant M and $\bar{v}$.

2.3 SUMMARY

Constructing nanoparticles from single polymer chains can tap the potential of ultrasmall sub-20nm particles while maintaining the strength of being polymeric. Fundamental topological discussion on the local structure, loops, in the SCNPs, improves our understanding of the formation of SCNPs, and thus, inspiring us to develop facile and versatile approaches to gain control on the global SCNP topology. While it’s challenging to perform topological characterization in the strict mathematical definition, current analytical tools enable us to infer the global topology of SCNPs. Furthermore, with controllable synthesis and careful characterization, investigation on how the topology affects certain properties could give insight on fundamental questions that has been left unanswered with the rigid nanoparticles.

2.4 REFERENCE

(1) Gu, Y.; Zhao, J.; Johnson, J. A. A (Macro)Molecular-Level Understanding of Polymer Network Topology. *TRECHEM* **2019**, *1* (3), 318–334. https://doi.org/10.1016/j.trechm.2019.02.017.

(2) Gu, Y.; Zhao, J.; Johnson, J. A. Polymer Networks: From Plastics and Gels to Porous Frameworks. *Angewandte Chemie International Edition* **2020**, *59* (13), 5022–5049. https://doi.org/10.1002/anie.201902900.

(3) Kuhn, W.; Balmer, G. Crosslinking of Single Linear Macromolecules. *J. Polym. Sci.* **1962**, *57* (165), 311–319. https://doi.org/10.1002/pol.1962.1205716524.

(4) Heidari, M.; Schiessel, H.; Mashaghi, A. Circuit Topology Analysis of Polymer Folding Reactions. *ACS Cent. Sci.* **2020**, *6* (6), 839–847. https://doi.org/10.1021/acscentsci.0c00308.

(5) ter Huurne, G. M.; de Windt, L. N. J.; Liu, Y.; Meijer, E. W.; Voets, I. K.; Palmans, A. R. A. Improving the Folding of Supramolecular Copolymers by Controlling the Assembly Pathway Complexity. *Macromolecules* **2017**, *50* (21), 8562–8569. https://doi.org/10.1021/acs.macromol.7b01769.

(6) Van Lokeren, L.; Maheut, G.; Ribot, F.; Escax, V.; Verbruggen, I.; Sanchez, C.; Martins, J. C.; Biesemans, M.; Willem, R. Characterization of Titanium Dioxide Nanoparticles Dispersed in Organic Ligand Solutions by Using a Diffusion-Ordered Spectroscopy-Based Strategy. *Chemistry – A European Journal* **2007**, *13* (24), 6957–6966. https://doi.org/10.1002/chem.200601722.

(7) Martin, J. E.; Eichinger, B. E. Dimensions of Intramolecularly Crosslinked Polymers. 2. Dilute Solution Thermodynamic Parameters and Photon Correlation Results on the Polystyrene/Cyclopentane System. *Macromolecules* **1983**, *16* (8), 1350–1358. https://doi.org/10.1021/ma00242a017.

(8) Martin, J. E.; Eichinger, B. E. Dimensions of Intramolecularly Crosslinked Polymers. 1. Theory. *Macromolecules* **1983**, *16* (8), 1345–1350. https://doi.org/10.1021/ma00242a016.

(9) Antonietti, M.; Sillescu, H.; Schmidt, M.; Schuch, H. Solution Properties and Dynamic Bulk Behavior of Intramolecular Cross-Linked Polystyrene. *Macromolecules* **1988**, *21* (3), 736–742. https://doi.org/10.1021/ma00181a031.

(10) Frank, M.; Burchard, W. Microgels by Intramolecular Crosslinking of Poly(Allylamine) Single Chains. *Die Makromolekulare Chemie, Rapid Communications* **1991**, *12* (11), 645–652. https://doi.org/10.1002/marc.1991.030121107.

(11) Pomposo, J. A.; Perez-Baena, I.; Lo Verso, F.; Moreno, A. J.; Arbe, A.; Colmenero, J. How Far Are Single-Chain Polymer Nanoparticles in Solution from the Globular State? *ACS Macro Lett.* **2014**, *3* (8), 767–772. https://doi.org/10.1021/mz500354q.

(12) Beck, J. B.; Killops, K. L.; Kang, T.; Sivanandan, K.; Bayles, A.; Mackay, M. E.; Wooley, K. L.; Hawker, C. J. Facile Preparation of Nanoparticles by Intramolecular Cross-Linking of Isocyanate Functionalized Copolymers. *Macromolecules* **2009**, *42* (15), 5629–5635. https://doi.org/10.1021/ma900899v.

(13) Chemistry (IUPAC), T. I. U. of P. and A. IUPAC - reduced viscosity (R05220) https://goldbook.iupac.org/terms/view/R05220 (accessed 2021 -10 -27). https://doi.org/10.1351/goldbook.R05220.

(14) Harding, S. E. The Intrinsic Viscosity of Biological Macromolecules. Progress in Measurement, Interpretation and Application to Structure in Dilute Solution. *Progress in Biophysics and Molecular Biology* **1997**, *68* (2), 207–262. https://doi.org/10.1016/S0079-6107(97)00027-8.

(15) Frank, P.; Prasher, A.; Tuten, B.; Chao, D.; Berda, E. Characterization of Single-Chain Polymer Folding Using Size Exclusion Chromatography with Multiple Modes of Detection. *Appl Petrochem Res* **2015**, *5* (1), 9–17. https://doi.org/10.1007/s13203-014-0046-1.

(16) Watanabe, K.; Tanaka, R.; Takada, K.; Kim, M.-J.; Lee, J.-S.; Tajima, K.; Isono, T.; Satoh, T. Intramolecular Olefin Metathesis as a Robust Tool to Synthesize Single-Chain Nanoparticles in a Size-Controlled Manner. *Polym. Chem.* **2016**, *7* (29), 4782–4792. https://doi.org/10.1039/C6PY00795C.

(17) Teraoka, I. *Polymer Solutions*; John Wiley & Sons, Inc, 2002.

(18) Nitsche, T.; Steinkoenig, J.; De Bruycker, K.; Bloesser, F. R.; Blanksby, S. J.; Blinco, J. P.; Barner-Kowollik, C. Mapping the Compaction of Discrete Polymer Chains by Size Exclusion Chromatography Coupled to High-Resolution Mass Spectrometry. *Macromolecules* **2019**, *52* (6), 2597–2606. https://doi.org/10.1021/acs.macromol.9b00203.

(19) Nitsche, T.; J. Blanksby, S.; P. Blinco, J.; Barner-Kowollik, C. Pushing the Limits of Single Chain Compaction Analysis by Observing Specific Size Reductions via High Resolution Mass Spectrometry. *Polymer Chemistry* **2020**, *11* (10), 1696–1701. https://doi.org/10.1039/C9PY01910C.

(20) Pomposo, J. A.; Perez-Baena, I.; Buruaga, L.; Alegría, A.; Moreno, A. J.; Colmenero, J. On the Apparent SEC Molecular Weight and Polydispersity Reduction upon Intramolecular Collapse of Polydisperse Chains to Unimolecular Nanoparticles. *Macromolecules* **2011**, *44* (21), 8644–8649. https://doi.org/10.1021/ma201070b.

(21) Latorre-Sánchez, A.; Alegría, A.; Verso, F. L.; Moreno, A. J.; Arbe, A.; Colmenero, J.; Pomposo, J. A. A Useful Methodology for Determining the Compaction Degree of Single-Chain Nanoparticles by Conventional SEC. *Particle & Particle Systems Characterization* **2016**, *33* (7), 373–381. https://doi.org/10.1002/ppsc.201500210.

(22) Engelke, J.; Brandt, J.; Barner-Kowollik, C.; Lederer, A. Strengths and Limitations of Size Exclusion Chromatography for Investigating Single Chain Folding – Current Status and Future Perspectives. **2019**. https://doi.org/10.1039/C9PY00336C.

(23) Engelke, J.; Tuten, B. T.; Schweins, R.; Komber, H.; Barner, L.; Plüschke, L.; Barner-Kowollik, C.; Lederer, A. An In-Depth Analysis Approach Enabling Precision Single Chain Nanoparticle Design. *Polym. Chem.* **2020**, *11* (41), 6559–6578. https://doi.org/10.1039/D0PY01045F.

(24) Cui, Z.; Cao, H.; Ding, Y.; Gao, P.; Lu, X.; Cai, Y. Compartmentalization of an ABC Triblock Copolymer Single-Chain Nanoparticle via Coordination-Driven Orthogonal Self-Assembly. *Polymer Chemistry* **2017**, *8* (24), 3755–3763. https://doi.org/10.1039/C7PY00582B.

(25) Roekel, H. W. H. van; M. Stals, P. J.; J. Gillissen, M. A.; J. Hilbers, P. A.; J. Markvoort, A.; Greef, T. F. A. de. Evaporative Self-Assembly of Single-Chain, Polymeric Nanoparticles. *Chemical Communications* **2013**, *49* (30), 3122–3124. https://doi.org/10.1039/C3CC40931G.

(26) Hosono, N.; Kushner, A. M.; Chung, J.; Palmans, A. R. A.; Guan, Z.; Meijer, E. W. Forced Unfolding of Single-Chain Polymeric Nanoparticles. *J. Am. Chem. Soc.* **2015**, *137* (21), 6880–6888. https://doi.org/10.1021/jacs.5b02967.

(27) Cherian, A. E.; Sun, F. C.; Sheiko, S. S.; Coates, G. W. Formation of Nanoparticles by Intramolecular Cross-Linking: Following the Reaction Progress of Single Polymer Chains by Atomic Force Microscopy. *J. Am. Chem. Soc.* **2007**, *129* (37), 11350–11351. https://doi.org/10.1021/ja074301l.

(28) Appel, E. A.; Dyson, J.; del Barrio, J.; Walsh, Z.; Scherman, O. A. Formation of Single-Chain Polymer Nanoparticles in Water through Host–Guest Interactions. *Angewandte Chemie International Edition* **2012**, *51* (17), 4185–4189. https://doi.org/10.1002/anie.201108659.

(29) Foster, E. J.; Berda, E. B.; Meijer, E. W. Metastable Supramolecular Polymer Nanoparticles via Intramolecular Collapse of Single Polymer Chains. *J. Am. Chem. Soc.* **2009**, *131* (20), 6964–6966. https://doi.org/10.1021/ja901687d.

(30) Adkins, C. T.; Muchalski, H.; Harth, E. Nanoparticles with Individual Site-Isolated Semiconducting Polymers from Intramolecular Chain Collapse Processes. *Macromolecules* **2009**, *42* (15), 5786–5792. https://doi.org/10.1021/ma9007913.

(31) Seo, M.; Beck, B. J.; Paulusse, J. M. J.; Hawker, C. J.; Kim, S. Y. Polymeric Nanoparticles via Noncovalent Cross-Linking of Linear Chains. *Macromolecules* **2008**, *41* (17), 6413–6418. https://doi.org/10.1021/ma8009678.

(32) Altintas, O.; Krolla-Sidenstein, P.; Gliemann, H.; Barner-Kowollik, C. Single-Chain Folding of Diblock Copolymers Driven by Orthogonal H-Donor and Acceptor Units. *Macromolecules* **2014**, *47* (17), 5877–5888. https://doi.org/10.1021/ma501186k.

(33) Perez-Baena, I.; Loinaz, I.; Padro, D.; García, I.; J. Grande, H.; Odriozola, I. Single-Chain Polyacrylic Nanoparticles with Multiple Gd(Iii) Centres as Potential MRI Contrast Agents. *Journal of Materials Chemistry* **2010**, *20* (33), 6916–6922. https://doi.org/10.1039/C0JM01025A.

(34) Cheng, C.-C.; Chang, F.-C.; Yen, H.-C.; Lee, D.-J.; Chiu, C.-W.; Xin, Z. Supramolecular Assembly Mediates the Formation of Single-Chain Polymeric Nanoparticles. *ACS Macro Lett.* **2015**, *4* (10), 1184–1188. https://doi.org/10.1021/acsmacrolett.5b00556.

(35) Ormategui, N.; García, I.; Padro, D.; Cabañero, G.; J. Grande, H.; Loinaz, I. Synthesis of Single Chain Thermoresponsive Polymer Nanoparticles. *Soft Matter* **2012**, *8* (3), 734–740. https://doi.org/10.1039/C1SM06310C.

(36) He, J.; Tremblay, L.; Lacelle, S.; Zhao, Y. Preparation of Polymer Single Chain Nanoparticles Using Intramolecular Photodimerization of Coumarin. *Soft Matter* **2011**, *7* (6), 2380–2386. https://doi.org/10.1039/C0SM01383H.

(37) Terashima, T.; Mes, T.; De Greef, T. F. A.; Gillissen, M. A. J.; Besenius, P.; Palmans, A. R. A.; Meijer, E. W. Single-Chain Folding of Polymers for Catalytic Systems in Water. *Journal of the American Chemical Society* **2011**, *133* (13), 4742–4745. https://doi.org/10.1021/ja2004494.

(38) Tuten, B. T.; Chao, D.; Lyon, C. K.; Berda, E. B. Single-Chain Polymer Nanoparticles via Reversible Disulfide Bridges. *Polymer Chemistry* **2012**, *3* (11), 3068. https://doi.org/10.1039/c2py20308a.

(39) Kröger, A. P. P.; Paats, J.-W. D.; Boonen, R. J. E. A.; Hamelmann, N. M.; Paulusse, J. M. J. Pentafluorophenyl-Based Single-Chain Polymer Nanoparticles as a Versatile Platform towards Protein Mimicry. *Polym. Chem.* **2020**, *11* (37), 6056–6065. https://doi.org/10.1039/D0PY00922A.

(40) Wen, J.; Yuan, L.; Yang, Y.; Liu, L.; Zhao, H. Self-Assembly of Monotethered Single-Chain Nanoparticle Shape Amphiphiles. *ACS Macro Lett.* **2013**, *2* (2), 100–106. https://doi.org/10.1021/mz300636x.

(41) Lambert, R.; Wirotius, A.-L.; Garmendia, S.; Berto, P.; Vignolle, J.; Taton, D. Pd(Ii)–NHC Coordination-Driven Formation of Water-Soluble Catalytically Active Single Chain Nanoparticles. *Polymer Chemistry* **2018**, *9* (23), 3199–3204. https://doi.org/10.1039/C8PY00326B.

(42) Berda, E. B.; Foster, E. J.; Meijer, E. W. Toward Controlling Folding in Synthetic Polymers: Fabricating and Characterizing Supramolecular Single-Chain Nanoparticles. *Macromolecules* **2010**, *43* (3), 1430–1437. https://doi.org/10.1021/ma902393h.

(43) Moreno, A. J.; Lo Verso, F.; Arbe, A.; Pomposo, J. A.; Colmenero, J. Concentrated Solutions of Single-Chain Nanoparticles: A Simple Model for Intrinsically Disordered Proteins under Crowding Conditions. *J. Phys. Chem. Lett.* **2016**, *7* (5), 838–844. https://doi.org/10.1021/acs.jpclett.6b00144.

(44) Johnson, C. S. Diffusion Ordered Nuclear Magnetic Resonance Spectroscopy: Principles and Applications. *Progress in Nuclear Magnetic Resonance Spectroscopy* **1999**, *34* (3–4), 203–256. https://doi.org/10.1016/S0079-6565(99)00003-5.

(45) Fischer, T. S.; Schulze-Sünninghausen, D.; Luy, B.; Altintas, O.; Barner-Kowollik, C. Stepwise Unfolding of Single-Chain Nanoparticles by Chemically Triggered Gates. *Angewandte Chemie International Edition* **2016**, *55* (37), 11276–11280. https://doi.org/10.1002/anie.201602894.

(46) Cui, Z.; Huang, L.; Ding, Y.; Zhu, X.; Lu, X.; Cai, Y. Compartmentalization and Unidirectional Cross-Domain Molecule Shuttling of Organometallic Single-Chain Nanoparticles. *ACS Macro Lett.* **2018**, *7* (5), 572–575. https://doi.org/10.1021/acsmacrolett.8b00199.

(47) S. Fischer, T.; Spann, S.; An, Q.; Luy, B.; Tsotsalas, M.; P. Blinco, J.; Mutlu, H.; Barner-Kowollik, C. Self-Reporting and Refoldable Profluorescent Single-Chain Nanoparticles. *Chemical Science* **2018**, *9* (20), 4696–4702. https://doi.org/10.1039/C8SC01009A.

(48) P. Cole, J.; J. Lessard, J.; J. Rodriguez, K.; M. Hanlon, A.; K. Reville, E.; P. Mancinelli, J.; B. Berda, E. Single-Chain Nanoparticles Containing Sequence-Defined Segments: Using Primary Structure Control to Promote Secondary and Tertiary Structures in Synthetic Protein Mimics. *Polymer Chemistry* **2017**, *8* (38), 5829–5835. https://doi.org/10.1039/C7PY01133D.

(49) Blasco, E.; Tuten, B. T.; Frisch, H.; Lederer, A.; Barner-Kowollik, C. Characterizing Single Chain Nanoparticles (SCNPs): A Critical Survey. *Polym. Chem.* **2017**, *8* (38), 5845–5851. https://doi.org/10.1039/C7PY01278K.

(50) Steinkoenig, J.; Nitsche, T.; Tuten, B. T.; Barner-Kowollik, C. Radical-Induced Single-Chain Collapse of Passerini Sequence-Regulated Polymers Assessed by High-Resolution Mass Spectrometry. *Macromolecules* **2018**, *51* (11), 3967–3974. https://doi.org/10.1021/acs.macromol.8b00577.

(51) Willenbacher, J.; Altintas, O.; Trouillet, V.; Knöfel, N.; J. Monteiro, M.; W. Roesky, P.; Barner-Kowollik, C. Pd-Complex Driven Formation of Single-Chain Nanoparticles. *Polymer Chemistry* **2015**, *6* (24), 4358–4365. https://doi.org/10.1039/C5PY00389J.

(52) Ralston, G. Introduction to Analytical Ultracentrifugation. 99.

(53) Schuck, P.; Zhao, H.; Brautigam, C. A.; Ghirlando, R. *Basic Principles of Analytical Ultracentrifugation*; CRC Press: Boca Raton, 2015. https://doi.org/10.1201/b19028.

(54) Maechtle, W.; Börger, L. *Analytical Ultracentrifugation of Polymers and Nanoparticles*, 2006th edition.; Springer: Berlin, 2014.

(55) Analytical Ultracentrifugation: Techniques and Methods; 2005. https://doi.org/10.1039/9781847552617.

(56) Brown, P. H.; Schuck, P. Macromolecular Size-and-Shape Distributions by Sedimentation Velocity Analytical Ultracentrifugation. *Biophysical Journal* **2006**, *90* (12), 4651–4661. https://doi.org/10.1529/biophysj.106.081372.

(57) Scott, D. J.; Harding, S. E.; Rowe, A. J. UltraScan - A Comprehensive Data Analysis Software Package for Analytical Ultracentrifugation Experiments. In *Analytical Ultracentrifugation*; 2005; pp 210–230. https://doi.org/10.1039/9781847552617-00210.

(58) Demeler, B.; Nguyen, T.-L.; Gorbet, G. E.; Schirf, V.; Brookes, E. H.; Mulvaney, P.; El-Ballouli, A. O.; Pan, J.; Bakr, O. M.; Demeler, A. K.; Hernandez Uribe, B. I.; Bhattarai, N.; Whetten, R. L. Characterization of Size, Anisotropy, and Density Heterogeneity of Nanoparticles by Sedimentation Velocity. *Anal. Chem.* **2014**, *86* (15), 7688–7695. https://doi.org/10.1021/ac501722r.

(59) Nourse, A.; Millar, D. B.; Minton, A. P. Physicochemical Characterization of Generation 5 Polyamidoamine Dendrimers. *Biopolymers* **2000**, *53* (4), 316–328. https://doi.org/10.1002/(SICI)1097-0282(20000405)53:4<316::AID-BIP4>3.0.CO;2-J.

Chapter 3 Cellular uptake

Due to their biocompatibility, biodegradability, drug-loading capability *et cetera*, polymeric nanoparticles have huge potential for drug delivery. The emergence of ultrasmall SCNPs could tap the potential that's unreachable for conventional polymeric nanoparticles. This chapter gives background information on the size-biodistribution relationship; informs the reader about the cellular uptake from the fundamental knowledge to common approaches to study this phenomenon; discusses the SCNPs' unique interaction mode with cells with some recent works from this field

3.1 WHY NANO?

Biological barriers provide the human body with protection but at the same time pose as challenge for drug delivery. Nanoparticles are designed as drug carriers to navigate biological barriers (systemic, local, and cellular). Nanoparticles' ability to permeate these biological barriers largely depends on their dimension.

Before we enter the discussion on the cellular level, let's briefly mention how size affects the way nanoparticles cross other biological barriers. The biodistribution[1] profile is deeply influenced by size. Nanoparticles that are smaller than 6 nm can undergo full **renal clearance**. This benefits their biocompatibility while limit their potential to short-time application.[2] Using liposomes, people have reported that liposomes smaller than 200 nm tend to accumulate in the **spleen** while those smaller than 70 nm are predominantly found in the **liver**.[3] Size-dependent biodistribution study has been conducted with gold nanoparticles of a series of different sizes (10~250 nm). Upon intravenous administration to mice or rats, only the smallest species (10 nm) were detected in the rodents' **brains**.[4,5]

Size also plays a key role in terms of **tumor uptake**, a study with gold nanoparticles indicated increased tumor penetration depths for smaller nanoparticles.[6] Nanoparticles within an optimal size range (not small enough for renal clearance[7] but not large enough to be rapidly recognized and trapped by the reticuloendothelial systems[8]) with long circulation times can leak preferentially into and retain in the tumor tissue due to poor lymphatic drainage, knows as enhanced permeability and retention (**EPR**) effect.[9-11] Similar works were also done with polyamidoamine dendrimers to show the crucial role of size in determining their cellular uptake and blood-circulation times.[12]

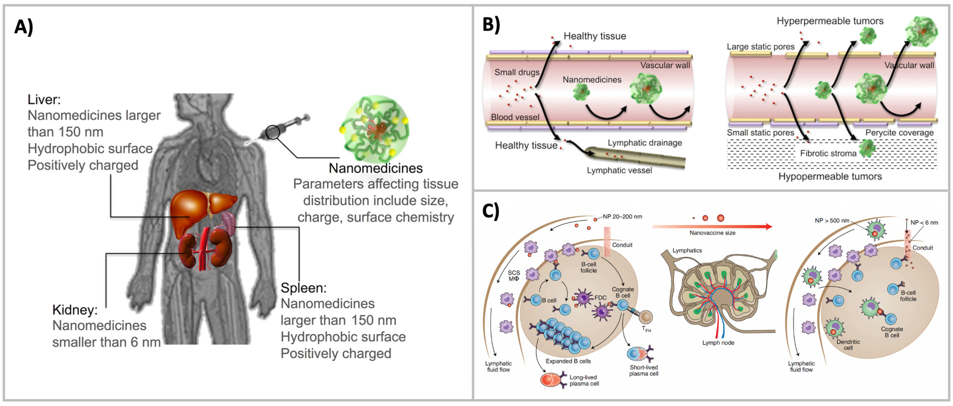
A)
Liver:
Nanomedicines larger than 150 nm
Hydrophobic surface
Positively charged
Nanomedicines
Parameters affecting tissue distribution include size, charge, surface chemistry
Kidney:
Nanomedicines smaller than 6 nm
Spleen:
Nanomedicines larger than 150 nm
Hydrophobic surface
Positively charged
B)
Healthy tissue
Small drugs
Nanomedicines
Vascular wall
Blood vessel
Healthy tissue
Lymphatic drainage
Lymphatic vessel
Hyperpermeable tumors
Large static pores
Vascular wall
Small static pores
Perycite coverage
Fibrotic stroma
Hypopermeable tumors
C)
NP 20–200 nm
Conduit
SCS MΦ
B-cell follicle
B cell
FDC
Cognate B cell
T_{FH}
Expanded B cells
Lymphatic fluid flow
Long-lived plasma cell
Short-lived plasma cell
Nanovaccine size
Lymphatics
Lymph node
NP > 500 nm
NP < 6 nm
Conduit
B-cell follicle
Cognate B cell
Dendritic cell
Lymphatic fluid flow

Figure 3.1 Size of nanoparticles affect their biological distribution

(Reproduced from ref[13] and ref[14])

3.2 EN ROUTE TO THE CYTOSOL

3.2.1 Cellular uptake pathways

Depending on the administration routes, various biological barriers are to be crossed before nanoparticles get to the neighborhood of targeted cells. Here, we only focus on the interaction between nanoparticles and cells.[15–17]

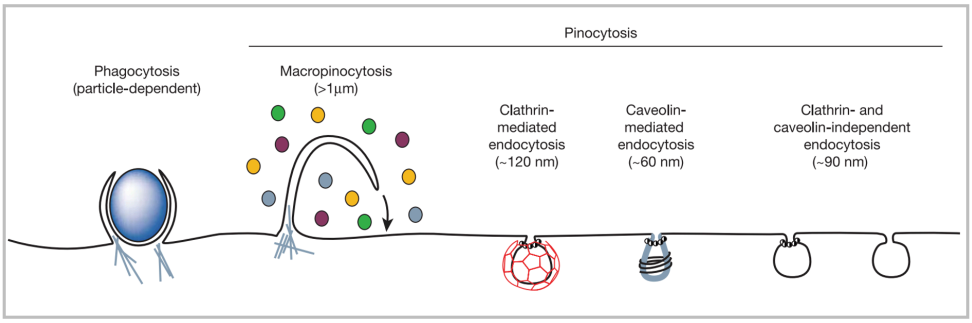
Pinocytosis
Phagocytosis (particle-dependent)
Macropinocytosis (>1μm)
Clathrin-mediated endocytosis (~120 nm)
Caveolin-mediated endocytosis (~60 nm)
Clathrin- and caveolin-independent endocytosis (~90 nm)

Figure 3.2 Main endocytic pathways.

(Reproduced from ref[18])

Packed via hydrophobic interaction, cellular membrane is phosphate lipid bilayers rich in proteins, cholesterols, sugars etc. It plays the role as biological barrier to defend cellular organelles while exchange with the external environment to selectively uptake nutrients. External substance enters cells via either energy-dependent or energy-independent routes.

The latter does not consume ATP and substance passes through the plasma membrane via passive diffusion. The energy-dependent route is in generally called endocytosis. Endocytosis can be categorized into phagocytosis (cell eating) and pinocytosis (cell drinking). **Phagocytosis** is usually carried out by phagocytes and associated with the uptake of large particles in the size range of over 500 nm. **Pinocytosis** can be further subdivided, depending on the mechanism and receptors involved, into macropinocytosis, clathrin-mediated endocytosis (CME), caveolae-dependent endocytosis, clathrin/caveolae-independent endocytosis. Macropinocytosis is similar to phagocytosis in that actins are involved in the extension of plasma membrane to engulf fluids and large particles. CME is the most well described endocytic mechanism. The name comes from the most important protein in the process, the triskelion clathrin. This pathway is a five-step event involving a set of protein machineries: initiation, cargo recognition, coat assembly, scission and un-coating. Another well-studied mechanism is called caveolae-dependent endocytosis. It's a common internalizing route since a third of the plasma membrane area is covered with the protein family of caveolins. Apart from the aforementioned pathways, the rest routes are independent from either clathrin or caveolae. Depending on the involvement of dynamine, the rest can be divided into dynamine-dependent (RhoA-dependent, Arf6-associated, flotillin-assisted) or dynamine-independent (CLIC-GEEC, flotillin-assisted).

3.2.2 Size dependency

Nanoparticles' size and shape affect the way they interact with cells.[19-23] A review published by Mauro de Sousa et al. summarized how the specific endocytic pathway is affected by the size/shape, as shown in Figure 3.3. Here we make a summary. We should first of all point out the size under this discussion is the effective size of nanoparticles in the certain cell culture medium since the environment affects the state of nanoparticles by the adsorption of protein corona[24] or causing nanoparticles to form aggregates due to pH, salt bridge *et cetera*. Some previous research works have shown that ultrasmall (<10 nm) Au nanoparticles with certain surface properties can passively translocate the cell membrane by direct penetration or pore formation. For phagocytosis and macropinocytosis, size is not considered critical as the former depends on the protein corona while the latter is non-specific. The size of clathrin-coated vesicles varies in the range of 50~150 nm depending on the cell type and due to the wide range of their dimension, it's the main pathway for most nanoparticles.

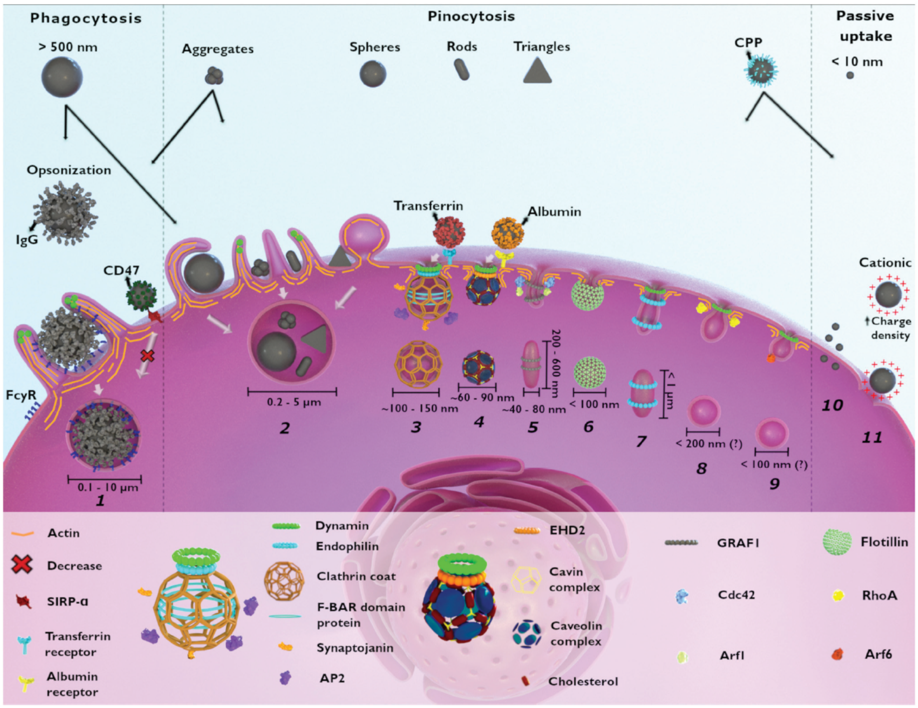
Phagocytosis
> 500 nm
Opsonization
IgG
CD47
FcγR
0.1 - 10 µm
1
Pinocytosis
Aggregates
Spheres
Rods
Triangles
CPP
Passive uptake
< 10 nm
Transferrin
Albumin
Cationic
↑Charge density
0.2 - 5 µm
2
~100 - 150 nm
3
~60 - 90 nm
4
~40 - 80 nm
200 - 600 nm
5
< 100 nm
6
< 1 µm
7
< 200 nm (?)
8
< 100 nm (?)
9
10
11
Actin
Decrease
SIRP-α
Transferrin receptor
Albumin receptor
Dynamin
Endophilin
Clathrin coat
F-BAR domain protein
Synaptojanin
AP2
EHD2
Cavin complex
Caveolin complex
Cholesterol
GRAF1
Cdc42
Arf1
Flotillin
RhoA
Arf6

Figure 3.3 The cellular uptake pathway is size/shape dependent.
(Reproduced from ref[15])

3.2.3 Endosomal escape

As mentioned above, the majority of nanoparticles enters cell via endocytosis, upon which they are entrapped in a vesicular structure, generally called the endosome.[25-27] The maturation of endosomes is accompanied with their acidification. The pH values in the endosomal compartment evolves from the physiological pH of ~7.4 to ~5.0 in the lysosome. The success of endosomal escape determines the cytosolic drug delivery while the failure usually leads to enzymatic degradation. However, the mechanism of endosomal escape is not well understood. Here we summarize some proposed mechanisms (Figure 3.4). **Membrane fusion** has been found to be the main cellular entry pathways for enveloped viruses, where the initial contact is initiated by the spike proteins' binding to cellular receptors and the conformational change of spike proteins drives the hydrophobic fusion between the virus' envelop and the lipid bilayer. Since the cell membrane shares the basic building blocks (phosphate lipids) with the endosomal membrane, the endosomal escape can also be driven by the fusion mechanism. This has been found on viruses[28], lipid nanoparticles[29], gold nanoparticles[30], etc. Another popular mechanism is **osmotic rupture**, or proton sponge effect, first proposed in 1995 by Behr and colleagues.[31,32] Some of the endocytosed nanoparticles exhibit some proton buffering capacity to prevent the drop of pH during the endosome's acidification. As a result, the proton pumps keep internalizing protons, followed with an influx of counter-ions such as chloride ions to main the charge neutrality. This process increases the internal osmotic pressure to drive the influx of water molecules and eventually ruptures the vesicle. Acidic condition can induce **particle swelling/dissociation to** destabilize the endosomal membrane and promote escape. The acidic condition in late endosome or lysosome provides excessive protons to be adsorbed by some polymeric nanoparticles. Upon protonation, these nanoparticles swell due to electrostatic repulsion. In the work by Irvine and coworkers,[33] the core of the polymeric micelle was pH-sensitive and thus its size underwent ~2.5 fold expansion from 200 nm to 550 nm, thus mechanically disrupting the endosome.

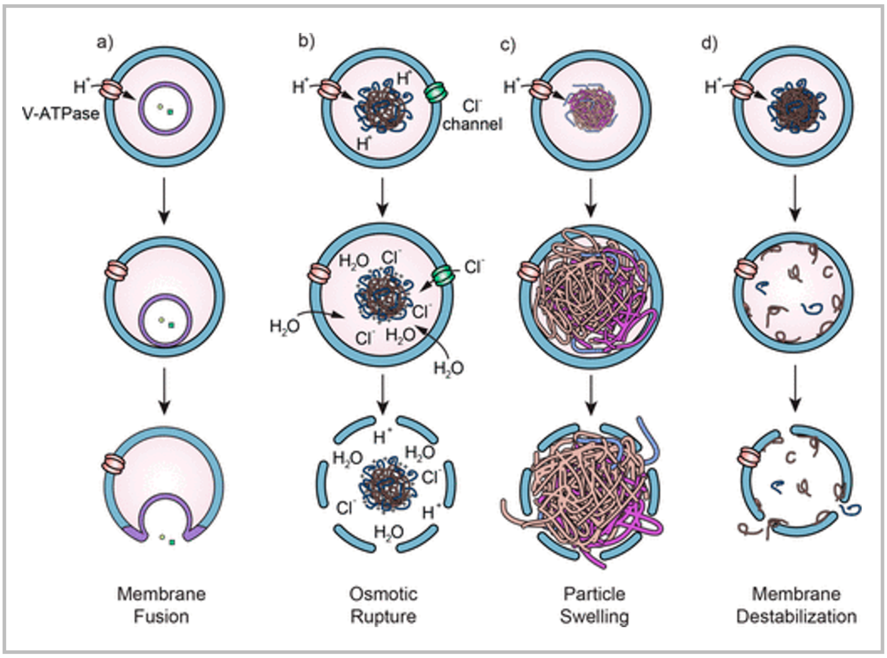
a)
b)
c)
d)
H^+
V-ATPase
Cl^- channel
H_2O
Cl^-
Membrane Fusion
Osmotic Rupture
Particle Swelling
Membrane Destabilization

Figure 3.4 Different endosomal escape mechanisms.

(Reproduced from ref[25])

3.2.4 Methods to study cellular uptake

This section reviews some common methods to study cellular uptake to prepare the reader for the discussion in Chapter 5.

Fluorescence pattern

A common method to study the localization of nanoparticles is via fluorescent microscopy. First, the material of interest is labelled with fluorescent dyes. Then the dye-labelled sample is incubated with cells under certain conditions, depending on the scientific question. Finally, fluorescent microscopy is applied to image the fluorescent emission of the dye (to represent the sample of interest) and often cases, sub cellular organelles (i.e. nucleus, endo/lysosomes, cellular membrane) are selectively stained for more localization information.

When answering if the sample is in the cytosol, the pattern of the fluorescent signal can be used as the first-hand qualitative information to aid the judgement. Labelled materials, if confined in the endocytic vesicles, the fluorescent signal appears as punctate spots; distribution in the cytosol, either via endosomal escape or passive translocation of cellular membrane, appears to be more uniform distribution of fluorescent signal, usually referred as “the diffuse pattern”. Shown in Figure 3.5 is one early work from this group where ultrasmall (~5 nm) AuNPs were synthesized and upon place exchange, decorated with a monolayer of a single type of thiols (Figure 3.5a, left), or binary mixtures of certain morphologies (random distribution or phase separation, as shown in Figure 3.5a, middle and right). The nanoparticles were incubated with cells at two temperatures, 37 °C or 4 °C. At 37 °C, the normal cell metabolism was maintained (Figure 3.5, b, c and d) while at 4 °C, the biological function of proteins and enzymes are inhibited to only allow passive diffusion (Figure 3.5, e, f and g).[34,35] We can clear observe that punctate spots and diffuse patter co-exist in Figure 3.5 b, while nearly no diffuse pattern exhibits in Figure 3.5 e, showing that the hydrophilic AuNPs mostly enter cells via active uptake. For the amiphilic Au NPs, when the binary ligands were ordered arranged, they could passively translocate the cellular membrane to appear the diffuse pattern at 4°C.

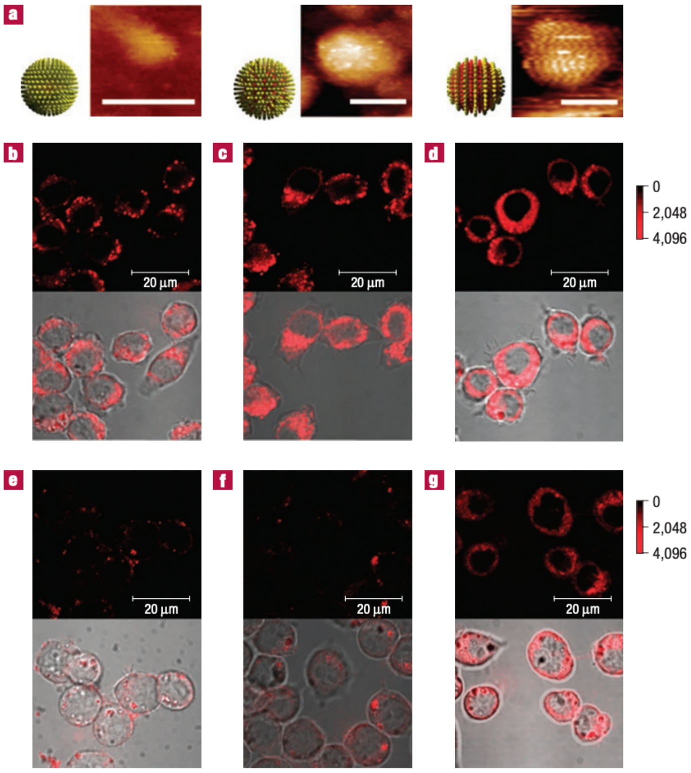

Figure 3.5 Using the fluorescent pattern to judge cytosolic localization of nanoparticles. (Reproduced from ref[36])

Endocytic inhibitor

As mentioned, there is a variety of endocytic mechanisms. To identify the certain cellular uptake pathways, researchers usually pretreated cells to deplete the level of certain signaling/receptor protein or substances such as cholesterol. This can be done by pretreating cells with chemical/pharmaceutical inhibitors or genetically knocking down the protein expression via RNA interference etc. The reader can be directed to the reviews for more thorough knowledge.[37] While such inhibitor assays have been widely used in the literature, they suffer from some limitations. For instance, they may lose efficacy in presence of serum; they show certain cytotoxicity; non-specific; their efficacy varies with cell lines. More detailed discussion about their pros and cons can be found in this review.[38]

GIGT assay

Apart from the fundamental investigation on the cellular uptake mechanisms, characterizing nanoparticles' level of cytosolic localization is of practical relevance. The current assays developed for this purpose have been summarized by some recent reviews (Plückthun[39], Montenegro[40] and Such[25]). Here, we briefly mention the mechanism of Glucocorticoid receptor Induced GFP Translocation (GIGT) assay.[41,42]

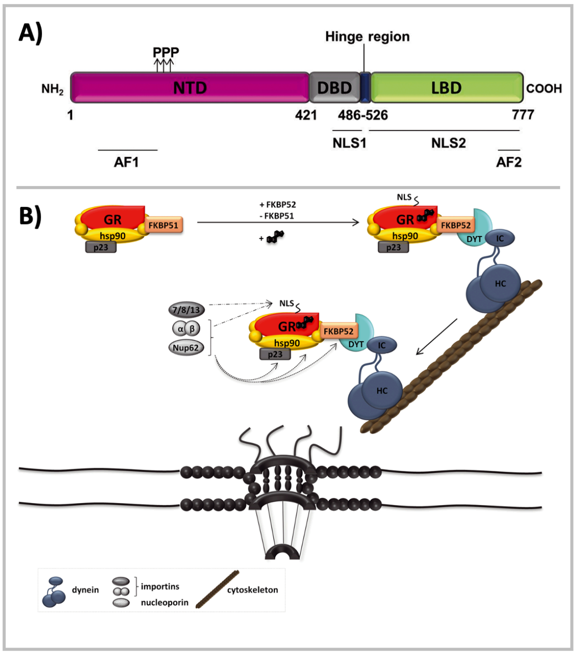
A)
Hinge region
PPP
NH_2
NTD
DBD
LBD
COOH
1
421
486-526
777
NLS1
NLS2
AF1
AF2
B)
GR
hsp90
p23
FKBP51
+ FKBP52
- FKBP51
NLS
FKBP52
DYT
IC
HC
7/8/13
α β
Nup62
dynein
importins
nucleoporin
cytoskeleton

Figure 3.6 The mechanism of GIGT assay.

A) Sub-molecular structure of GR; B) the working principle of GR-induced nucleus transportation. (Reproduced from ref[42])

Glucocorticoid receptors (GR) are widely expressed and reside in the cytosol of almost all types of mammalian cells. GR is a modular protein composed of three major domains: the N-terminal domain (NTD), the central DNA-binding domain (DBD), and the C-terminal ligand-binding domain (LBD). In the absence of ligands, GR resides in the cytoplasm as chaperon complex, which guides the conformation of GR. Binding with glucocorticoids, such as cortisol, dexamethasone etc., triggers the rapid active transport of the receptor-glucocorticoid complex along cytoskeleton towards the nuclear pore complex, as shown in Figure 3.6.[42] In 1997, Macara and coworkers constructed the plasmid encoding the chimeric protein of GR-GFP where the GFP epitope serves as the reporter.[43] Due to the small size of GR-GFP proteins, they can freely diffuse through the nuclear pores. The nuclear transportation due to the binding with steroid-tagged molecule-of-interest results in a brighter GFP signal in the nucleus region than the cytosol. The GFP signal ratio of nucleus against cytosol can be taken as the relative measure to the cytosolic level of the ligands, reflecting the cytosolic accessing ability of the molecule-of-interest, regardless of the pathways. This assay has been applied to study the cytosolic access of synthetic molecules for drug delivery. To name a few, Liu and coworkers[44] tagged dexamethasone onto a library of peptides to screen for the sequence that enhances endosomal escape; Schepartz and cowork[45] studied how the arginine topology affects the cell permeability of miniature proteins; Holub et al.[46] compared GIGT assay with GIGI (glucocorticoidinduced eGFP induction) assay; Montenegro and coworkers[47] developed a group of cell penetrating peptides for the delivery of Cas9 and used this approach to characterize their membrane permeability.

3.3 CELLULAR UPTAKE OF SCNPS

Unlike conventional polymeric nanostructures, SCNPs are ultrasmall falling the diameter range of <20 nm and some of them possess unique dimensions comparable to the characteristic thickness of the lipid bilayer (~5 nm). Moreover, comparing to rigid nanoparticle such as gold nanoparticles which cannot be deformed by the lipid bilayer, the softness[48,49] of SCNPs can give rise to different modes of action. Considering the huge size difference between a SCNP and a cell, we can simplify the lipid bilayer as a flat surface with negative charge. With internal restriction due to the crosslinking, the softness of SCNPs lies in between the precursor polymer chain and those widely investigated rigid inorganic nanoparticles. Are they prone to deformation upon adsorption to the lipid bilayer? While SCNPs possesses some unique features and thus potentially leading to unique interacting modes with cells, related topics are not widely studied in the current literature. Here we mentioned two recent works (one is simulation and the other is based on experimental investigation) for discussion.

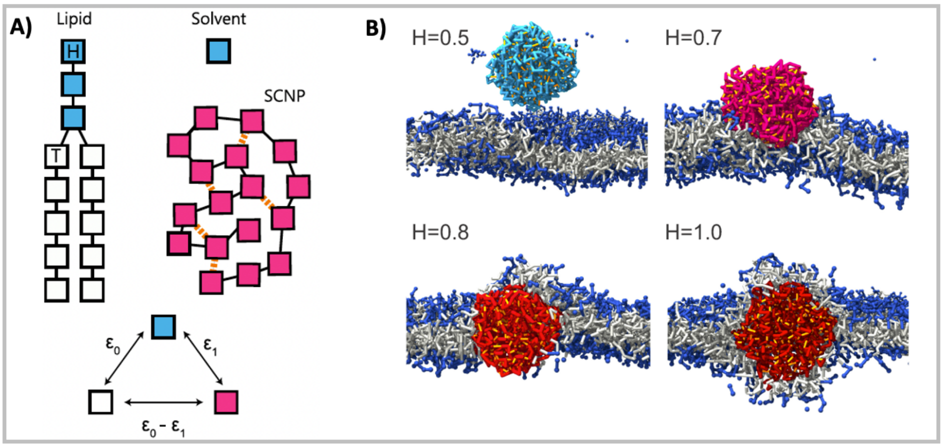

Figure 3.7 SCNPs' interacting modes with cells as an interplay between rigidity and hydrophobicity.

A) The coarse-grained model showing the interaction between the SCNPs and the lipids; B) typical snapshots of the SCNP interacting with lipid bilayer for different hydrophobicities H with fixed chain length and cross-link density. (Reproduced from ref[50])

Guo et al.[50] studied the interaction of SCNPs with the lipid bilayer using the Bond Fluctuation Model. Their coarse-grained simulation showed that the fully hydrophilic SCNPs would preferentially stay in the solvent; increasing the hydrophobicity of the precursor would favor the interaction with the lipid bilayer, leading to SCNPs' insertion; when the hydrophobicity of the SCNPs exceeds the critical value, the SCNPs can be fully embedded inside the lipid bilayer. They also predict that a second critical hydrophobicity where the SCNPs could cause the topological transition of the lipid bilayer.

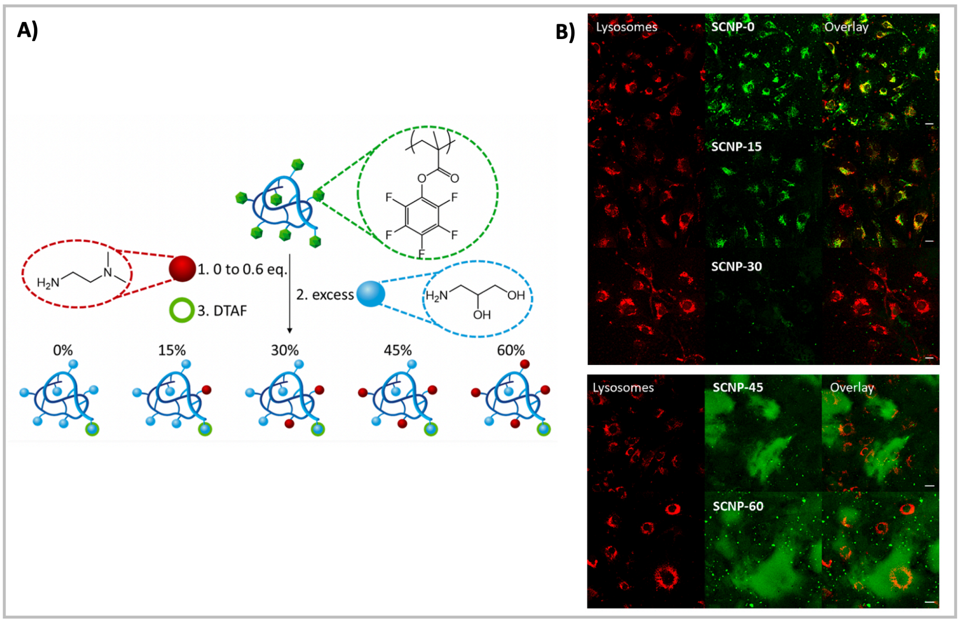

Figure 3.8 Cytosolic delivery of SCNPs highly depends on their surface charge (Reproduced from ref[52])

Recently, increasing numbers of experimental studies on this topic are appearing.[51–53] In one recent work[52] by Paulusse and co-workers, they investigated how the surface charge affect the uptake of SCNPs of ~10 nm. They first synthesized the active ester functionalized SCNPs with intramolecular thiol-Michael addition. By functionalizing with tertiary amines from 0 to 60 mol%, a series of SCNPs with different surface cationic charges were obtained (Figure 3.8). The confocal microscopy revealed successful cytosolic delivery of SCNPs with high degrees of functionalization

(45% and 60%), while SCNPs with low amounts (0% to 30%) of tertiary amines showed high degrees of colocalization with lysosomes (Figure 3.8).

3.4 SUMMARY

When nanoparticles are designed for medicinal purpose, their size plays a key role in determining their biological fate and cellular uptake pathways. Understanding the cellular uptake mechanism and especially characterizing the cytosolic level of nanoparticles upon cellular uptake can rationalize the design of drug carriers.

The dimension of SCNPs earns them some advantages such as quick elimination, deep tissue penetration, passive tumour retention *et cetera*. Experimental investigation on SCNPs' mode of cellular uptake is a key step towards developing them as efficient drug carriers.

3.5 REFERENCE

(1) Pharmacokinetics and Biodistribution of Nanoparticles | Molecular Pharmaceutics https://pubs.acs.org/doi/abs/10.1021/mp800049w.

(2) Clearance properties of nano-sized particles and molecules as imaging agents: considerations and caveats | Nanomedicine https://www.futuremedicine.com/doi/abs/10.2217/17435889.3.5.703.

(3) Liu, D.; Mori, A.; Huang, L. Role of Liposome Size and RES Blockade in Controlling Biodistribution and Tumor Uptake of GM1-Containing Liposomes. *Biochimica et Biophysica Acta (BBA) – Biomembranes* **1992**, *1104* (1), 95–101. https://doi.org/10.1016/0005-2736(92)90136-A.

(4) De Jong, W. H.; Hagens, W. I.; Krystek, P.; Burger, M. C.; Sips, A. J. A. M.; Geertsma, R. E. Particle Size-Dependent Organ Distribution of Gold Nanoparticles after Intravenous Administration. *Biomaterials* **2008**, *29* (12), 1912–1919. https://doi.org/10.1016/j.biomaterials.2007.12.037.

(5) Sonavane, G.; Tomoda, K.; Makino, K. Biodistribution of Colloidal Gold Nanoparticles after Intravenous Administration: Effect of Particle Size. *Colloids and Surfaces B: Biointerfaces* **2008**, *66* (2), 274–280. https://doi.org/10.1016/j.colsurfb.2008.07.004.

(6) Sykes, E. A.; Dai, Q.; Sarsons, C. D.; Chen, J.; Rocheleau, J. V.; Hwang, D. M.; Zheng, G.; Cramb, D. T.; Rinker, K. D.; Chan, W. C. W. Tailoring Nanoparticle Designs to Target Cancer Based on Tumor Pathophysiology. *PNAS* **2016**, *113* (9), E1142–E1151. https://doi.org/10.1073/pnas.1521265113.

(7) Longmire, M.; Choyke, P. L.; Kobayashi, H. Clearance Properties of Nano-Sized Particles and Molecules as Imaging Agents: Considerations and Caveats. *Nanomedicine* **2008**, *3* (5), 703–717. https://doi.org/10.2217/17435889.3.5.703.

(8) Kobayashi, H.; Brechbiel, M. W. Nano-Sized MRI Contrast Agents with Dendrimer Cores. *Advanced Drug Delivery Reviews* **2005**, *57* (15), 2271–2286. https://doi.org/10.1016/j.addr.2005.09.016.

(9) Matsumura, Y.; Maeda, H. A New Concept for Macromolecular Therapeutics in Cancer Chemotherapy: Mechanism of Tumoritropic Accumulation of Proteins and the Antitumor Agent Smancs. *Cancer Res* **1986**, *46* (12 Part 1), 6387–6392.

(10) A Retrospective 30 Years After Discovery of the Enhanced Permeability and Retention Effect of Solid Tumors: Next-Generation Chemotherapeutics and Photodynamic Therapy—Problems, Solutions, and Prospects – Maeda – 2016 – Microcirculation – Wiley Online Library https://onlinelibrary.wiley.com/doi/full/10.1111/micc.12228.

(11) Nakamura, Y.; Mochida, A.; Choyke, P. L.; Kobayashi, H. Nanodrug Delivery: Is the Enhanced Permeability and Retention Effect Sufficient for Curing Cancer? *Bioconjugate Chem.* **2016**, *27* (10), 2225–2238. https://doi.org/10.1021/acs.bioconjchem.6b00437.

(12) Zhang, F.; Trent Magruder, J.; Lin, Y.-A.; Crawford, T. C.; Grimm, J. C.; Sciortino, C. M.; Wilson, M. A.; Blue, M. E.; Kannan, S.; Johnston, M. V.; Baumgartner, W. A.; Kannan, R. M.

Generation-6 Hydroxyl PAMAM Dendrimers Improve CNS Penetration from Intravenous Administration in a Large Animal Brain Injury Model. *J Control Release* **2017**, *249*, 173–182. https://doi.org/10.1016/j.jconrel.2017.01.032.

(13) Singh, A. Eliciting B Cell Immunity against Infectious Diseases Using Nanovaccines. *Nature Nanotechnology* **2020**, 1–9. https://doi.org/10.1038/s41565-020-00790-3.

(14) Cabral, H.; Miyata, K.; Osada, K.; Kataoka, K. Block Copolymer Micelles in Nanomedicine Applications. *Chem. Rev.* **2018**, *118* (14), 6844–6892. https://doi.org/10.1021/acs.chemrev.8b00199.

(15) Almeida, M. S. de; Susnik, E.; Drasler, B.; Taladriz-Blanco, P.; Petri-Fink, A.; Rothen-Rutishauser, B. Understanding Nanoparticle Endocytosis to Improve Targeting Strategies in Nanomedicine. *Chem. Soc. Rev.* **2021**. https://doi.org/10.1039/D0CS01127D.

(16) Rennick, J. J.; Johnston, A. P. R.; Parton, R. G. Key Principles and Methods for Studying the Endocytosis of Biological and Nanoparticle Therapeutics. *Nature Nanotechnology* **2021**, *16* (3), 266–276. https://doi.org/10.1038/s41565-021-00858-8.

(17) Petros, R. A.; DeSimone, J. M. Strategies in the Design of Nanoparticles for Therapeutic Applications. *Nat Rev Drug Discov* **2010**, *9* (8), 615–627. https://doi.org/10.1038/nrd2591.

(18) Conner, S. D.; Schmid, S. L. Regulated Portals of Entry into the Cell. *Nature* **2003**, *422* (6927), 37–44. https://doi.org/10.1038/nature01451.

(19) Chithrani, B. D.; Ghazani, A. A.; Chan, W. C. W. Determining the Size and Shape Dependence of Gold Nanoparticle Uptake into Mammalian Cells. *Nano Lett.* **2006**, *6* (4), 662–668. https://doi.org/10.1021/nl052396o.

(20) Rejman, J.; Oberle, V.; Zuhorn, I. S.; Hoekstra, D. Size-Dependent Internalization of Particles via the Pathways of Clathrin- and Caveolae-Mediated Endocytosis. *Biochemical Journal* **2004**, *377* (1), 159–169. https://doi.org/10.1042/bj20031253.

(21) Dasgupta, S.; Auth, T.; Gompper, G. Shape and Orientation Matter for the Cellular Uptake of Nonspherical Particles. *Nano Lett.* **2014**, *14* (2), 687–693. https://doi.org/10.1021/nl403949h.

(22) Vácha, R.; Martinez-Veracoechea, F. J.; Frenkel, D. Receptor-Mediated Endocytosis of Nanoparticles of Various Shapes. *Nano Lett.* **2011**, *11* (12), 5391–5395. https://doi.org/10.1021/nl2030213.

(23) Cong, V. T.; Wang, W.; Tilley, R. D.; Sharbeen, G.; Phillips, P. A.; Gaus, K.; Gooding, J. J. Can the Shape of Nanoparticles Enable the Targeting to Cancer Cells over Healthy Cells? *Advanced Functional Materials n/a* (n/a), 2007880. https://doi.org/10.1002/adfm.202007880.

(24) Digiacomo, L.; Cardarelli, F.; Pozzi, D.; Palchetti, S.; Digman, M. A.; Gratton, E.; Capriotti, A. L.; Mahmoudi, M.; Caracciolo, G. An Apolipoprotein-Enriched Biomolecular Corona Switches the Cellular Uptake Mechanism and Trafficking Pathway of Lipid Nanoparticles. *Nanoscale* **2017**, *9* (44), 17254–17262. https://doi.org/10.1039/C7NR06437C.

(25) Smith, S. A.; Selby, L. I.; Johnston, A. P. R.; Such, G. K. The Endosomal Escape of Nanoparticles: Toward More Efficient Cellular Delivery. *Bioconjugate Chem.* **2019**, *30* (2), 263–272. https://doi.org/10.1021/acs.bioconjchem.8b00732.

(26) Selby, L. I.; Cortez-Jugo, C. M.; Such, G. K.; Johnston, A. P. R. Nanoescapology: Progress toward Understanding the Endosomal Escape of Polymeric Nanoparticles. *WIREs Nanomedicine and Nanobiotechnology* **2017**, *9* (5), e1452. https://doi.org/10.1002/wnan.1452.

(27) Bus, T.; Traeger, A.; Schubert, U. S. The Great Escape: How Cationic Polyplexes Overcome the Endosomal Barrier. *J. Mater. Chem. B* **2018**, *6* (43), 6904–6918. https://doi.org/10.1039/C8TB00967H.

(28) Dimitrov, D. S. Virus Entry: Molecular Mechanisms and Biomedical Applications. *Nat Rev Microbiol* **2004**, *2* (2), 109–122. https://doi.org/10.1038/nrmicro817.

(29) Multi-layered nanoparticles for penetrating the endosome and nuclear membrane via a step-wise membrane fusion process – ScienceDirect https://www.sciencedirect.com/science/article/abs/pii/S0142961209001574?via%3Dihub.

(30) Mout, R.; Ray, M.; Tay, T.; Sasaki, K.; Yesilbag Tonga, G.; Rotello, V. M. General Strategy for Direct Cytosolic Protein Delivery via Protein–Nanoparticle Co-Engineering. *ACS Nano* **2017**, *11* (6), 6416–6421. https://doi.org/10.1021/acsnano.7b02884.

(31) Boussif, O.; Lezoualc'h, F.; Zanta, M. A.; Mergny, M. D.; Scherman, D.; Demeneix, B.; Behr, J. P. A Versatile Vector for Gene and Oligonucleotide Transfer into Cells in Culture and in Vivo: Polyethylenimine. *PNAS* **1995**, *92* (16), 7297–7301. https://doi.org/10.1073/pnas.92.16.7297.

(32) Behr, J.-P. The Proton Sponge: A Trick to Enter Cells the Viruses Did Not Exploit. *CHIMIA International Journal for Chemistry* **1997**, *51* (1–2), 34–36.

(33) Hu, Y.; Litwin, T.; Nagaraja, A. R.; Kwong, B.; Katz, J.; Watson, N.; Irvine, D. J. Cytosolic Delivery of Membrane-Impermeable Molecules in Dendritic Cells Using PH-Responsive Core−Shell Nanoparticles. *Nano Lett.* **2007**, *7* (10), 3056–3064. https://doi.org/10.1021/nl071542i.

(34) Saraste, J.; Palade, G. E.; Farquhar, M. G. Temperature-Sensitive Steps in the Transport of Secretory Proteins through the Golgi Complex in Exocrine Pancreatic Cells. *PNAS* **1986**, *83* (17), 6425–6429. https://doi.org/10.1073/pnas.83.17.6425.

(35) Iacopetta, B. J.; Morgan, E. H. The Kinetics of Transferrin Endocytosis and Iron Uptake from Transferrin in Rabbit Reticulocytes. *Journal of Biological Chemistry* **1983**, *258* (15), 9108–9115. https://doi.org/10.1016/S0021-9258(17)44637-0.

(36) Verma, A.; Uzun, O.; Hu, Y.; Hu, Y.; Han, H.-S.; Watson, N.; Chen, S.; Irvine, D. J.; Stellacci, F. Surface-Structure-Regulated Cell-Membrane Penetration by Monolayer-Protected Nanoparticles. *Nature Materials* **2008**, *7* (7), 588–595. https://doi.org/10.1038/nmat2202.

(37) Dutta, D.; Donaldson, J. G. Search for Inhibitors of Endocytosis. *Cellular Logistics* **2012**, *2* (4), 203–208. https://doi.org/10.4161/cl.23967.

(38) Francia, V.; Reker-Smit, C.; Boel, G.; Salvati, A. Limits and Challenges in Using Transport Inhibitors to Characterize How Nano-Sized Drug Carriers Enter Cells. *Nanomedicine* **2019**, *14* (12), 1533–1549. https://doi.org/10.2217/nnm-2018-0446.

(39) Deprey, K.; Becker, L.; Kritzer, J.; Plückthun, A. Trapped! A Critical Evaluation of Methods for Measuring Total Cellular Uptake versus Cytosolic Localization. *Bioconjugate Chem.* **2019**, *30* (4), 1006–1027. https://doi.org/10.1021/acs.bioconjchem.9b00112.

(40) Méndez-Ardoy, A.; Lostalé-Seijo, I.; Montenegro, J. Where in the Cell Is Our Cargo? Methods Currently Used To Study Intracellular Cytosolic Localisation. *ChemBioChem* **2019**, *20* (4), 488–498. https://doi.org/10.1002/cbic.201800390.

(41) Yu, P.; Liu, B.; Kodadek, T. A High-Throughput Assay for Assessing the Cell Permeability of Combinatorial Libraries. *Nat Biotechnol* **2005**, *23* (6), 746–751. https://doi.org/10.1038/nbt1099.

(42) Vandevyver, S.; Dejager, L.; Libert, C. On the Trail of the Glucocorticoid Receptor: Into the Nucleus and Back. *Traffic* **2012**, *13* (3), 364–374. https://doi.org/10.1111/j.1600-0854.2011.01288.x.

(43) Carey, K. L.; Richards, S. A.; Lounsbury, K. M.; Macara, I. G. Evidence Using a Green Fluorescent Protein-Glucocorticoid Receptor Chimera That the Ran/TC4 GTPase Mediates an Essential Function Independent of Nuclear Protein Import. *Journal of Cell Biology* **1996**, *133* (5), 985–996. https://doi.org/10.1083/jcb.133.5.985.

(44) Li, M.; Tao, Y.; Shu, Y.; LaRochelle, J. R.; Steinauer, A.; Thompson, D.; Schepartz, A.; Chen, Z.-Y.; Liu, D. R. Discovery and Characterization of a Peptide That Enhances Endosomal Escape of Delivered Proteins in Vitro and in Vivo. *J. Am. Chem. Soc.* **2015**, *137* (44), 14084–14093. https://doi.org/10.1021/jacs.5b05694.

(45) Appelbaum, J. S.; LaRochelle, J. R.; Smith, B. A.; Balkin, D. M.; Holub, J. M.; Schepartz, A. Arginine Topology Controls Escape of Minimally Cationic Proteins from Early Endosomes to the Cytoplasm. *Chemistry & Biology* **2012**, *19* (7), 819–830. https://doi.org/10.1016/j.chembiol.2012.05.022.

(46) Holub, J. M.; LaRochelle, J. R.; Appelbaum, J. S.; Schepartz, A. Improved Assays for Determining the Cytosolic Access of Peptides, Proteins, and Their Mimetics. *Biochemistry* **2013**, *52* (50), 9036–9046. https://doi.org/10.1021/bi401069g.

(47) Lostalé-Seijo, I.; Louzao, I.; Juanes, M.; Montenegro, J. Peptide/Cas9 Nanostructures for Ribonucleoprotein Cell Membrane Transport and Gene Edition. *Chem. Sci.* **2017**, *8* (12), 7923–7931. https://doi.org/10.1039/C7SC03918B.

(48) Moreno, A. J.; Bacova, P.; Verso, F. L.; Arbe, A.; Colmenero, J.; Pomposo, J. A. Effect of Chain Stiffness on the Structure of Single-Chain Polymer Nanoparticles. *J. Phys.: Condens. Matter* **2017**, *30* (3), 034001. https://doi.org/10.1088/1361-648X/aa9f5c.

(49) Song, X.; Ma, J.; Long, T.; Xu, X.; Zhao, S.; Liu, H. Mechanochemical Cellular Membrane Internalization of Nanohydrogels: A Large-Scale Mesoscopic Simulation. *ACS Appl. Mater. Interfaces* **2021**, *13* (1), 123–134. https://doi.org/10.1021/acsami.0c16688.

(50) Guo, Y.; Werner, M.; Li, W.; Sommer, J.-U.; Baulin, V. A. Shape-Adaptive Single-Chain Nanoparticles Interacting with Lipid Membranes. *Macromolecules* **2019**, *52* (24), 9578–9584. https://doi.org/10.1021/acs.macromol.9b02102.

(51) Hamilton, S. K.; Harth, E. Molecular Dendritic Transporter Nanoparticle Vectors Provide Efficient Intracellular Delivery of Peptides. *ACS Nano* **2009**, *3* (2), 402–410. https://doi.org/10.1021/nn800679z.

(52) Hamelmann, N. M.; Paats, J.-W. D.; Paulusse, J. M. J. Cytosolic Delivery of Single-Chain Polymer Nanoparticles. *ACS Macro Lett.* **2021**, *10* (11), 1443–1449. https://doi.org/10.1021/acsmacrolett.1c00558.

(53) Kröger, A. P. P.; Komil, M. I.; Hamelmann, N. M.; Juan, A.; Stenzel, M. H.; Paulusse, J. M. J. Glucose Single-Chain Polymer Nanoparticles for Cellular Targeting. *ACS Macro Lett.* **2019**, *8* (1), 95–101. https://doi.org/10.1021/acsmacrolett.8b00812.

(54) Batty, C. J.; Bachelder, E. M.; Ainslie, K. M. Historical Perspective of Clinical Nano and Microparticle Formulations for Delivery of Therapeutics. *Trends in Molecular Medicine* **2021**, *27* (6), 516–519. https://doi.org/10.1016/j.molmed.2021.04.002.

(55) Kröger, A. P. P.; Paulusse, J. M. J. Single-Chain Polymer Nanoparticles in Controlled Drug Delivery and Targeted Imaging. *Journal of Controlled Release* **2018**, *286*, 326–347. https://doi.org/10.1016/j.jconrel.2018.07.041.

Chapter 4 Control and Characterization of SCNP Topology

This chapter discusses how two key factors, the initial chain conformation and cross-linker length, affect the global topology of SCNPs. To this end, a set of analytical tools were applied. And we examination the cytotoxicity profile of SCNPs with different topologies.

Disclosure: This chapter is adapted from the published work entitled Control and Characteirzation of the Compactness of Single-Chain Nanoparticles, by Suiyang Liao*, Lixia Wei, Luciano A. Abriata and Francesco Stellacci* on *Macromolecules* (doi: 10.1021/acs.macromol.1c02071)

4.1 ABSTRACT

Polymers when self-cross-linked into single-chain nanoparticles bear some resemblance to folded proteins; yet proteins have clear energy landscapes that determine precisely folded structures, while single-chain polymer nanoparticles (SCNPs) have more undefined structures. There have been initial reports showing that some structural parameters in SCNPs can be con-trolled, for example compactness. Here, we construct SCNPs from poly(allylamine) (MW ~22,000 Da) with dicarboxylic acids (HOOC-R-COOH) in solvent conditions where the initial chains adopt either extended or collapsed conformation. The spacer groups R that we used were $-CH_2CH_2-$, $-(CH_2S)_2-$ or $–(CH_2CH_2)_3-$ whose length can be estimated to vary from ~4 to ~12 Å. We present a systematic study that uses several characterization techniques (^{1}H-NMR DOSY, viscometry, analytical ultracentrifugation, and ^{1}H-NMR T_2 relaxation) to show that both initial reaction conditions as well as length of the cross-linking molecules determine the final topology of SCNPs. Specifically, when short cross-linking molecules are applied, short-range loops dominate and the cross-linking process fails to achieve global chain compaction, leading to less compact SCNPs. When the chain is pre-collapsed (0.1 M water solution of NaCl or 10 vol% ethanol as opposed to DI water) the particles resulting after cross-linking are more compact. Of utmost practical relevance, we show that particles that are essentially chemically identical but differ only in topology have different toxicity when interacting with HeLa cells, the more compact ones being less toxic.

4.2 INTRODUCTION

Proteins are mono-disperse sequence-defined polymers. It is accepted that, for most proteins, the sequence determines a single shape that a protein folds into. Recently, synthetic polymers have been used as precursor for single-chain polymer nanoparticles by a process of intra-chain cross-linking that bears some resemblance to collapsed states *en route* to protein folding.[1,2] However, unlike its natural counterpart, the folding/collapsing process of synthetic polymer chains is stochastic due to its self-repeating nature and the lack of precisely defined interactions. Thus, controlling the final topology is challenging.

The understanding of intramolecular loops provides the guidance for the tuning the topology of SCNPs.[3,4] Each crosslinking event connects two functional sites from the linear backbone to generate a loop. The loop size is defined as the contour distance between the two cross-linked sites. The competition between local compaction (forming short-range loops) and global compaction (forming long-range loops) determines the probability distribution of intramolecular loop sizes, thus defining the final SCNP topology, as illustrated in Scheme 1. However, under conventional conditions, due to the swelling effect and the self-avoiding nature in highly diluted good solvents, intra-molecular collapsing of polymer chains tends to form short-range loops, thus generating less compact topologies.[5]

To favor the formation of long-range loops, chemists have been expanding the arsenal of covalent single-chain techniques, such as Michael addition with tri-functional cross-linkers,[6] orthogonal reactions (hetero-functional cross-linkers,[7] and step-wise folding[8,9]), thiol-yne click[10] and etc. Moreover, supramolecular interactions have been exploited to construct SCNPs. The work from Morishima et al.[11] shows that bulky hydrophobic groups can promote intramolecular self-association. Amphiphilic copolymers (Sawamoto[12] et al.) bearing poly(ethylene glycol) and hydrophobic olefin pendants are able to self-fold in aqueous conditions. With the inspiration from the folding of natural biomacromolecules that is largely dominated by hydrogen bonds, Barner-Kowollik and co-workers[13] decorated the polymer chains with pairs of complementary hydrogen bonding motifs for full orthogonal recognition; Meijer and co-workers[15] introduced onto poly(norbornenes) chains 2-ureido-pyrimidinone (Upy) protected groups to reveal H-bonding interaction upon UV cleavage. Multiple non-covalent interactions can be combined in a cooperative manner for the compaction of SCNPs. Benzene-1,3,5-tricarboxamide (BTA)[16] was applied as recognition unit to form helical stacks due to pi-interaction and stabilization from threefold hydrogen bonding.[14] Revealed by Palmans and Meijer et al, the self-assembly pathway of BTA-decorated amphiphilic polymer chains can be tuned by the hydrophobic content[15], as well as the formation order of covalent and hydrogen bonds[16].

Carefully manipulating the conformation of the precursor chains holds vast potential as a facile yet versatile approach to control them topology of SCNPs. Pomposo and co-workers added an extra ring-closing step of precusor linear chain and found a higher shrinking factor for such single-ring nanoparticles.[17] Similar result through molecular dynamic simulation by Formanek et al.[18] revealed that cyclic precursors reach higher compaction than their linear counterparts. Due to size-exclusion effect, polymer chains are more compact in crowded molecular environment. Such phenomenon inspired researchers to apply crowding molecules to pre-collapse precursor chains before cross-linking for compact SCNPs.[19–22] Another effective strategy to manipulate the precursor conformation is via the solvent quality.[23–27] For example, Sommer and co-workers[23] used Monte-Carlo simulation to show that cross-linking in good or poor solvent could determine the compactness of the single-chain product. One would also reasonably expect the cross-linkers to affect the single-chain compaction. Here, if we restrict to external cross-linkers to simplify our discussion, many questions await further investigation. For instance, comparing to widely-applied bifunctional cross-linkers, does higher valency such as tridentate ones[6] promote compaction? The work by Moreno et al.[7] showed that hetero-bifunctional cross-linkers performed better than the homo-bifunctional ones. Besides, the length of cross-linkers[10] can determine the contour distance between the backbone moieties and in turn affect the final compactness of SCNPs.

Moreover, characterizing the topology of SCNPs requires careful and systematic investigation.[28,29] Direct size and shape imaging can be achieved with microscopic tools[30–32] such as SEM (scanning electron microscopy), negative staining TEM (transmission electron microscopy) and AFM (atomic force microscopy),[33,34] but they are inevitably prone to drying effects[6]. Scattering techniques such as DLS (dynamic light scattering), SLS (static light scattering) and SAXS (small angle X-ray scattering) are widely used for nanoparticle size-and-shape characterization but for polymer nanoparticles they suffer from low optical contrast. SEC (size exclusion chromatography) is widely employed to determine SCNPs compactness by separating particles according to their hydrodynamic volume; however, it is not trivial to meet the ideal SEC conditions with no enthalpic interaction with the columns occurs.[35–40]

As discussed, there is a body of literature that has shown the potential of implementing either pre-collapsing or cross-linker length as versatile strategies for controlling the topology of SCNPs. Unfortunately, the diverse precursor library and characterization tools applied renders hard a generalization of the results as they are difficult to compare. To fill this gap, this work adopts a simple homopolymer (pre-collapsed in different ways) and a set of bifunctional cross-linkers (three spacer lengths) to generate SCNPs as shown Scheme 4.1. All SCNPs underwent careful structural evaluation by multiple analytical tools.

The model polymer chains chosen here is a type of cationic polyelectrolyte called poly(allylamine)/PALA (average MW ~22,000 and PDI ~1.52) and the cross-linkers are bicarboxylic acids with different spacer lengths. The SCNPs were characterized by a suite of analytical tools. Namely we used ^{1}H-NMR DOSY (diffusion-ordered spectroscopy), viscometry and SV-AUC (sedimentation velocity-analytical ultracentrifugation) to determine diffusion coefficient, intrinsic viscosity, and sedimentation coefficient respectively. All three properties depend on particle size, that in turn can be uniquely linked to particle compactness when the SCNPs derive from the same polymer precursor. Furthermore, we used ^{1}H-NMR T_2 relaxation as an indication of chain mobility within nanoparticles, a feature related to SCNP topology. PALA, as the main component of Renagel[41], an FDA-approved drug to treat hyperphosphatemia, holds potential to be developed as drug delivery platform while its cytotoxicity needs to be mitigated. We performed cell proliferation assays to explore the relationships between topology and cytotoxicity of these cationic polyelectrolyte nanoparticles.

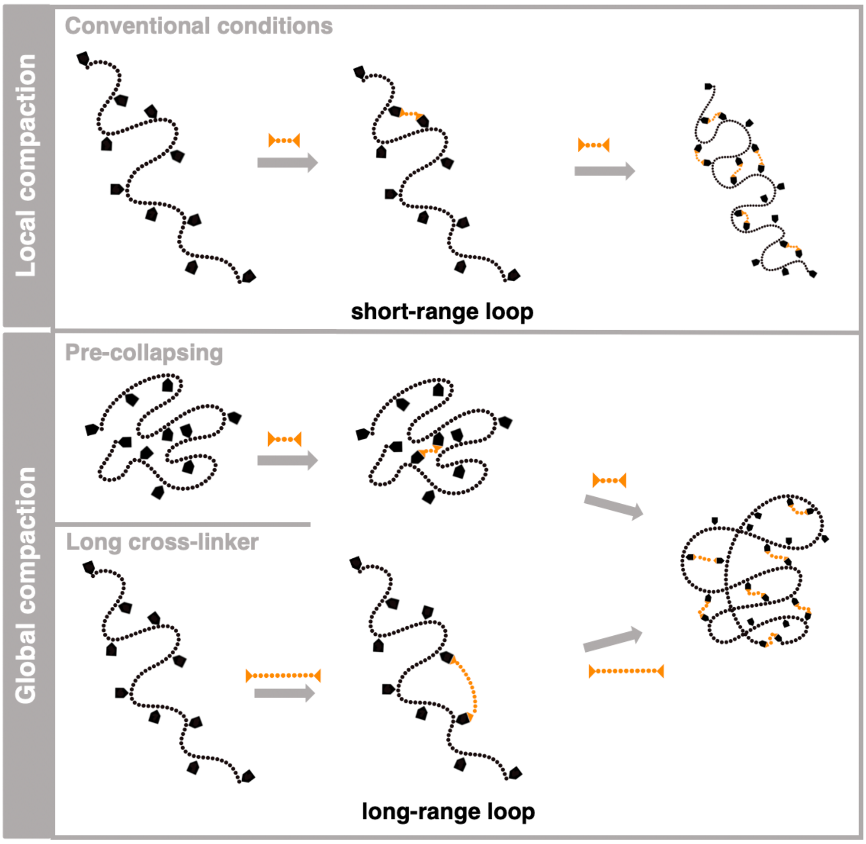

Scheme 4.1 Illustration of the interplay between short-range (top) and long-range (bottom) loops and the global topology of SCNPs. This scheme also illustrates the major finding of this work. Compact SCNP can be achieved either by pre-collapsing the polymer chain or by using longer cross-linking molecules, in both cases we believe that long-range loops are achieved

4.3 RESULTS AND DISCUSSION

We prepared SCNPs *via* amide bond formation as shown Figure 4.1A. The nature of the library of all nine SCNPs is shown in Table 1; they differ either in the cross-linker used or in the initial reaction conditions. PALA was dissolved into diluted solutions (~1 mg/ml, below the critical concentration to avoid the inter-chain entanglement) under the chosen solvent conditions (ultrapure water, 100 mM NaCl or 10 vol% ethanol-water mixture) to predefine the polymer conformation. In water, the electrostatic repulsion among the cationic amines present the PALA chains as random coil-like; in 100 mM NaCl aqueous solution the ionic strength screens electrostatic repulsion thus collapsing the precursor chains via counter-ion condensation;[42] in 10/90 ethanol/water binary mixture, ethanol molecules work as osmolytes to strengthen the water molecule network and promote the intra-chain hydrophobic effect to induce pre-collapsing.[43] To examine the influence from the length of cross-linkers, three types of dicarboxylic acids (succinic acids, dithiodiglycolic acids and suberic acids) with various spacer lengths varying from ~4 to ~12 Å were applied for amidation. The cross-linking density were kept within a certain range (40% ±10%) to ensure that the resulting particles can be compared. Moreover, PALA was conjugated with 40% amine conversion to a type of linear carboxylic acid (2-[2-(2-Methoxyethoxy)ethoxy]acetic acid; this product is referred as EGPALA thereafter; synthesis and characterization in SI) as control. The reaction procedures and the calculation for the cross-linking density can be found more in details in SI. The ^{1}H NMR spectra in Figure 4.1B were used as a first characterization to support formation of the nanoparticles.

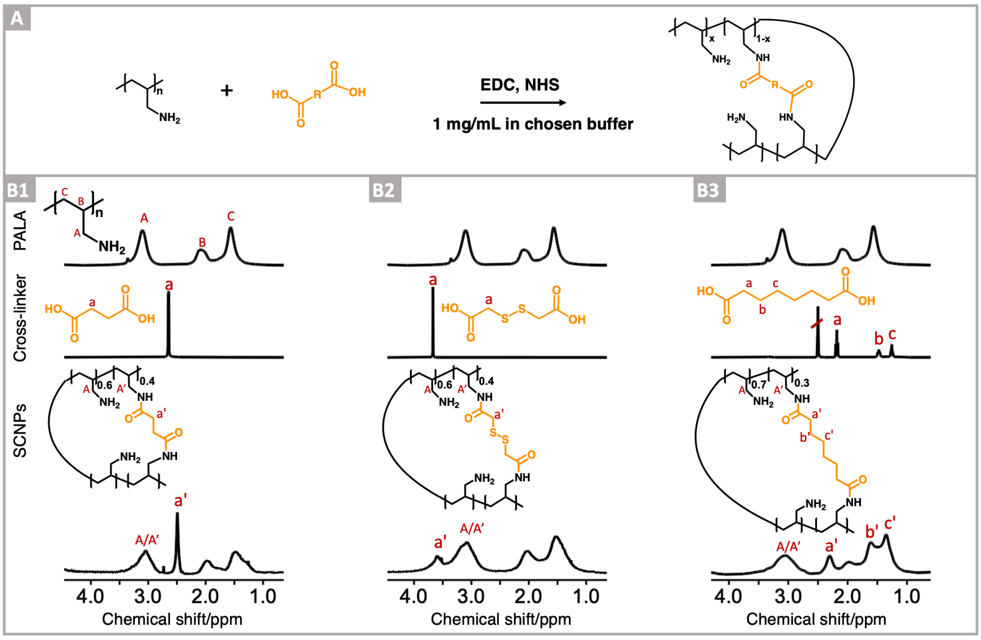

Figure 4.1 PALA SCNPs crosslinked with dicarboxylic acids.

A) The general amidation scheme for cross-linking poly(allylamine) chains with dicarboxylic acids under a certain solvent condition; B) ^{1}H-NMR spectra of SCNPs formation via dicarboxylic acids of three different lengths. The cross-linkers are, in B1) R= $-CH_2CH_2-$, succinic acids; in B2) R= $-CH_2SSCH_2-$, dithiodiglycolic acids; in B3) R= $-CH_2CH_2CH_2CH_2CH_2CH_2-$, suberic acids.

The intramolecular cross-linking of linear polymer chains leads to size reduction. The more the size reduction the more the SCNPs' topology deviates from a chain. We performed DOSY NMR and viscometry for size characterization from

SCNPs' Brownian diffusion and their intrinsic viscosity/overlapping concentration, respectively. The PALA precursor (linear topology) and a PAMAM dendrimer of generation 5.0 (molecular weight=28824.81 g/mol, comparable to SCNPs; ideal sphere) were measured as reference materials.

Throughout all DOSY measurements, the diffusion time Δ (300 ms) and the gradient pulse duration δ (5 ms) were fixed. For each sample, the regression analysis of Stejskal Tanner equation was performed on the three types of protons (denoted as A, B, and C in Figure 4.1B1) from the original PALA backbone. Results are reported as mean ± SD (standard deviation) from measurements on two independent samples in Figure 4.2. For each cross-linking scheme (solvent condition and crosslinker), the data shown are for two independent reactions, each batch has a separate data point in the figure to illustrate the reproducibility of the data. Higher self-diffusion coefficients indicate faster Brownian motion, that results from smaller size, in our case this means more compact topology.

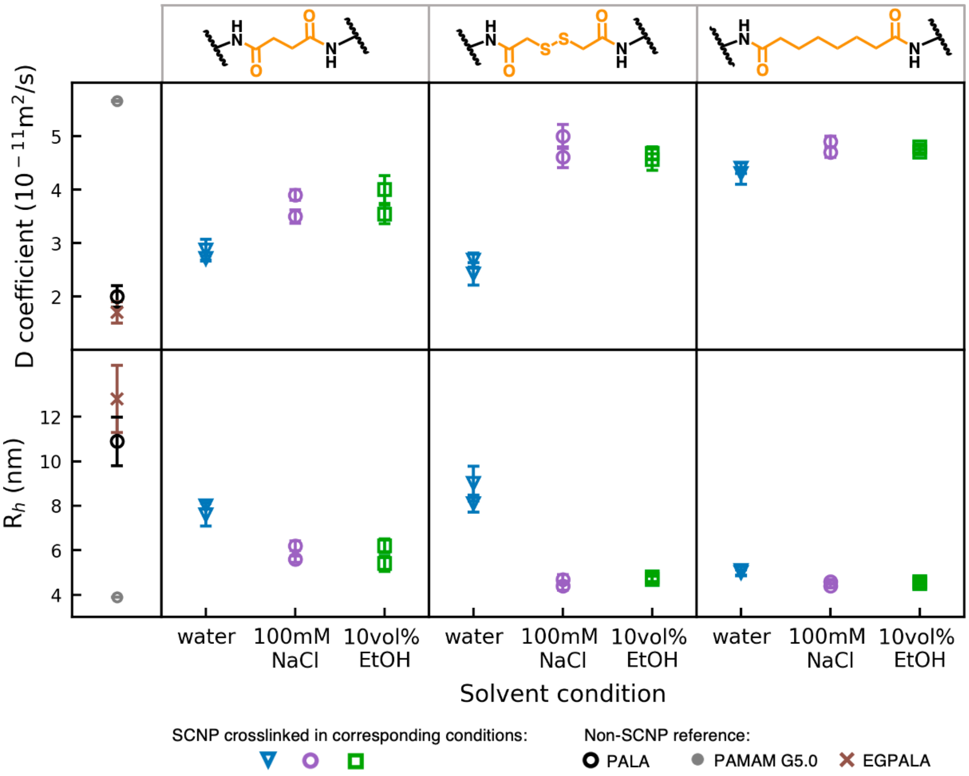

Figure 4.2 Plots of diffusion coefficients (panels in the upper row) determined from DOSY-NMR.

Measurements were done for all nine SCNPs studies and the reference materials. Each SCNPs synthesis was duplicated to test reproducibility and each datapoint represents an independent batch. Panels in the lower row present the hydrodynamic radius converted from the corresponding diffusion coefficients with the Stokes-Einstein equation for more intuitive interpretation of size. Analyzing results are reported as mean ± SD.

Topology can also be assessed by the reduction of gyration radius, that can be probed with viscosity measurement. The empirical Huggins Equation (see SI) shows that the slope of the specific viscosity vs polymer concentration (in dilute condition) is related to the radius of gyration. The larger the slope in the plot the larger the gyration radius, and in our case the lower the compactness. For each sample/reference, the viscosity-concentration dependency was measured with an Anton-Paar Lovis module through a rolling-ball mechanism to yield Figure 4.3.

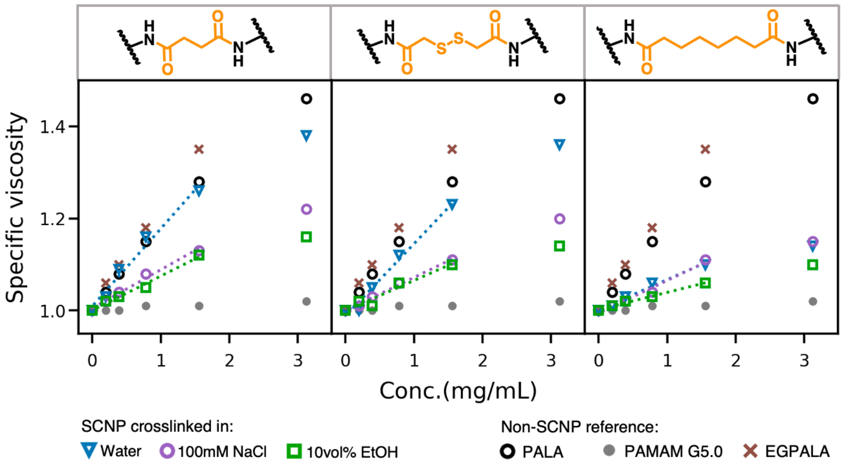

Figure 4.3 Viscosity-concentration plots for SCNP solutions.

Linear fitting in the diluted regime reveals the intrinsic viscosity; the dashed lines show the fitting results. In each panel, the PALA and PAMAM G5.0 data series are presented as conformational references (totally linear and ideally spherical, respectively).

We used SV-AUC because of its unmatched ability to characterize sedimentation coefficient (related to size) and frictional ratio (related to shape) of particles at the same time.[44–46] SV-AUC is a hydrodynamic tool to separate particles in solution by their sedimentation behavior under a strong centrifugal field. The sedimentation process introduces a concentration gradient that in turn induces a diffusion flux. In a typical SV-AUC experiment, concentration profiles are recorded as a spatiotemporal dataset *c(r, t)* with respect to time *t* and to distance to the rotational center *r*; by fitting with Lamm equation, the concentration profile *c(r, t)* can be transformed into a function of *s* (sedimentation coefficient) and *D* (diffusion coefficient). Next, by constraining one parameter out of *Mw*, f/f_0 (frictional ratio) or $\bar{v}$ (partial specific volume), the other two can be determined by the measurements, as they are restricted by Svedberg equation (SI). The frictional ratio f/f_0 is related to the anisotropy of the analyte with an ideal sphere having a frictional ratio of 1 and a larger frictional ratio indicating higher anisotropy. Each spatiotemporal dataset *c(r, t)* was analyzed with the continuous *c(s, ff0)* model in the SEDFIT[47,48] software developed by Schuck et al.[49,50] Data analysis is discussed in detail in SI. The results are shown as contours plots in Figure 4.4. We should point out an important result in the AUC characterization of our SCNPs. In SCNPs it is often important to determine whether all (or at least most) particles in the samples are indeed single-chain. AUC allows very precise determination of *Mw* distribution. The data shown Figure 4.4 are all narrow single three-dimensional peaks, which means that the analytes all have very narrow *Mw* distribution. Hence, we can conclude that the particles are all made of the same number of polymer chains, and the analysis of the sedimentation coefficient then indicates that such number has to be 1. If our samples were to contain particles made of multiple polymer chains (in a single particle or as aggregates of multiple particles) such particles could be present only below the (very low) AUC detection limit. As a reference, in SI we show how the AUC of particles containing multiple chains of polymer looks like.

In Figure 4.4. we show contour plots derived from the AUC analysis of our nine SCNPs with sedimentation coefficient on the x-axis and frictional ratio on the y-axis. Sedimentation coefficients depend on size, density, shape and molecular weight, as a consequence we did not use them for deep interpretation of the data. The frictional ratio depends on shape. We notice that all particles that we assume to be compact have frictional ratios very close to 1, indicating that they have the expected topology. The other depart significantly from 1 indicating more anisotropic geometry and sparse topology.

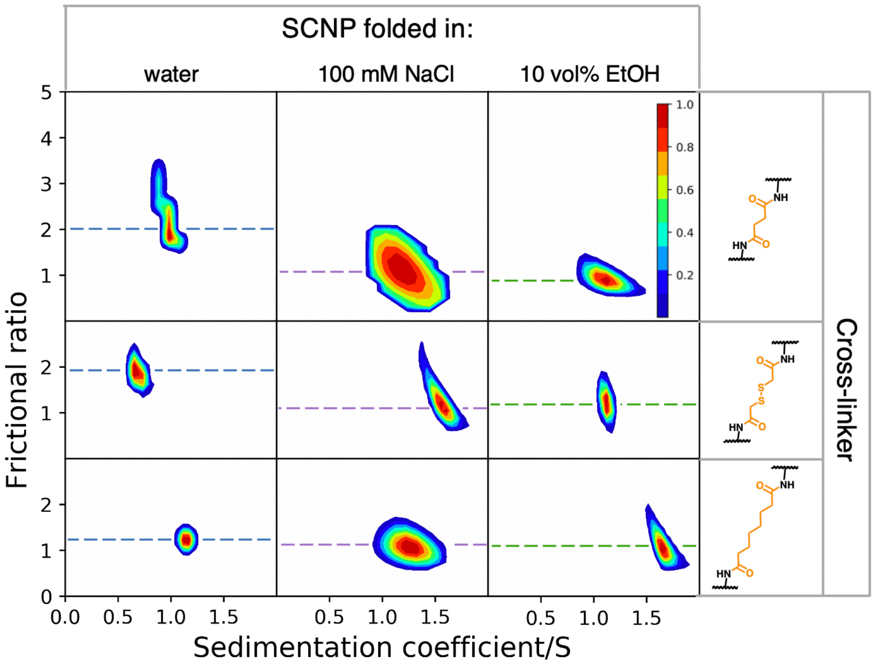

Figure 4.4 Contour plots of sedimentation coefficients vs frictional ratio for SCNPs. The contour plot in each panel represents one batch of SCNPs synthesized under the conditions indicated. Loading concentrations were fixed for all measurements. Peak normalization was performed for comparison. Dashed lines mark the average values of f/f_0 to guide the eyes. The color scheme is consistent with other figures.

As mentioned earlier, unlike rigid inorganic nanoparticles, polymeric NPs can deform. This likely gives place to an interplay between local and global compaction, and to variable degrees of rigidity/flexibility across the polymer. To probe this idea, we conducted ^1H T_2 relaxation NMR experiments at 500 MHz.[51] Transverse relaxation is a complex phenomenon modulated by global tumbling and internal dynamics, widely exploited as a cue for dynamics in polymers.[52,53]

In Figure 4.5 we compare the T_2 values of the CH_2 protons alpha to the amine/amide, whose signals are well resolved in all spectra, across PALA, EGPALA and the nine SCNPs. Precursor PALA and the two least compact SCNPs (#1 and #4 in Table 1, crosslinked in water with succinic acid and dithiodiglicolic acid, respectively) display T_2 values from 25 to 30 ms for this CH_2. Under the same concentration and with similar overall size, the other SCNPs, more compact according to our earlier characterization, show faster T_2 decays reaching T_2 values in the range from 14 to 20 ms. This reveals different dynamics for the tested CH_2 protons across the polymers, indicating that the conditions under which collapse was induced affect the tumbling and motions inside the resulting SCNPs. In the works of Pinto et al.[52,53] it was shown that the T_2s of ^1H nuclei in a dendrimer polymer increase with the distance from the core, where the CH_2 protons have higher flexibility due to being in less compact regions. Consistently, we infer that across our SCNPs the CH_2 group is more flexible in the least compact SCNPs, or equivalently that these protons experience a more rigid environment in the more compact SCNPs.

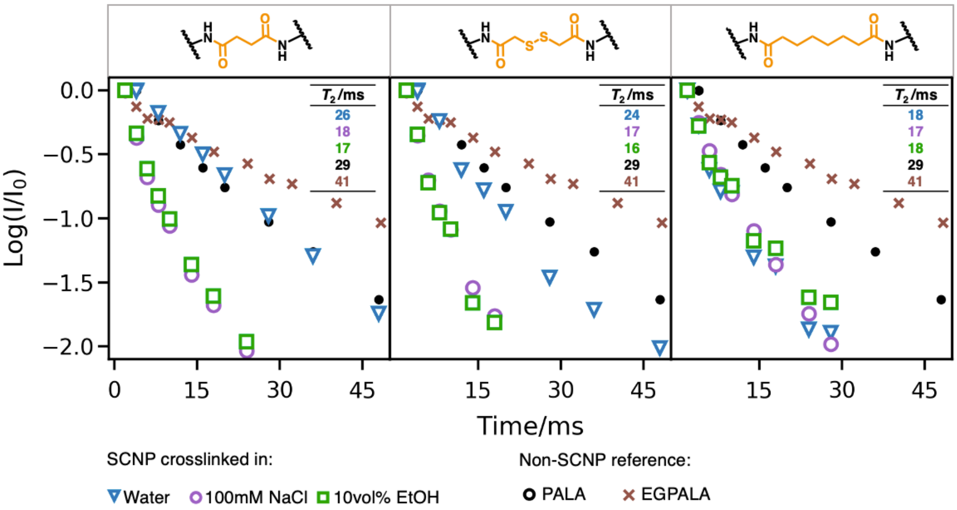

Figure 4.5 NMR relaxation of PALA SCNPs.

Signal decays in T_2 relaxation experiments for the CH_2 protons in position alpha to the amine/amide of the precursor PALA, EGPALA and SCNPs.

We decided to investigate a structure-property relationship to better evidence the importance of the characterizations that we performed. As an example, we chose cytotoxicity. Cationic polymers form a large group of drug carrier for intracellular delivery.[54–56] It is known that cationic nature boosts the cellular uptake but also causes cytotoxicity.[57,58] Previous structure-property investigations have covered various physicochemical characteristics that lead to such cytotoxicity.[57–61] We studied the cytotoxicity of our SCNPs' on HeLa cells by measuring their viability with MTS assay. MTS assay is a colorimetric assay based on the cellular metabolic reduction of a yellow tetrazolium salt to purple formazan products. For each SCNP, a wide concentration range was covered to complete the sigmoidal curve to determine the IC_{50} values, as shown in Figure 4.6. We find that the two less compact SCNPs lead to lower IC_{50} when compared to the compact ones. We can state that there is a correlation between compactness and cytotoxicity.

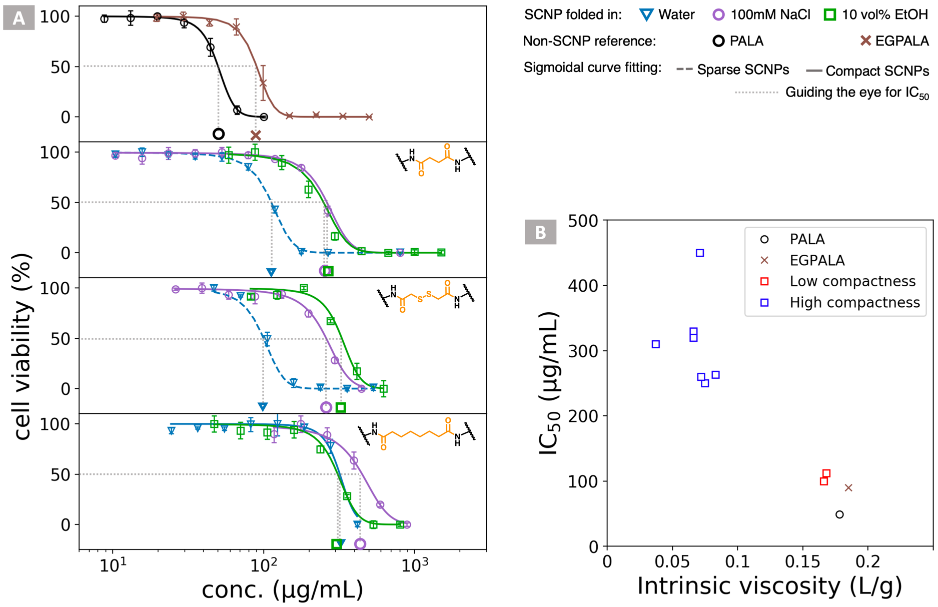

Figure 4.6 Topology-cytotoxicity relationship.

A) HeLa cell viability via MTS assay upon 24-hour incubation with SCNPs. Each data point represents three independent experiments and reported as mean ± SD. B) The scatter plot to elucidate the correlation between cytotoxicity (IC_{50}) and compactness (the intrinsic viscosity is chosen as the representative parameter)

4.4 SUMMARY

To conclude, our work provides as a platform to examine how the initial chain conformation and the length of the cross-linking molecules affect the final topology of SCNPs. The use of several characterization techniques has allowed us to conclude that polymer chains that are pre-collapsed and/or longer cross-linkers lead to more compact nanoparticles. We found that if starting from an open conformation, shorter cross-linkers could not efficiently connect contour-distant functional groups, thus generating sparse and flexible SCNPs; whereas a pre-collapsed chain presents functional groups in a more confined space and allows global compaction even via short cross-linkers. When relatively long cross-linkers are applied, however the initial chain conformation, high compactness can be achieved. We have also found that compactness can be correlated to cytotoxicity for PALA SCNPs. Polycationic SCNPs of higher compactness present lower cytotoxicity. Considering that SCNPs of various compactness do not necessarily differ in size, we believe that it's the structural flexibility that allows the sparse SCNPs to bind better with the negative cellular membrane. In turn, due to the higher conformational entropy penalty upon binding with less compact cationic PALA SCNPs, the cellular membrane is more prone to lose its structural integrity, thus leading to higher cytotoxicity. The understanding of SCNP compactness could improve their use and efficacy as drug carriers.

Table 1. Summary of characterization results

SCNPs			DOSY	Viscometry	Relaxation	SV-AUC			MTS
#	-R-[i]	Solvent	D[ii]	$[\eta]$[iii] /L·g^{-1}	T_2/ms	S[iv]	D[v]	f/f_0	IC$_{50}$/μg·mL^{-1}
1	$-CH_2CH_2-$	water	3.0	0.168	26	0.8	4.5	2.3	112
2		100 mM NaCl	4.0	0.083	17	1.2	16	1.1	263
3		10 vol% EtOH	4.0	0.075	18	1.4	25	1.2	250
4	$-(CH_2S)_2-$	water	2.8	0.166	24	0.7	6.0	2.2	100
5		100 mM NaCl	5.0	0.072	16	1.6	17	1.2	260
6		10 vol% EtOH	4.8	0.066	17	1.1	17	1.3	330
7	$-(CH_2CH_2)_3-$	water	4.5	0.066	18	1.2	10	1.2	320
8		100 mM NaCl	4.9	0.071	18	1.3	30	1.0	450
9		10 vol% EtOH	4.9	0.037	17	1.6	15	1.1	310
EGPALA			1.7	0.185	41	N.A.[vi]			90
PALA			2.0	0.178	29	N.A.			49

[i] Spacer group as shown in Scheme 4.1

[ii] Self-diffusion coefficient with unit of 1×10^{-11} m^2·s^{-1}

[iii] Intrinsic viscosity

[iv] Sedimentation coefficient with unit of Svedberg, 1 Svedberg = 1×10^{-13} s

[v] Mutual-diffusion coefficient with unit of 1×10^{-11} m^2·s^{-1}

[vi] Not Applicable

4.5 SUPPLMENTARY INFORMATION

4.5.1 Synthesis and purification

Chemical Information

PALA (Polyallylamine hydrochloride, CAS 71550-12-4), succinic acid (CAS 110-15-6), dithiodiglycolic acid (CAS 505-73-7), suberic acid (CAS 505-48-6), EDC (CAS 22572-40-3), and NHS (6066-82-6) were purchased from Sigma-Aldrich and used without further purification.

Cross-linking reaction

150 mg parent polymer PALA was dispersed into 150ml chosen reaction conditions as discussed in the paper to form dilute precursor solution. To crosslink 50% of the primary amines, around 96mg succinic acids (2 molar excess to 50% of the amines) were dissolved into 10 ml corresponding buffer, followed with the addition of EDC and NHS (both at 1.5 molar excess to carboxylic groups) for activation and stabilization. The activated crosslinker solution was then transferred into an additional funnel. While stirring the precursor solution in a 250 ml round bottom flask, the crosslinker solution was added dropwise at ~1 drop/s. The reaction was kept at room temperature overnight.

Pre-collapsing of PALA

To show the solvent-induced compaction of PALA, DLS was performed in the corresponding solvent conditions. Figure S1 shows size distribution by volume (with viscosity correction).

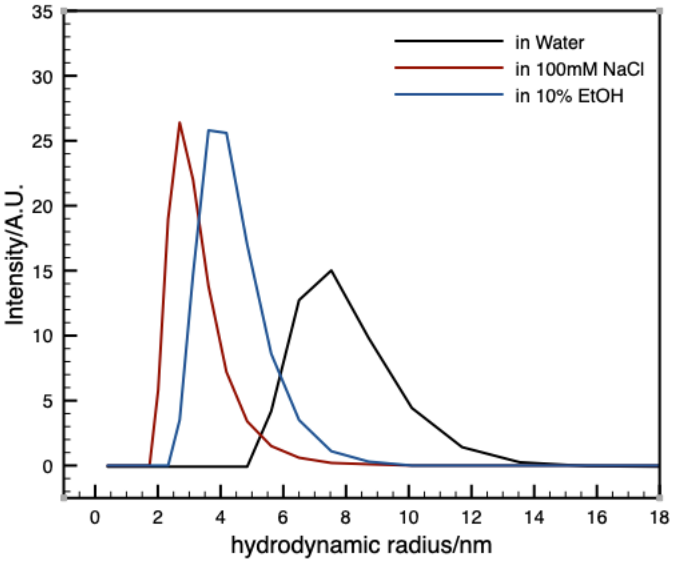

Figure S 4.1 DLS size distribution (by volume) of PALA in different solvent conditions.

Purification

Ultrafiltration was performed on the reaction mixture with Amicon® Ultra-15 filter (Mw cutoff: 3,000 Da) to concentrate the final product, which was later washed with ultrapure water for multiple rounds to desalt. The concentrated sample underwent extensive dialysis in ultrapure water before the final concentrating step. Finally, the sample was freeze dried into dry powder.

EG-PALA

The structure-cytotoxicity relationship was also evidence by conjugating the PALA chain with 2-[2-(2-Methoxyethoxy)ethoxy]acetic acid via amidation, to yield a similar ratio of free primary amine groups. The proton NMR is shown in Figure S4.2. The final product is referred as EG-PALA. It shows similar zeta-potential profile to the SCNPs in the work. (Figure S4.2)

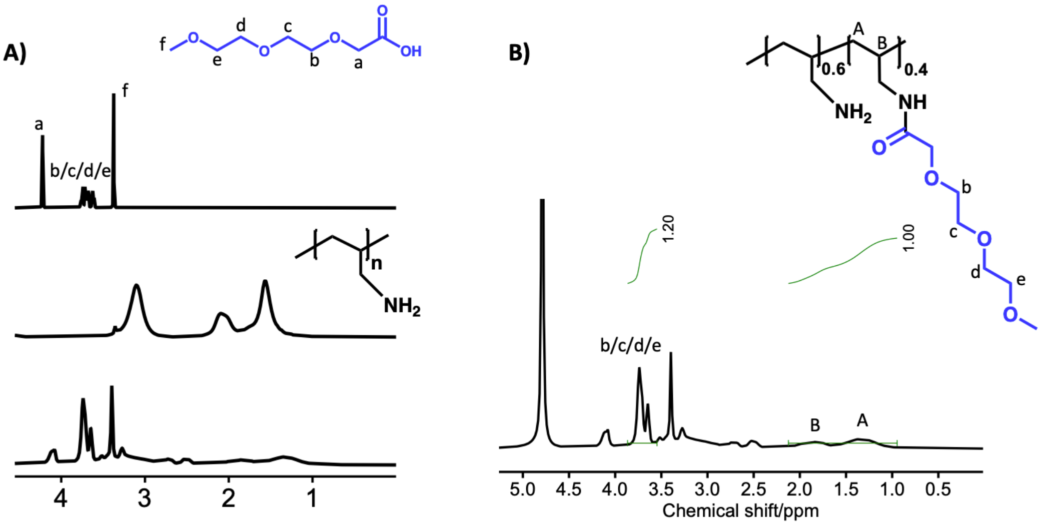

Figure S4.2 A) proton NMR of (from top to bottom) 2-[2-(2-Methoxyethoxy)ethoxy]acetic acid; PALA; EG-PALA; B) Ligand conjugation ratio is quantified to be 40%, comparable to the cross-linking ratio of the SCNPs in this work

4.5.2 Analytical methods

^{1}H NMR and cross-linking density

^{1}H NMR spectra were obtained using excitation sculpting centered on the water resonance in spectral widths of around 14 ppm wit 16k points. Resonance assignments were straightforward from chemical shifts of the ^{1}H resonances. The cross-linking density was quantified as the ratio of the amide (quantified by the signal from the cross-linker protons) to the initial primary amines (quantified by the signal from the backbone protons).

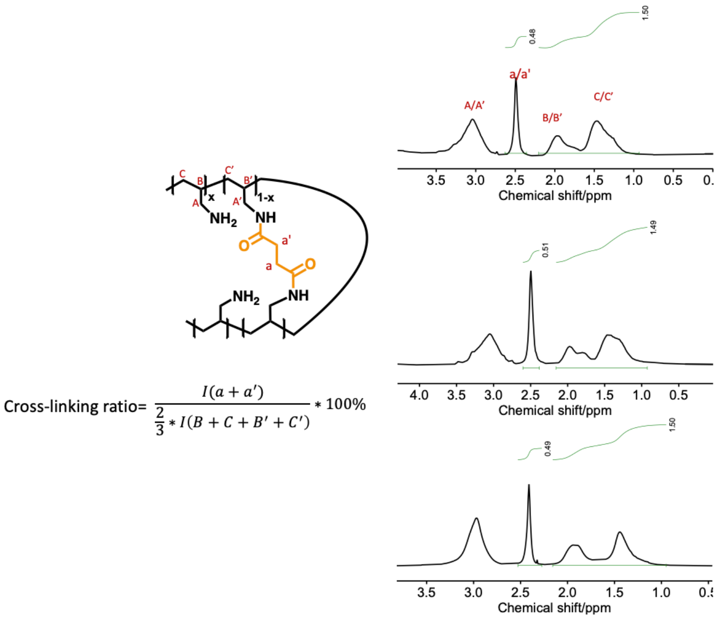

$$\text{Cross-linking ratio}=\frac{I(a+a')}{\frac{2}{3}*I(B+C+B'+C')}*100\%$$

Figure S 4.3 ^{1}H NMR of succinic acid cross-linked SCNPs

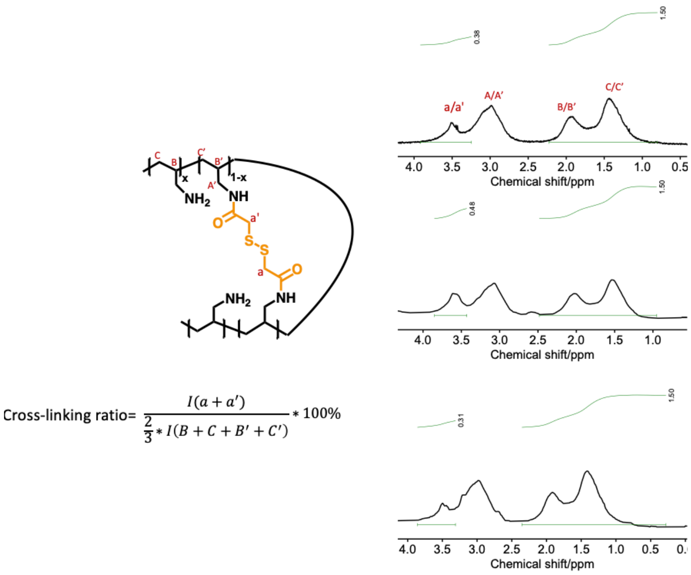

$$\text{Cross-linking ratio}=\frac{I(a+a')}{\frac{2}{3}*I(B+C+B'+C')}*100\%$$

Figure S 4.4 ^{1}H NMR of dithiodiglycolic acid cross-linked SCNPs

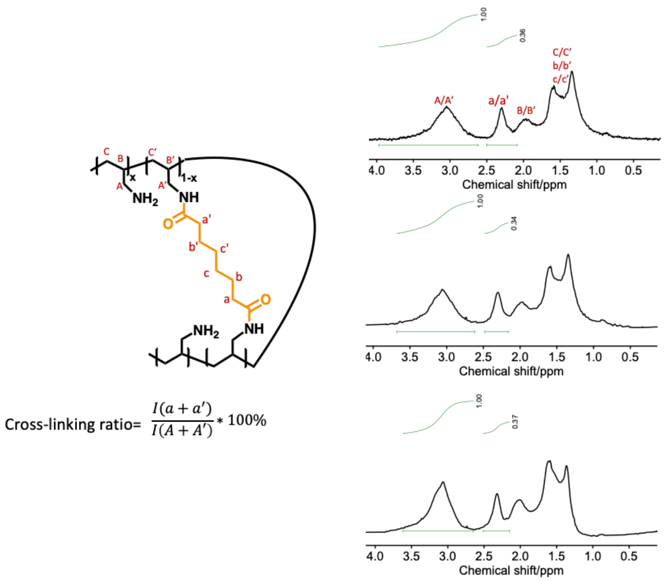

Figure S 4.5 ^{1}H NMR of suberic acid cross-linked SCNPs

DOSY NMR

DOSY NMR is a chromatographic tool to differentiate species by both diffusion and chemical shift. First, a magnetic field gradient is applied to spatially label the spins; then during the spin echo, the spins refocus to various degree depending on the rate of Brownian motion, thus generating a signal decay; the signal decay is fitted with the Stejskal Tanner equation to obtain the diffusion coefficient. The DOSY NMR experiments were conducted at 25 °C on an autosampler Bruker Avance I Neo (^{1}H: 400 MHz) with 5mm Smart BBFO-Plusz ATMA probe. All spectra were acquired using the Bruker pulse program ledbpgp2s with a diffusion gradient of 300 ms, a diffusion time of 5000 µs and a squared gradient ramp from 2 to 98%.

Basic data processing such as baseline correction, phase correction and peak integration were performed with MestReNova (version 14.1.2). Data Fitting of the DOSY signal decay was achieved with python scripting.

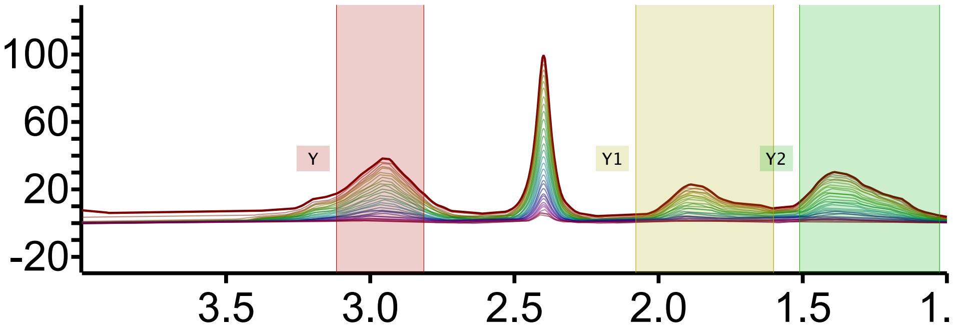

Figure S 4.6 Signal integration example (processed in Mestrenova)

For a better visualization of such exponential decay, the natural logarithms of normalized signal intensities were plotted against q^2 (the description of q can be found under the equation) so that the slope directly indicates the rate of diffusion. Figure S 4.6 shows the representative signal decay (proton A/A' as denoted in Figure 4.1) from each SCNP batch.

$$\frac{I(q)}{I_0} = \exp[-Dq^2(\Delta - \delta/3)] \qquad (S1)$$

q = γ gδ

γ: proton gyromagnetic ratio

g : gradient amplitude

δ: gradient pulse duration

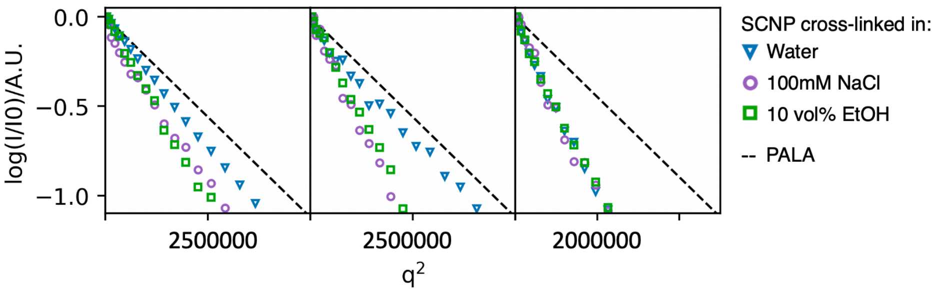

Figure S 4.7 Scatter plots showing DOSY signal decay. (cross-linkers are succnic acids, dithiodiglycolic acids, and suberic acids, respectively in the panels from left to right)

Viscometry

The specific viscosities (the ratio of the absolute viscosity to that of the reference fluid, herein, water) were plotted against solution concentration and the slope measures the SCNPs' contribution to the overall viscosity. The intrinsic viscosity was obtained by fitting each viscosity-concentration series with Huggins equation.

To study the viscosity's dependence on the concentration of polymeric analytes, PALA/SCNPs/PAMAM G5 dendrimers were dissolved into ultrapure water. With a two-fold serial dilution, sample solutions with concentrations of 3.125, 1.56, 0.78, 0.39, 0.2 mg/ml were prepared for measurement.

Viscosity measurements were conducted on an Anton Paar Lovis 2000 rolling-ball viscometer at 20°C. The apparent viscosity η were corrected with the viscosity of water η_0 to be listed as relative viscosity as listed below.

Table S2. Relative viscosity η/η_0

			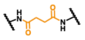			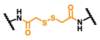			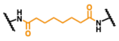		
conc (mg/ml)	PALA	PAMAM G5	▼	○	□	▼	○	□	▼	○	□
3.125	1.46	1.02	1.38	1.22	1.16	1.36	1.20	1.14	1.14	1.15	1.10
1.56	1.28	1.01	1.26	1.13	1.12	1.23	1.11	1.10	1.1	1.11	1.06
0.78	1.15	1.01	1.16	1.08	1.05	1.12	1.06	1.06	1.06	1.04	1.03
0.39	1.08	1.00	1.09	1.04	1.03	1.05	1.03	1.01	1.03	1.02	1.02
0.2	1.04	1.00	1.03	1.02	1.02	1.00	1.01	1.02	1.01	1.01	1.01
0	1.00	1.00	1.00	1.00	1.00	1.00	1.00	1.00	1.00	1.00	1.00

The dependence of relative viscosity on concentration can be described in the form of power series with high-order terms being negligible, due to the dilute nature of our sample solution. ($[\eta]$: intrinsic viscosity; k_h: Huggins coefficient)

Equation S1. Relative viscosity – concentration relationship

$$\frac{\eta}{\eta_0} = 1 + [\eta]c + k_h[\eta]^2c^2$$

SV-AUC

AUC was performed using a Beckman Optima XL-A, An-60 Ti rotor. All SCNP solutions were prepared freshly in ultrapure water to obtain final solutions that had 0.5~1.0 OD (optical density) absorbance at 230 nm in AUC cells (double sector titanium centerpieces with quartz windows; the optical path length is 1.2 cm). All measurements were made at 20 °C, 60,000 r.p.m. (with radial step size of 0.003 cm) with sufficient duration to ensure complete sedimentation. Pilot runs at varying concentrations were performed to ensure that the sedimentation and diffusion coefficients were not concentration dependent. Data ranges from 50-100 scans were chosen to represent the whole transporting process.

$$\frac{\partial c}{\partial t} = D\left(\frac{\partial^2 c}{\partial r^2} + \frac{1}{r}\frac{\partial c}{\partial r}\right) - \omega^2 s(r\frac{\partial c}{\partial r} + 2c)$$

$$M = \frac{RTs}{(1 - \bar{v}\rho)D}$$

As the cross-linking densities were fixed within a comparable range for all nine SCNPs, we made the assumption that the final SCNP share the same molecular mass of 30 ± 3 kDa. With the assumption, various values of partial specific volume were tested until the main peak obtained the assumed MW of 30 kDa. Then all the fitting parameters were transferred into the 2D model, c(s, ff_0), to resolve the frictional ratio.

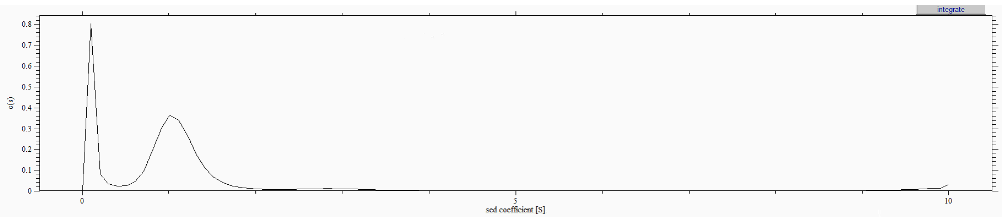

Figure S 4.8 1D distribution of c(s)

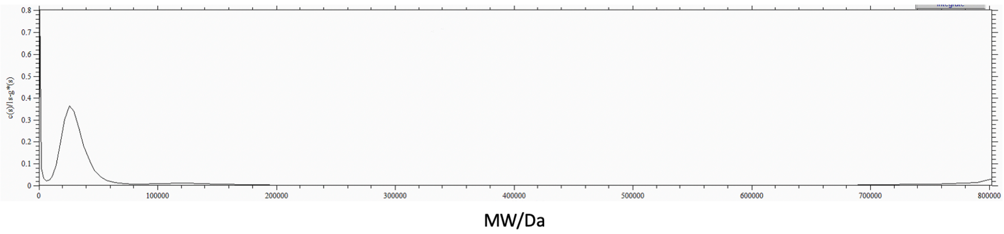

Figure S 4.9 1D distribution of c(M)

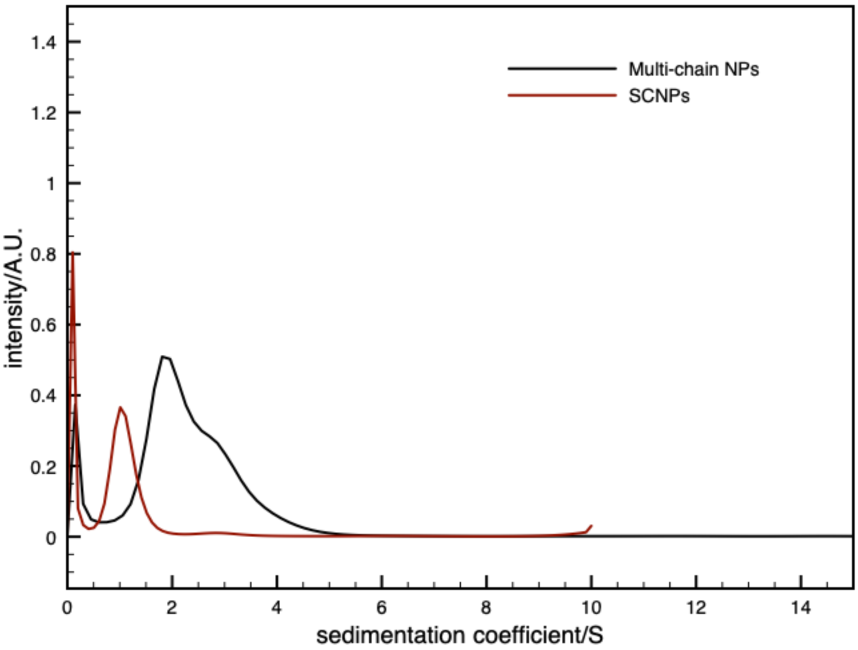

Figure S 4.10 Distribution of sedimentation coefficient on SCNPs and multi-chain NPs (cross-linked above the critical concentration)

NMR T_2 relaxation

Samples for NMR spectroscopy were prepared at 2 g/L concentrations dissolved from powders with 500 µL of 100% D_2O. All experiments were carried out in a Bruker 500 MHz spectrometer equipped with a 5 mm ^{1}H,^{13}C,^{15}N BBI probe and an Avance Neo console. All NMR data was acquired and processed with Topspin 4 and analyzed with MestreNova 14.1.2.

^{1}H T_2 relaxation was measured using a spin echo sequence that removes J modulation[51] using CPMG delays (in s) of 0.0020155, 0.004031, 1.03194, 0.0060465, 0.008062, 0.0100775, 0.0141085, 0.0181395, 0.024186, 0.028217, 0.032248, 0.04031, 0.048372, 0.056434, 0.064496, 0.072558, 0.08062, 0.088682, 0.096744, 0.104806, 0.112868, 0.12093, 0.128992, 0.193488, 0.257984, 0.386976, 0.515968, 0.773952, 1.03194, 0.0020155, 2.06387

SEC

SEC analysis was performed using an Agilent PL-GPC 50 equipped with a refractive index detector. The mobile phase was acetate buffer at a flow of 1.0 mL/min at 40 °C. Samples were filtered prior to analysis and results were calibrated with PEG standards.

Zeta-potential

The charge density from cationic moieties plays a key role in determining the cytotoxicity. With comparable cross-linking densities, all SCNPs show similar zeta-potential values.

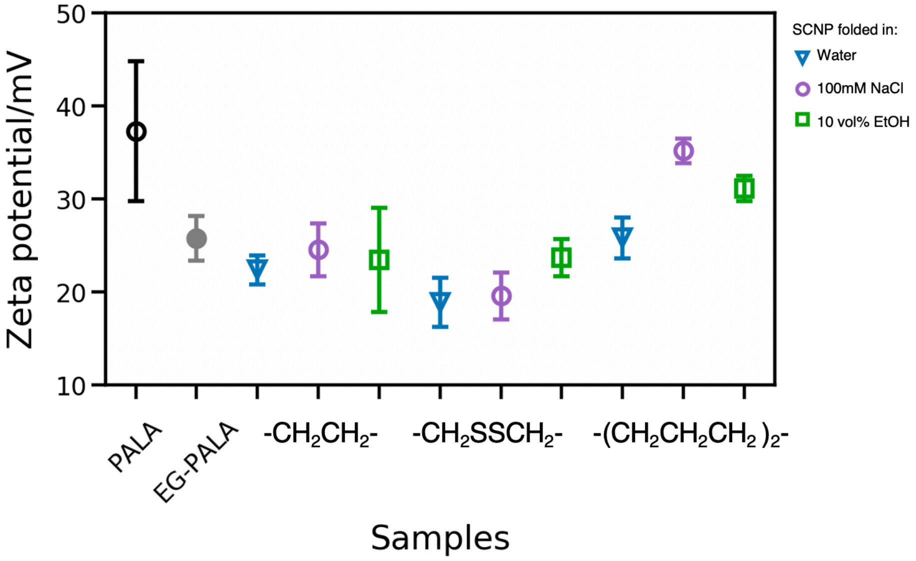

Figure S 4.11 Scatter plot with all SCNPs and reference materials' zeta potential results (plotted as mean ± SD)

4.5.3 MTS assay

Cell cytotoxicity in this work was performed on Hela cell line with MTS assay. Hela cells were plated 12 hours before with seeding density 1.5×10^4 in 200 μL DMEM medium supplemented with 10% fetal bovine serum (FBS) and 1% Penicillin Streptomycin in 96-well plates. Samples were added in fixed volume 20 μL with different concentrations into each well and incubated together with cells for 24 hours at 37°C in 5% CO_2 environment. Afterwards, materials containing cell medium was removed and cells were washed with 1x phosphate-buffered saline (PBS) twice. Then 10 μL MTS tetrazolium compound was added together with 90 μL original DMEM medium (without FBS or Pen strep supplement) into each well and followed with incubation (37°C and 5% CO_2) for 4 hours. Measurement of cell proliferation was checked via absorbance at 490 nm with a Tecan Plate Reader.

4.6 REFERENCE

(1) Kuhn, W.; Balmer, G. Crosslinking of Single Linear Macromolecules. *Journal of Polymer Science* **1962**, *57* (165), 311–319. https://doi.org/10.1002/pol.1962.1205716524.

(2) Harth, E.; Horn, B. V.; Lee, V. Y.; Germack, D. S.; Gonzales, C. P.; Miller, R. D.; Hawker, C. J. A Facile Approach to Architecturally Defined Nanoparticles via Intramolecular Chain Collapse. *J. Am. Chem. Soc.* **2002**, *124* (29), 8653–8660. https://doi.org/10.1021/ja026208x.

(3) Wang, J.; Wang, R.; Gu, Y.; Sourakov, A.; Olsen, B. D.; Johnson, J. A. Counting Loops in Sidechain-Crosslinked Polymers from Elastic Solids to Single-Chain Nanoparticles. *Chem. Sci.* **2019**, *10* (20), 5332–5337. https://doi.org/10.1039/C9SC01297D.

(4) Gu, Y.; Zhao, J.; Johnson, J. A. A (Macro)Molecular-Level Understanding of Polymer Network Topology. *TRECHEM* **2019**, *1* (3), 318–334. https://doi.org/10.1016/j.trechm.2019.02.017.

(5) Pomposo, J. A.; Perez-Baena, I.; Lo Verso, F.; Moreno, A. J.; Arbe, A.; Colmenero, J. How Far Are Single-Chain Polymer Nanoparticles in Solution from the Globular State? *ACS Macro Lett.* **2014**, *3* (8), 767–772. https://doi.org/10.1021/mz500354q.

(6) Sanchez-Sanchez, A.; Akbari, S.; Etxeberria, A.; Arbe, A.; Gasser, U.; Moreno, A. J.; Colmenero, J.; Pomposo, J. A. "Michael" Nanocarriers Mimicking Transient-Binding Disordered Proteins. *ACS Macro Lett.* **2013**, *2* (6), 491–495. https://doi.org/10.1021/mz400173c.

(7) Moreno, A. J.; Lo Verso, F.; Sanchez-Sanchez, A.; Arbe, A.; Colmenero, J.; Pomposo, J. A. Advantages of Orthogonal Folding of Single Polymer Chains to Soft Nanoparticles. *Macromolecules* **2013**, *46* (24), 9748–9759. https://doi.org/10.1021/ma4021399.

(8) Verso, F. L.; A. Pomposo, J.; Colmenero, J.; J. Moreno, A. Multi-Orthogonal Folding of Single Polymer Chains into Soft Nanoparticles. *Soft Matter* **2014**, *10* (27), 4813–4821. https://doi.org/10.1039/C4SM00459K.

(9) Chao, D.; Jia, X.; Tuten, B.; Wang, C.; Berda, E. B. Controlled Folding of a Novel Electroactive Polyolefin via Multiple Sequential Orthogonal Intra-Chain Interactions. *Chem. Commun.* **2013**, *49* (39), 4178–4180. https://doi.org/10.1039/C2CC37157J.

(10) Perez-Baena, I.; Asenjo-Sanz, I.; Arbe, A.; Moreno, A. J.; Lo Verso, F.; Colmenero, J.; Pomposo, J. A. Efficient Route to Compact Single-Chain Nanoparticles: Photoactivated Synthesis via Thiol–Yne Coupling Reaction. *Macromolecules* **2014**, *47* (23), 8270–8280. https://doi.org/10.1021/ma5017133.

(11) Morishima, Y.; Nomura, S.; Ikeda, T.; Seki, M.; Kamachi, M. Characterization of Unimolecular Micelles of Random Copolymers of Sodium 2-(Acrylamido)-2-Methylpropanesulfonate and Methacrylamides Bearing Bulky Hydrophobic Substituents. *Macromolecules* **1995**, *28* (8), 2874–2881. https://doi.org/10.1021/ma00112a037.

(12) Terashima, T.; Sugita, T.; Sawamoto, M. Single-Chain Crosslinked Star Polymers via Intramolecular Crosslinking of Self-Folding Amphiphilic Copolymers in Water. *Polym J* **2015**, *47* (10), 667–677. https://doi.org/10.1038/pj.2015.54.

(13) Altintas, O.; Lejeune, E.; Gerstel, P.; Barner-Kowollik, C. Bioinspired Dual Self-Folding of Single Polymer Chains via Reversible Hydrogen Bonding. *Polym. Chem.* **2012**, *3* (3), 640–651. https://doi.org/10.1039/C1PY00392E.

(14) Mes, T.; van der Weegen, R.; Palmans, A. R. A.; Meijer, E. W. Single-Chain Polymeric Nanoparticles by Stepwise Folding. *Angewandte Chemie International Edition* **2011**, *50* (22), 5085–5089. https://doi.org/10.1002/anie.201100104.

(15) ter Huurne, G. M.; de Windt, L. N. J.; Liu, Y.; Meijer, E. W.; Voets, I. K.; Palmans, A. R. A. Improving the Folding of Supramolecular Copolymers by Controlling the Assembly Pathway Complexity. *Macromolecules* **2017**, *50* (21), 8562–8569. https://doi.org/10.1021/acs.macromol.7b01769.

(16) ter Huurne, G. M.; Voets, I. K.; Palmans, A. R. A.; Meijer, E. W. Effect of Intra- versus Intermolecular Cross-Linking on the Supramolecular Folding of a Polymer Chain. *Macromolecules* **2018**, *51* (21), 8853–8861. https://doi.org/10.1021/acs.macromol.8b01623.

(17) Rubio-Cervilla, J.; Frisch, H.; Barner-Kowollik, C.; Pomposo, J. A. Synthesis of Single-Ring Nanoparticles Mimicking Natural Cyclotides by a Stepwise Folding-Activation-Collapse Process. *Macromolecular Rapid Communications* **2019**, *40* (1), 1800491. https://doi.org/10.1002/marc.201800491.

(18) Formanek, M.; Moreno, A. J. Effects of Precursor Topology and Synthesis under Crowding Conditions on the Structure of Single-Chain Polymer Nanoparticles. *Soft Matter* **2017**, *13* (37), 6430–6438. https://doi.org/10.1039/C7SM01547J.

(19) Oberdisse, J.; González-Burgos, M.; Mendia, A.; Arbe, A.; Moreno, A. J.; Pomposo, J. A.; Radulescu, A.; Colmenero, J. Effect of Molecular Crowding on Conformation and Interactions of Single-Chain Nanoparticles. *Macromolecules* **2019**, *52* (11), 4295–4305. https://doi.org/10.1021/acs.macromol.9b00506.

(20) Verde-Sesto, E.; Arbe, A.; Moreno, A. J.; Cangialosi, D.; Alegría, A.; Colmenero, J.; Pomposo, J. A. Single-Chain Nanoparticles: Opportunities Provided by Internal and External Confinement. *Mater. Horiz.* **2020**, *7* (9), 2292–2313. https://doi.org/10.1039/D0MH00846J.

(21) González-Burgos, M.; Arbe, A.; Moreno, A. J.; Pomposo, J. A.; Radulescu, A.; Colmenero, J. Crowding the Environment of Single-Chain Nanoparticles: A Combined Study by SANS and Simulations. *Macromolecules* **2018**, *51* (4), 1573–1585. https://doi.org/10.1021/acs.macromol.7b02438.

(22) Moreno, A. J.; Lo Verso, F.; Arbe, A.; Pomposo, J. A.; Colmenero, J. Concentrated Solutions of Single-Chain Nanoparticles: A Simple Model for Intrinsically Disordered Proteins under Crowding Conditions. *J. Phys. Chem. Lett.* **2016**, *7* (5), 838–844. https://doi.org/10.1021/acs.jpclett.6b00144.

(23) Rabbel, H.; Breier, P.; Sommer, J.-U. Swelling Behavior of Single-Chain Polymer Nanoparticles: Theory and Simulation. *Macromolecules* **2017**, *50* (18), 7410–7418. https://doi.org/10.1021/acs.macromol.7b01379.

(24) Scheutz, G. M.; Elgoyhen, J.; Bentz, K. C.; Xia, Y.; Sun, H.; Zhao, J.; Savin, D. A.; Sumerlin, B. S. Mediating Covalent Crosslinking of Single-Chain Nanoparticles through Solvophobicity in Organic Solvents. *Polym. Chem.* **2021**. https://doi.org/10.1039/D1PY00780G.

(25) H. Liu, C.; D. Dugas, L.; I. Bowman, J.; Chidanguro, T.; F. Storey, R.; C. Simon, Y. Forcing Single-Chain Nanoparticle Collapse through Hydrophobic Solvent Interactions in Comb Copolymers. *Polymer Chemistry* **2020**, *11* (2), 292–297. https://doi.org/10.1039/C9PY01235D.

(26) Zhang, Y.-Y.; Jia, X.-M.; Shi, R.; Li, S.-J.; Zhao, H.; Qian, H.-J.; Lu, Z.-Y. Synthesis of Polymer Single-Chain Nanoparticle with High Compactness in Cosolvent Condition: A Computer Simulation Study. *Macromolecular Rapid Communications* **2020**, *41* (24), 1900655. https://doi.org/10.1002/marc.201900655.

(27) Verso, F. L.; A. Pomposo, J.; Colmenero, J.; J. Moreno, A. Simulation Guided Design of Globular Single-Chain Nanoparticles by Tuning the Solvent Quality. *Soft Matter* **2015**, *11* (7), 1369–1375. https://doi.org/10.1039/C4SM02475C.

(28) Blasco, E.; Tuten, B. T.; Frisch, H.; Lederer, A.; Barner-Kowollik, C. Characterizing Single Chain Nanoparticles (SCNPs): A Critical Survey. *Polym. Chem.* **2017**, *8* (38), 5845–5851. https://doi.org/10.1039/C7PY01278K.

(29) Hanlon, A. M.; Lyon, C. K.; Berda, E. B. What Is Next in Single-Chain Nanoparticles? *Macromolecules* **2016**, *49* (1), 2–14. https://doi.org/10.1021/acs.macromol.5b01456.

(30) Cheng, C.-C.; Chang, F.-C.; Yen, H.-C.; Lee, D.-J.; Chiu, C.-W.; Xin, Z. Supramolecular Assembly Mediates the Formation of Single-Chain Polymeric Nanoparticles. *ACS Macro Lett.* **2015**, *4* (10), 1184–1188. https://doi.org/10.1021/acsmacrolett.5b00556.

(31) S. Fischer, T.; Spann, S.; An, Q.; Luy, B.; Tsotsalas, M.; P. Blinco, J.; Mutlu, H.; Barner-Kowollik, C. Self-Reporting and Refoldable Profluorescent Single-Chain Nanoparticles. Chemical Science 2018, 9 (20), 4696–4702. https://doi.org/10.1039/C8SC01009A.

(32) Cui, Z.; Cao, H.; Ding, Y.; Gao, P.; Lu, X.; Cai, Y. Compartmentalization of an ABC Triblock Copolymer Single-Chain Nanoparticle via Coordination-Driven Orthogonal Self-Assembly. Polymer Chemistry 2017, 8 (24), 3755–3763. https://doi.org/10.1039/C7PY00582B.

(33) Berda, E. B.; Foster, E. J.; Meijer, E. W. Toward Controlling Folding in Synthetic Polymers: Fabricating and Characterizing Supramolecular Single-Chain Nanoparticles. Macromolecules 2010, 43 (3), 1430–1437. https://doi.org/10.1021/ma902393h.

(34) Foster, E. J.; Berda, E. B.; Meijer, E. W. Tuning the Size of Supramolecular Single-Chain Polymer Nanoparticles. J. Polym. Sci. A Polym. Chem. 2011, 49 (1), 118–126. https://doi.org/10.1002/pola.24426.

(35) Latorre-Sánchez, A.; Alegría, A.; Verso, F. L.; Moreno, A. J.; Arbe, A.; Colmenero, J.; Pomposo, J. A. A Useful Methodology for Determining the Compaction Degree of Single-Chain Nanoparticles by Conventional SEC. Particle & Particle Systems Characterization 2016, 33 (7), 373–381. https://doi.org/10.1002/ppsc.201500210.

(36) Frank, P.; Prasher, A.; Tuten, B.; Chao, D.; Berda, E. Characterization of Single-Chain Polymer Folding Using Size Exclusion Chromatography with Multiple Modes of Detection. Appl Petrochem Res 2015, 5 (1), 9–17. https://doi.org/10.1007/s13203-014-0046-1.

(37) Engelke, J.; Tuten, B. T.; Schweins, R.; Komber, H.; Barner, L.; Plüschke, L.; Barner-Kowollik, C.; Lederer, A. An In-Depth Analysis Approach Enabling Precision Single Chain Nanoparticle Design. Polym. Chem. 2020, 11 (41), 6559–6578. https://doi.org/10.1039/D0PY01045F.

(38) Engelke, J.; Brandt, J.; Barner-Kowollik, C.; Lederer, A. Strengths and Limitations of Size Exclusion Chromatography for Investigating Single Chain Folding – Current Status and Future Perspectives. 2019. https://doi.org/10.1039/C9PY00336C.

(39) Pomposo, J. A.; Perez-Baena, I.; Buruaga, L.; Alegría, A.; Moreno, A. J.; Colmenero, J. On the Apparent SEC Molecular Weight and Polydispersity Reduction upon Intramolecular Collapse of Polydisperse Chains to Unimolecular Nanoparticles. Macromolecules 2011, 44 (21), 8644–8649. https://doi.org/10.1021/ma201070b.

(40) Nitsche, T.; Steinkoenig, J.; De Bruycker, K.; Bloesser, F. R.; Blanksby, S. J.; Blinco, J. P.; Barner-Kowollik, C. Mapping the Compaction of Discrete Polymer Chains by Size Exclusion Chromatography Coupled to High-Resolution Mass Spectrometry. Macromolecules 2019, 52 (6), 2597–2606. https://doi.org/10.1021/acs.macromol.9b00203.

(41) Hegde, D. A.; Choudhary, V. S.; Bhide, Y. S. Process for the Preparation of Sevelamer Hydrochloride and Formulation Thereof. US7846425B2, December 7, 2010.

(42) Manning, G. S. Counterion Condensation on Charged Spheres, Cylinders, and Planes. J. Phys. Chem. B 2007, 111 (29), 8554–8559. https://doi.org/10.1021/jp0670844.

(43) Mukherji, D.; Marques, C. M.; Kremer, K. Polymer Collapse in Miscible Good Solvents Is a Generic Phenomenon Driven by Preferential Adsorption. Nature Communications 2014, 5 (1), 4882. https://doi.org/10.1038/ncomms5882.

(44) Carney, R. P.; Kim, J. Y.; Qian, H.; Jin, R.; Mehenni, H.; Stellacci, F.; Bakr, O. M. Determination of Nanoparticle Size Distribution Together with Density or Molecular Weight by 2D Analytical Ultracentrifugation. Nature Communications 2011, 2 (1). https://doi.org/10.1038/ncomms1338.

(45) Bekdemir, A.; Stellacci, F. A Centrifugation-Based Physicochemical Characterization Method for the Interaction between Proteins and Nanoparticles. Nature Communications 2016, 7 (1), 13121. https://doi.org/10.1038/ncomms13121.

(46) Bekdemir, A.; Liao, S.; Stellacci, F. On the Effect of Ligand Shell Heterogeneity on Nanoparticle/Protein Binding Thermodynamics. Colloids and Surfaces B: Biointerfaces 2019, 174, 367–373. https://doi.org/10.1016/j.colsurfb.2018.11.027.

(47) Dam, J.; Schuck, P. Calculating Sedimentation Coefficient Distributions by Direct Modeling of Sedimentation Velocity Concentration Profiles. In Methods in Enzymology; Numerical Computer Methods, Part E; Academic Press, 2004; Vol. 384, pp 185–212. https://doi.org/10.1016/S0076-6879(04)84012-6.

(48) Schuck, P. analytical ultracentrifugation direct boundary 93 odelling with sedfit http://www.analyticalultracentrifugation.com/ (accessed 2021 -06 -25).

(49) Brown, P. H.; Schuck, P. Macromolecular Size-and-Shape Distributions by Sedimentation Velocity Analytical Ultracentrifugation. Biophysical Journal 2006, 90 (12), 4651–4661. https://doi.org/10.1529/biophysj.106.081372.

(50) Schuck, P.; Perugini, M. A.; Gonzales, N. R.; Howlett, G. J.; Schubert, D. Size-Distribution Analysis of Proteins by Analytical Ultracentrifugation: Strategies and Application to Model Systems. Biophysical Journal 2002, 82 (2), 1096–1111. https://doi.org/10.1016/S0006-3495(02)75469-6.

(51) Aguilar, J. A.; Nilsson, M.; Bodenhausen, G.; Morris, G. A. Spin Echo NMR Spectra without J Modulation. Chem. Commun. 2011, 48 (6), 811–813. https://doi.org/10.1039/C1CC16699A.

(52) Pinto, L. F.; Riguera, R.; Fernandez-Megia, E. Stepwise Filtering of the Internal Layers of Dendrimers by Transverse-Relaxation-Edited NMR. J. Am. Chem. Soc. 2013, 135 (31), 11513–11516. https://doi.org/10.1021/ja4059348.

(53) Pinto, L. F.; Correa, J.; Martin-Pastor, M.; Riguera, R.; Fernandez-Megia, E. The Dynamics of Dendrimers by NMR Relaxation: Interpretation Pitfalls. J. Am. Chem. Soc. 2013, 135 (5), 1972–1977. https://doi.org/10.1021/ja311908n.

(54) Bernkop-Schnürch, A.; Dünnhaupt, S. Chitosan-Based Drug Delivery Systems. European Journal of Pharmaceutics and Biopharmaceutics 2012, 81 (3), 463–469. https://doi.org/10.1016/j.ejpb.2012.04.007.

(55) Cabral, H.; Kataoka, K. Progress of Drug-Loaded Polymeric Micelles into Clinical Studies. Journal of Controlled Release 2014, 190, 465–476. https://doi.org/10.1016/j.jconrel.2014.06.042.

(56) Bono, N.; Ponti, F.; Mantovani, D.; Candiani, G. Non-Viral in Vitro Gene Delivery: It Is Now Time to Set the Bar! Pharmaceutics 2020, 12 (2), 183. https://doi.org/10.3390/pharmaceutics12020183.

(57) Cai, J.; Yue, Y.; Rui, D.; Zhang, Y.; Liu, S.; Wu, C. Effect of Chain Length on Cytotoxicity and Endocytosis of Cationic Polymers. Macromolecules 2011, 44 (7), 2050–2057. https://doi.org/10.1021/ma102498g.

(58) Fischer, D.; Li, Y.; Ahlemeyer, B.; Krieglstein, J.; Kissel, T. In Vitro Cytotoxicity Testing of Polycations: Influence of Polymer Structure on Cell Viability and Hemolysis. Biomaterials 2003, 24 (7), 1121–1131. https://doi.org/10.1016/S0142-9612(02)00445-3.

(59) Kumar, D.; Mutreja, I.; Chitcholtan, K.; Sykes, P. Cytotoxicity and Cellular Uptake of Different Sized Gold Nanoparticles in Ovarian Cancer Cells. Nanotechnology 2017, 28 (47), 475101. https://doi.org/10.1088/1361-6528/aa935e.

(60) Sultana, S.; Djaker, N.; Boca-Farcau, S.; Salerno, M.; Charnaux, N.; Astilean, S.; Hlawaty, H.; de la Chapelle, M. L. Comparative Toxicity Evaluation of Flower-Shaped and Spherical Gold Nanoparticles on Human Endothelial Cells. Nanotechnology 2015, 26 (5), 055101. https://doi.org/10.1088/0957-4484/26/5/055101.

(61) Lin, J.; Zhang, H.; Chen, Z.; Zheng, Y. Penetration of Lipid Membranes by Gold Nanoparticles: Insights into Cellular Uptake, Cytotoxicity, and Their Relationship. ACS Nano 2010, 4 (9), 5421–5429. https://doi.org/10.1021/nn1010792.

Chapter 5 Cellular Uptake Discriminates SCNP Topological Isomers

The current paradigm of nanoparticles' cellular uptake profiles was largely built with rigid materials, such gold nanoparticles. However, such "geometry-property" relationship can not necessarily be directly translated to soft materials without a defined geometry. This chapter discusses if there's "topology-property" relationship that's overlooked by the community.

Disclosure: The work in this chapter is in preparation for a manuscript to be submitted

5.1 ABSTRACT

Cationic polymers form a group of vehicles for intracellular drug delivery. The prerequisite for rational carrier design is our understanding of how they interact with cells and their ability to access the cytosol. The established literature landscape has largely related the cellular interacting properties to geometrical factors (size and shape) using rigid model systems such as Au nanoparticles. However, how polymeric nanoparticles with distinct topologies interact with cells needs further examination. Therefore, in this work, we use single-chain nanoparticles as model system to answer this question. We deliberately construct SCNPs with distinct topologies (sparse versus compact), as evidenced with a set of analytical tools. Due to the flexibility of polymer nanoparticles, the two topologies converge geometrically when placed in the incubation medium, PBS buffer. The observation with fluorescent microscopy and endocytic inhibitor assays, we found that the two SCNPs, differing in topology while geometrically identical, interact with cells differently. Finally, we construct SCNPs with dynamic covalent chemistry, namely, disulfide bonds. The disulfide pairs can be reshuffled by a redox cycle in a certain solvent system, allowing for topological transformation to create SCNP topological isomers. The SCNP topological isomerism can be sensitively and accurately captured by SV-AUC. A type of end-point assay, called GIGT assay, was performed to investigate these SCNP topological isomers' ability to access the cytosol.

5.2 INTRODUCTION

Most of the biological macromolecules, such as peptides, proteins, plasmids, siRNA and mRNA, requires cytosolic presence to perform their biological function.[1] Due to the anionic nature, they cannot cross the negatively charged cellular membranes, not to mention their fragility against enzymatic degradation. Thus, developing suitable vehicles to carry these biological payloads is key to the success for the delivery purpose. The fundamental study on the structure-property relationship to understand which physical parameters of the vehicle affect their interaction with cells is of paramount practical relevance towards rational design.

To date, most of the discussion approaches this question through the geometrical descriptors, i.e., size[2,3] and shape[4–6]. The main reason is the availability of materials. The size question can be easily answered with inorganic (Au, silica etc.) or organic nanoparticles such as dendrimers; the shape question is answered with Au nanoparticles.[7] These rigid nanoparticles differ in their geometries but converge in the topological space. And the corresponding works don't provide us with information about how topology affects their interaction with cells. Moreover, their rigid nature doesn't allow us to probe the effect of conformational flexibility, which allows for structural responsiveness to external stimulus such pH, ionic strength, and guest-binding.

Recent advancement in single-chain technology allows us to construct polymeric nanoparticles with tunable topologies.[8,9] Single-chain polymeric nanoparticles (SCNPs), as the name suggests, are constructed by intra-molecularly cross-linking reaction to compact the linear precursor into nanoparticles. Their typical size range is 5~20 nm. The single-chain reaction can also be understood by topological terms. Single-chain reactions introduce a secondary topology, loop, to the linear topology of the precursor.[10] Depending on the loop sizes, the final products' topology departs to various extend from the initial linearity. When small loops dominate, locally cross-linked domains are formed to resemble the "beads-on-string" model; we call such topology "sparse". When large loops dominate, the precursor is compacted in a global manner to resemble the "globule-like" model; we call such topology "compact". Due to the presence of the uncross-linked hinge, the sparse topology is expected to be more flexible than the compact one. The cross-linking reaction can be approximated as covalently "freeze" the precursor chain conformation. Thus, an effective approach to tune the topology of SCNPs is to place the precursor under certain solvent conditions prior to cross-linking. We recently reported our systematic study on this.[11]

In this work, we hypothesize that cells can recognize topological difference and react differently. We cross-linked polyallylamine (PALA) with succinic acids under different solvent conditions to generate SCNPs of two topologies, sparse or compact. The topological characterization was done in pure water, which is good solvent condition to allow for sufficient swelling[12]. Since PBS buffer was chosen as the incubation medium to avoid ambiguity of protein corona, we also performed characterization in PBS. Due to deprotonation and counter-ion condensation, the two topologically different SCNPs share very similar geometrical identities. To study their interaction with cells, we first made observation with confocal laser scanning microscopy (CLSM) after incubation under 37 °C and 4 °C; then we performed inhibitor assay, trying to identify the specific cellular uptake pathways. Finally, to understand the cytosolic accessing ability of a certain topology, we cross-linked the same PALA precursor with dithiodiglycolic acid. With redox cycle in various solvent condition, the disulfide pairing reshuffled to transform the overall topology. Thus, we obtained two topological groups (sparse vs. compact) of SCNPs. Then we performed Glucocorticoid induced GFP translocation (GIGT) assay to compare their ability to access the cytosol.[13,14]

5.3 SCHEME AND CHARACTERIZATION

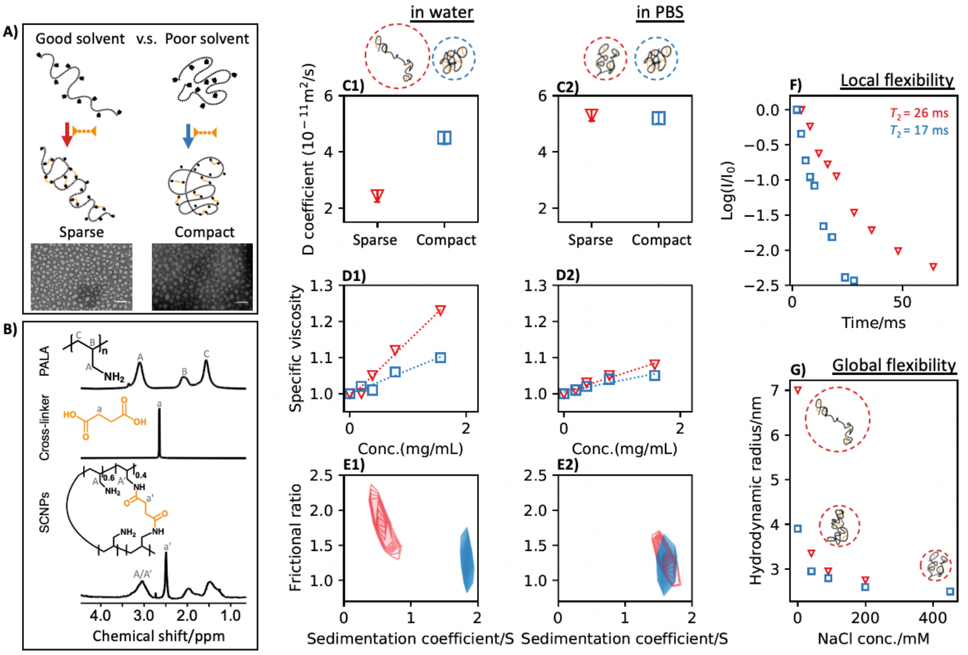

Figure 5.1 Control and characterization of the topology of SCNPs.

A) Scheme of the single-chain compaction with or without pre-collapsing the precursor chain. Samples were stained with uranyl acetate for better contrast in TEM, scale bar: 50 nm. B) ^{1}H NMR spectra of the precursor PALA, cross-linker and final SCNPs. C1, C2) Scatter plots showing DOSY results in water or PBS; D1, D2) Plots showing viscosity-concentration dependency in water or PBS. The slope of the linear fitting (dashed line) in the diluted regime reveals the intrinsic viscosity; E1, E2) Contour plots of sedimentation coefficients vs frictional ratio from 2D analysis of SV-AUC runs in water or PBS; F) Signal decay by T_2 ^{1}H NMR probing the segmental rigidity; G) Scatter plots showing size dependency on ionic strength to probe the overall flexibility of the SCNPs. The size here is the hydrodynamic radius converted from diffusion coefficients (DOSY NMR) via Einstein-Stokes equation.

Briefly, we first dissolved PALA chain below the overlap concentration, in water or ethanol (10%)-water mixture, to tune the chain conformation; then the solution of succinic acids, after activating with EDC and NHS, was added to the PALA solution drop wisely to form amide bonds with PALA. (Scheme in Figure 5.1A; see Supporting Information for more detail) After purification and lyophilization, the SCNPs were stored in dry powder form for further characterization. With knowledge from our previous work, the two SCNPs produced in water or ethanol (10%)-water mixture, exhibit distinct topology. Herein, they are called sparse SCNPs and compact SCNPs, to ease the communication. The reaction was validated with ^{1}H-NMR in Figure 5.1B with the cross-linking density being ~40%. Under the dry condition of negative staining TEM, both SCNPs show the diameter of ~20 nm. As mentioned, we characterized both SCNPs under two types of solvent conditions (water and PBS) with DOSY NMR, viscometry and SV-AUC. In water (or D_2O), the two topologies are significantly different in terms of the three geometrical descriptors (the hydrodynamic radius, gyration radius and anisotropy). However, when both topologies were placed in PBS, characterization results revealed the convergence in the geometrical space[15], mostly due to the high ionic strength. Moreover, the two distinct topologies should also differ in their conformational flexibility, locally and globally. We conducted ^{1}HNMR T_2 relaxation experiments to probe the segmental rigidity. Indeed, the compact topology shows faster signal decay and larger T_2 value than the sparse topology. Polyelectrolytes are known of their counter-ion condensation behavior. We used this phenomenon to probe the global conformational flexibility. SCNPs were dissolved in D_2O with various NaCl molarities. DOSY NMR experiments were performed, and the results were converted into hydrodynamic radius through the Einstein-Stokes relationship. Shown in Figure 5.1G, the overall size depends on the counter-ion concentration, and the sparse topology show more responsiveness than the compact one (size reduction: 65% versus 35%). With these results, we can confidently claim that the two types of SCNPs are conformers, being presumably identical in their molecular formula but differing in the arrangement of cross-linking sites.

5.4 CELL PENETRATION OBSERVED WITH CLSM

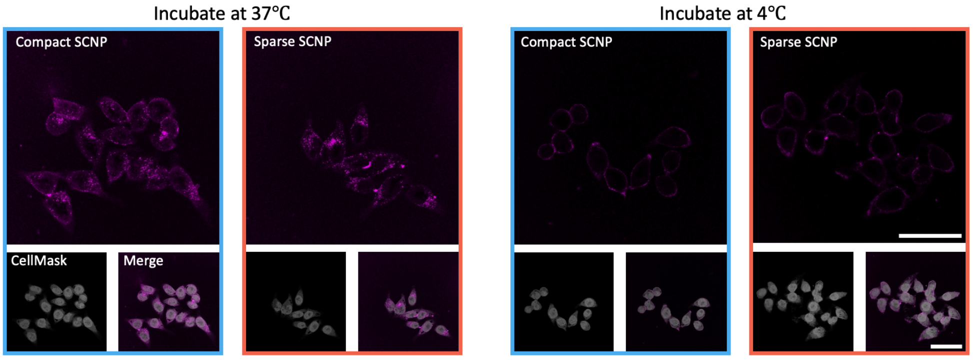

Figure 5.2 Cell penetration assay observed with CLSM.

HeLa cells (pseudo color: grey) were incubated with SCNPs (pseudo color: magenta) under 37°C or 4°C. Blue frames: compact SCNPs; Red frames: sparse SCNPs. Scale bar: 50 µm.

We used HeLa cell line as model to study the cell penetration of PALA SCNPs. SCNPs were fluorescently labelled with Alexa Flour 647 (AF647). Incubation was performed under two temperatures (37°C or 4°C, to allow or inhibit active cellular uptake). Cells were stained with DAPI (targeting nucleus) and HCS CellMask Blue (targeting cytosol). Shown in Figure 5.2 is a representative slice from a set of z-stack images. At the incubation temperature of 37 °C, AF647 channels representing SCNPs display two patterns, diffuse and punctate pattern. The diffuse pattern usually indicates cytosolic distribution while punctate pattern is the result of confinement, most likely endosomal entrapment. The images show that the compact SCNPs exhibit clear diffuse pattern, along with some punctate spots; for the sparse SCNPs, the punctate pattern dominates. Low temperature at 4°C effectively blocked the bioactivity of most proteins, thus the active cellular uptake mechanism[16,17]. In either case, we observed no punctate spots but surface accumulation from electrostatic attraction.[18] This renders it hard to judge the possibility of passive diffusion. Worth noting is that multi-chain nanoparticles showed no diffuse pattern at 37°C and no accumulation/penetration was found at 4°C. (see SI) Such comparison indicates that the interaction with cells is diffusion-limited.

5.5 ENDOCYTOCI INHIBITOR ASSAY

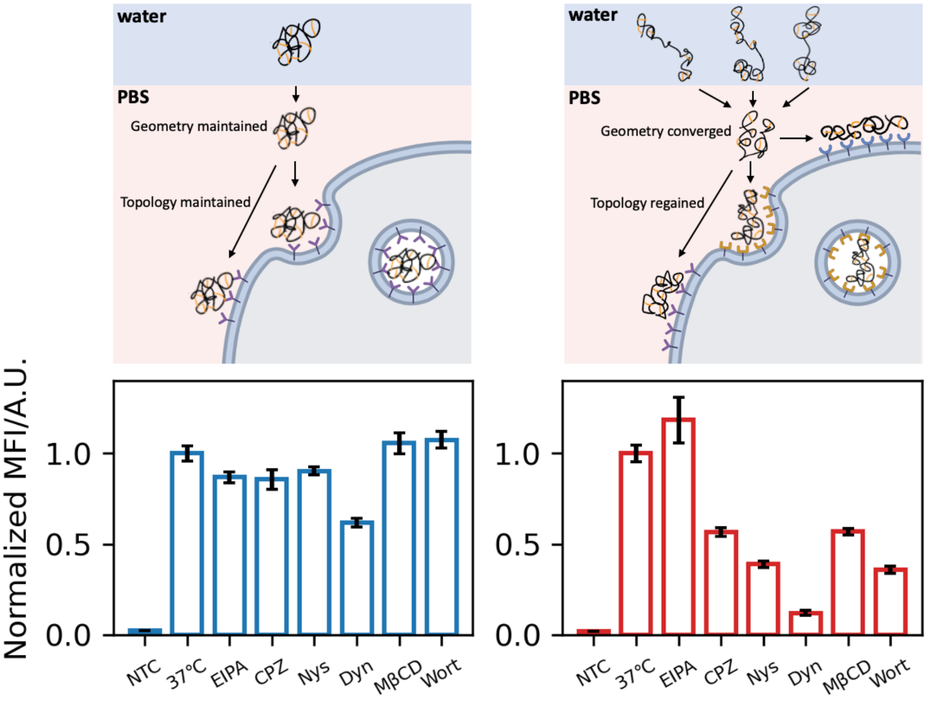

Figure 5.3 Endocytic inhibitor assay.

Bar plots of mean fluorescent intensity of the SCNPs (via FACS, normalized with the results from 37 °C) upon incubation with HeLa cells pre-treated with the indicted endocytic inhibitors. Left and right panels are the results from SCNPs of compact and sparse topologies, respectively. The error bar is one standard deviation from triplicated experiments. NTC: Non-treated control.

We performed endocytic inhibitor assay to investigate the uptake pathway(s). The chosen inhibitors are, chlorpromazine (CPZ, inhibitor of clathrin-mediated endocytosis), dynasore (Dyn, inhibitor dynamin-dependent endocytosis), 5-(N-Ethyl-N-isopropyl)amiloride (EIPA, inhibitor for macropinocytosis), methyl-β-cyclodextrin (MβCD, a cholesterol-depletion agent to inhibit lipid raft), nystatin (Nys, inhibitor of caveolae-mediated endocytosis), and wortmannin (Wort, inhibitor for phosphoinositide 3-kinase). In brief, cells were pretreated with the chose inhibitor before washing away for incubation with SCNPs. After incubation, the free SCNPs were washed away and cells were harvested for FACS, inspecting the AF647 signal from the internalized SCNPs. (Details see SI) The bar plot in Figure 5.3 shows the normalized mean fluorescent intensity (MFI, interpreted as the median of the distribution of AF647 signal; MFI of each experiment was normalized by the 37°C result) For the compact SCNPs, we found dynamin is both affective to mitigate the MFI by ~40% while results from other inhibitors didn't show significant difference comparing to the 37°C condition. The cellular entry of the sparse SCNPs is mainly dynamin-dependent. The MFI values are decreased by ~90% after dynasore treatment. We also notice decreasing after the treatment of other inhibitors, such as CPZ, Nys, MβCD and Wort, as strong proof that the sparse SCNPs enter cells by interacting a variety of receptors. In both SCNPs, not surprisingly, EIPA didn't show significant effect as macropinocytosis is generally the main pathway for entities larger than 1 μm. Combining the characterizing results, SCNPs of two distinct topologies exhibit little geometrical difference in PBS buffer. However, the cells can distinguish them and respond distinctly, revealing the interaction mode depends on topology instead of geometry. One likely explanation is that upon binding to the cellular membrane, the flexibility of sparse SCNPs allows for unfolding to generate multivalent contact, thus triggering various uptake mechanisms.

5.6 SOLVENT-GUIDED RESHUFFLE

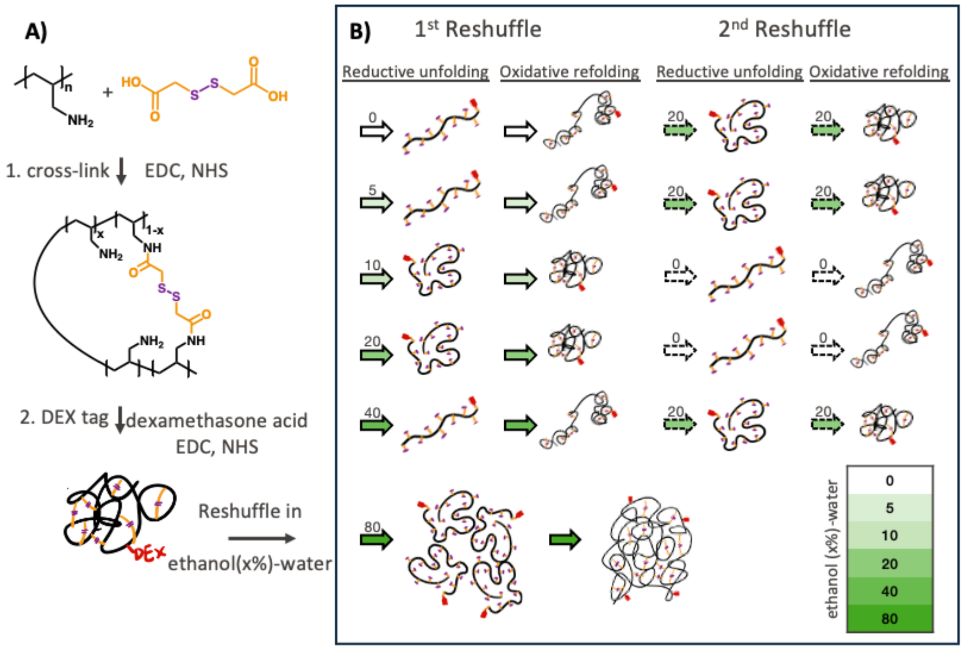
A)
n
NH2
HO
S
S
O
OH
1. cross-link
EDC, NHS
x
1-x
NH2
NH
S
S
NH2
NH
2. DEX tag
dexamethasone acid
EDC, NHS
DEX
Reshuffle in
ethanol(x%)-water
B)
1st Reshuffle
2nd Reshuffle
Reductive unfolding
Oxidative refolding
Reductive unfolding
Oxidative refolding
0
5
10
20
40
80
ethanol (x%)-water

Figure 5.4 Solvent-guided topological reshuffle.

A) The synthetic route to construct SCNPs containing disulfide bonds followed with DEX conjugation; B) Schematic workflow of the reshuffle experiments

Although the inhibitor assays provide some information, they also suffer from inherent limitations such as non-specificity and cytotoxicity.[19] Moreover, the wide range of inhibitor choices, together with dosage and incubation time applied by different researchers make their works hard to compare. We decided to investigate if the topology affects SCNPs' ability to access the cytosol, with more practical relevance. Evaluation of the cytosolic access is done with GIGT assay.[20–22] This assay requires labelling the sample-of-interest with dexamethasone (DEX). Two criteria should be met. First, the labelling ratio be low so that the DEX does not dominate the interaction; second, the labelling ratio should be strictly identical across all sample to be compared. Combining the two criteria, it becomes synthetically demanding as well as analytically challenging. To circumvent this issue, we upgraded the SCNPs. Inspired by the seminal work from Anfinsen on protein folding, we constructed SCNPs with dithiodiglycolic acids. (Figure 5.4A; See SI for synthetic details) The disulfide bonds can be cleaved with dithiothreitol (DTT) to revert the SCNPs into the linear topology, where the chain conformation is immediately dictated by the solvent quality (tuned by varying the composition of the water-ethanol mixture). Repairing the disulfide bonds by dialyzing away the DTT against the same solvent, the linear chains recross-linked back as SCNPs with certain topologies. Such redox cycle allows us to reshuffle only the disulfide pairing while leaving the molecular formula the same, creating topological isomers. Simple 1D SV-AUC experiments can sensitively capture the topological variation. With the identical MW and density, these isomers experience the same centrifugal force and buoyancy, but only different viscosity drag depending on the topology. Thus, the final 1D distribution of sedimentation coefficients can be simply interpreted as the topological spectrum.

As shown in the scheme panel of Figure 5.4A, PALA was first cross-linked with dithiodiglycolic acids into parental SCNPs. The we covalently tagged the SCNPs with dexamethasone acids (DEX). Then, we performed two rounds of reshuffles. In the 1st Reshuffle, a series of ethanol fraction (0%, 5%, 10%, 20%, 40%, and 80%) was utilized.

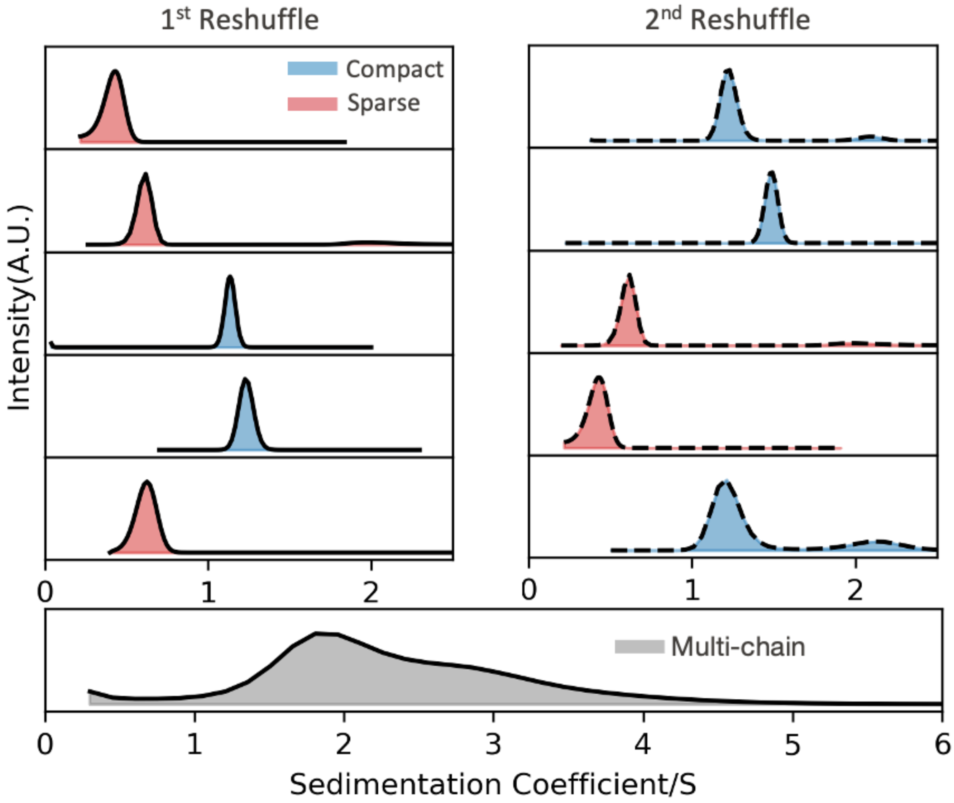

Figure 5.5 Distribution of sedimentation coefficients of all samples.
Products after 1st and 2nd reshuffle are indicated as solid and dashed line. Blue: compact SCNPs; Red: sparse SCNPs; Grey: multi-chain nanoparticles.

The resulting six new batches were profiled with AUC, shown in Figure 5.5 with solid lines and color-coded to indicate the topology. Additionally, the results identify water and 20% EtOH to be good and poor solvents, respectively. In 80% EtOH, the SCNPs aggregated, and the redox cycle transformed the aggregates into MCNP (multi-chain nanoparticles) with simultaneous events of intra and inter-chain interaction. From each of the five topological isomers, a portion was taken for the 2nd Reshuffle in a more guided way, where the compact topology was transformed to be sparse and vice versa. AUC profiling results were shown as dashed line in Figure 5.5. Eventually, we obtained ten batches of SCNPs as topological isomers. Each of the two topology types (compact or sparse) contains five bathes.

5.7 GIGT: CYTOSOL-ACCESSING ABILITY

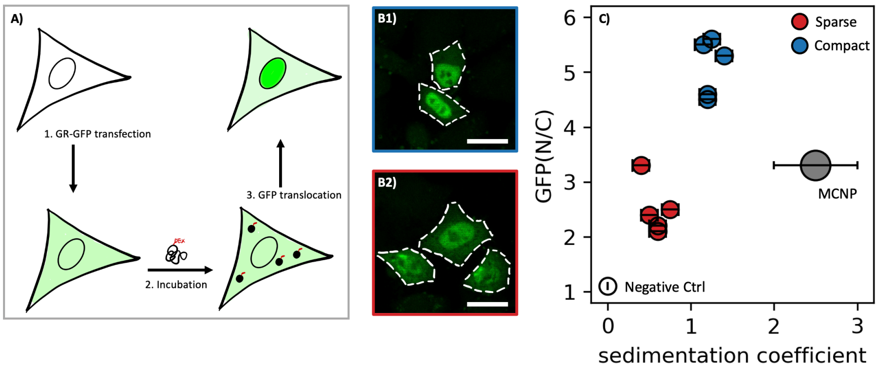

Figure 5.6 Schematic illustration and result of GIGT assay.

A) Schematic illustration of the workflow of GIGT assay; B) Representative CLSM images of GFP nuclear translocation upon incubation with DEX-tagged compact (blue frame) or sparse (red frame) SCNPs. White dashed lines indicate the rim of cells to guide the eyes (scale bar: 20 µm). C) Scatter plot showing the correlation between the GFP translocation efficiency and the topology of SCNPs. GFP(N/C) stands for the ratio between the nuclear and cytosolic GFP signal. (Negative control: transfected cells without incubation with any samples)

As shown in Figure 5.6A, in GIGT assay, cells are first transfected with the plasmid pK7-GR-GFP to express the chimeric proteins.[23] When the GR part binds with cytosolic steroids (i.e. dexamethasone), the active nuclear transportation is triggered. Along with GR, the GFP part reports the translocation efficiency by comparing its nucleus (N) level with its cytosolic (C) level (representative images are shown in Figure 5.6B). Quantitatively, the ratio GFP(N/C), is taken as the relative measure of the cytosolic level of DEX. Since all the samples are isomers with the same DEX conjugation, the GFP(N/C) also describes the samples' ability to access the cytosol.

The eleven samples of DEX-tagged nanoparticles (ten SCNP topological isomers and the MCNPs) underwent GIGT assay. (See SI for experimental details and image processing) The results are summarized as the scatter plot in Figure 5.6C. First, by comparing with the negative control, we found all eleven samples enter the cytosol. It's not surprising since cationic polymers are known for their ability to escape from endosomal entrapment through the proton sponge effect.[24] Data points from the SCNPs as topological isomers can be divided into two clusters. The upper right cluster comes from the compact ones while the lower left the sparse ones. This distribution pattern with statistical significance indicates a strong correlation between the samples' topology and their ability to enter the cytosol.

5.8 SUMMARY

In this work, we demonstrate that single-chain nanoparticles as topological isomers, while sharing the geometrical identity (size and shape) in the incubation medium, interact with cells in distinct manners. The characterization on their structural flexibility directs us to infer that upon adsorption to the cell surface driven by Coulombic attraction, the one with the sparse topology could unfold to generate multivalent contact, in comparison to its counterpart with the compact topology. The difference in the enthalpy-driven step leads to distinct cellular uptake pathways. Thus, the topology, instead of the geometry, dictates the interaction with cells and the nanoparticles' ability to access the cytosol.

5.9 SUPPLEMENTARY INFORMATION

5.9.1 Synthesis and Purification

Chemical information

PALA (Polyallylamine hydrochloride, CAS 71550-12-4), succinic acid (CAS 110-15-6), dithiodiglycolic acid (CAS 505-73-7), EDC (CAS 22572-40-3), and NHS (6066-82-6) were purchased from Sigma-Aldrich and used without further purification. Dexamethasone acid (CAS 37927-01-8, product of Toronto Research Chemicals) was the purchased from Chemie Brunschwig AG. DL-dithiothreitol (CAS 3483-12-3) was purchased from Acros Organics.

Cross-linking reaction

150 mg parent polymer PALA was dispersed into 150ml chosen reaction conditions as discussed in the paper to form dilute precursor solution. To crosslink 50% of the primary amines, around 96mg succinic acids (2 molar excess to 50% of the amines) were dissolved into 10 ml corresponding buffer, followed with the addition of EDC and NHS (both at 1.5 molar excess to carboxylic groups) for activation and stabilization. The activated crosslinker solution was then transferred into an additional funnel. While stirring the precursor solution in a 250 ml round bottom flask, the crosslinker solution was added dropwise at ~1 drop/s. The reaction was kept at room temperature overnight.

In the disulfide-containing SCNPs, 150 mg dithiodiglycolic acid was used (instead of succinic acids) and the rest were kept the same.

Purification

Ultrafiltration was performed on the reaction mixture with Amicon® Ultra-15 filter (Mw cutoff: 3,000 Da) to concentrate the final product, which was later washed with ultrapure water for multiple rounds to desalt. The concentrated sample underwent extensive dialysis in ultrapure water before the final concentrating step. Finally, the sample was freeze dried into dry powder.

AF647 labelling

AlexaFluor 647 NHS Ester (Succinimidyl Ester) was purchased from ThermoFisher and dissolved into dry DMSO as 10mg/mL solution. 2 μL NHS-dye solution was added to 200uL SCNP solution (1mg/mL) and then incubate at 37°C in a thermomixer for 2 hours. The SCNPs has MW of around 30 kDa. This labelling stoichiometry ensure 3-fold molar excess of AF647 against SCNPs. Upon labelling and purification, UV-vis was applied to confirm that the labelling efficiency for both samples to be comparable.

Dexamethasone conjugation

400 µL dexamethasone acid solution (in DMSO, 10mg/mL) was first activated with EDC and NHS (1.5-fold molar excess) and then added into 30 mL disulfide-containing SCNPs aqueous solution (1mg/mL). The dexamethasone acid was in 10-fold molar excess to SCNPs. The reaction mixture was kept stirring at room temperature for 4 hours. The final product was concentrated, washed via ultrafiltration, and referred to as DEX-SCNP.

Disulfide reshuffle

DEX-SCNP powder was dissolved in water as 10 mg/mL solution. Six aliquots, 0.5 mL each, were prepared for the 1st reshuffle. Certain quantify of ethanol/water was added to each aliquot to tune the binary solvent system to form a series of ethanol fraction (0%, 5%, 10%, 20%, 40%, and 80%). The final SCNP concentration was kept ~1 mg/mL, below the overlap concentration. In each, DTT was added (final molarity is 100 mM) to cleave the disulfide bonds. The reaction was kept stir at room temperature in a thermomixer for 30 min. Then each aliquot was dialyzed in the same solvent system overnight, where the excessive DTT was removed, and disulfide bonds were reformed by oxidation with the dissolved oxygen.

Six samples generated with the 1st reshuffle was profiled with SV-AUC. The AUC results identified pure water and 20% ethanol-water to be good and poor solvents, respectively.

The resulting five SCNPs from the 1st reshuffle underwent the 2nd reshuffle, the goal of which was to reverse the topology with the identified solvent conditions. In brief, an aliquot of the sparse SCNPs underwent the redox cycle in 20% ethanol-water to generate a new compact batch and an aliquot of the compact SCNPs underwent the redox cycle in pure water to generate a new sparse batch.

5.9.2 Analytical Methods

Negative staining TEM

On one side of the parafilm, put some droplets of water and 1% (mass) uranyl acetate dihydrate solution (UA). Transfer 4 µL of SCNPs solution (1 mg/mL) onto the TEM grid and keep for 1.5 minutes. Remove the excessive sample with filter paper. Rinse the sample with water by contacting the grid's sample side with the water droplet. Remove the water with filter paper. Staining with UA by contacting the grid's sample side with the UA droplet for 30 seconds. Remove the UA with filter paper.

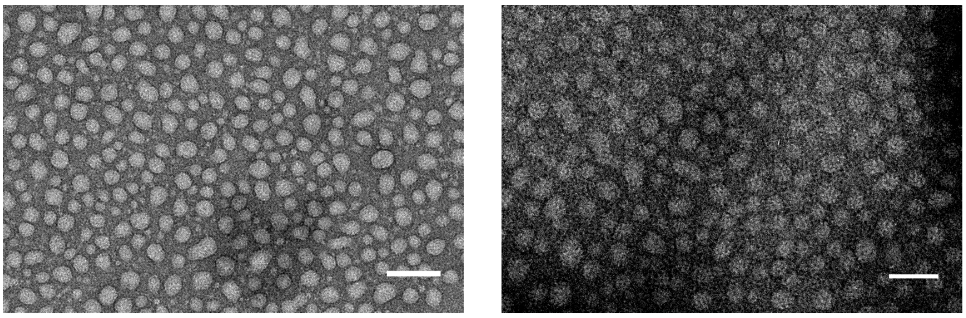

Figure S 5.1 Negative staining TEM images of SCNPs (left: sparse; right: compact). Scale bar: 50 nm

^{1}H NMR

^{1}H NMR spectra were obtained using excitation sculpting centered on the water resonance in spectral widths of around 14 ppm wit 16k points. Resonance assignments were straightforward from chemical shifts of the ^{1}H resonances. The cross-linking density was quantified as the ratio of the amide (quantified by the signal from the cross-linker protons) to the initial primary amines (quantified by the signal from the backbone protons).

Cross-linking density

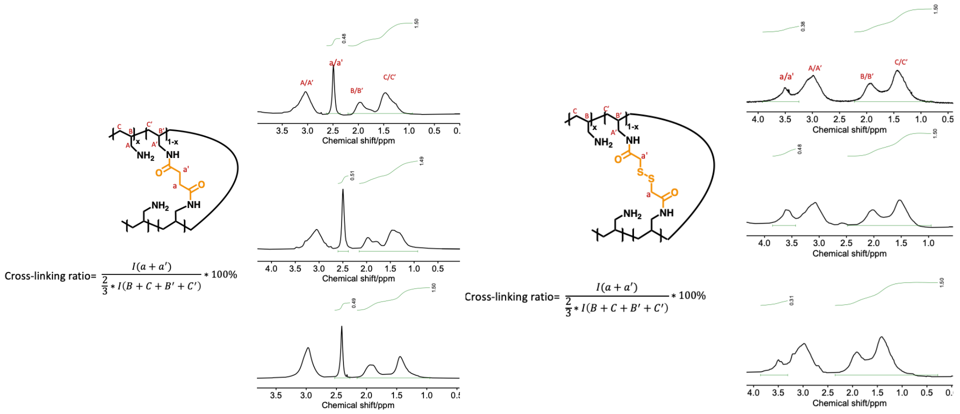

Figure S 5.2 ^{1}H NMR of succinic acid (left) and dithiodiglycolic acid (right) cross-linked SCNPs.

DEX tag

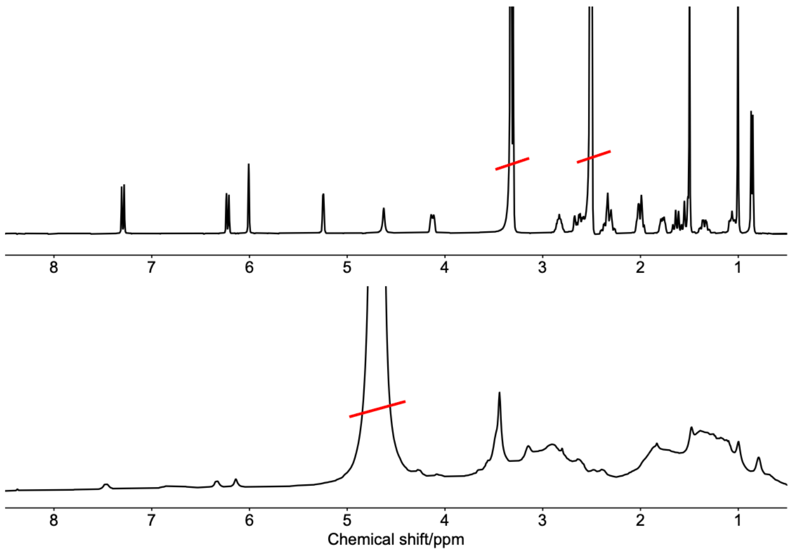

Figure S 5.3 ^{1}H NMR of dexamethasone acid (in d6-DMSO, upper) and DEX-SCNP (in D_2O, lower). The solvent residual peaks are crossed with the red lines.

DOSY NMR

The DOSY NMR experiments were conducted at 25 °C on an autosampler Bruker Avance I Neo (^{1}H: 400 MHz) with 5mm Smart BBFO-Plusz ATMA probe. All spectra were acquired using the Bruker pulse program ledbpgp2s with a diffusion gradient of 300 ms, a diffusion time of 5000 μs and a squared gradient ramp from 2 to 98%. Basic data processing such as baseline correction, phase correction and peak integration were performed with MestReNova (version 14.1.2). Data Fitting of the DOSY signal decay was achieved with python scripting.

Viscometry

Viscosity measurements were conducted on an Anton Paar Lovis 2000 rolling-ball viscometer at 20°C. The apparent viscosity η were corrected with the viscosity of water η_0 to be listed as relative viscosity.

SV-AUC

AUC was performed using a Beckman Optima XL-A, An-60 Ti rotor. All SCNP solutions were prepared freshly in the chosen buffer (ultrapure water or 1X PBS) as 1mg/mL solution to give 0.5~1.0 OD (optical density) absorbance at 230 nm in AUC cells (double sector titanium centerpieces with quartz windows; the optical path length is 1.2 cm). All measurements were made at 20 °C, 60,000 r.p.m. (with radial step size of 0.003 cm) with sufficient duration to ensure complete sedimentation. Data ranges from 50-100 scans were chosen to represent the whole transporting process.

5.9.3 Cell penetration assay

Sample preparation

Two types of SCNPs (sparse or compact topology), AF-647 labelled in the same way with comparable conjugation efficiency were used.

A 24 mm*24 mm glass cover slip was placed in each well of a 6-well cell culture plate 12 h prior to the experiment. Then, HeLa cells were seeded at 3 x 10^5 cells/well and cultured in Dulbecco's modified Eagle medium (DMEM; ThermoFisher 31966021) supplemented with 10 vol% fetal bovine serum and 1 vol% Pen-Strap at 37 °C in a humidified atmosphere of 5% CO_2. On the day of assay, after removing the culture medium and replenish with 1X PBS buffer, 10 µL SCNP aqueous solution (1 mg/ml, labelled with AF 647) was added into each well. After a 2-hour incubation period (under 37°C in an incubator or under 4°C in a fridge), cells were stained with HCS Cell Mask^{TM} Blue Stain (Invitrogen), following the vender's standard protocol. In brief, cells were washed with 1X PBS twice and then fixed with 4% paraformaldehyde (PFA) PBS solution. Cells were washed with PBS buffer twice to remove PFA. To stain cells with HCS CellMask, in each well, 2mL Triton® X-100 PBS solution (5000-fold dilution) was applied and incubate for 15 min; cells were washed twice to remove Triton® X-100; 2mL HCS CellMask solution (working conc.:

0.5 µg/mL in PBS buffer) was added and incubate for 30min; cells were washed 2~3 times with PBS buffer. The coverslips were dried in air. To seal the sample, 10 µL Prolong^{TM} Antifade Diamond Mountant with DAPI (ThermoFisher P36962) was dropped on a 75 by 26mm microscope slide; then the coverslip was placed on top of the mountant with cells facing inside; nail polish was applied to seal the rim of the coverslip. CLSM imaging was performed within the same day and the sample slides were stored under 4°C in fridge for long-term storage.

CLSM

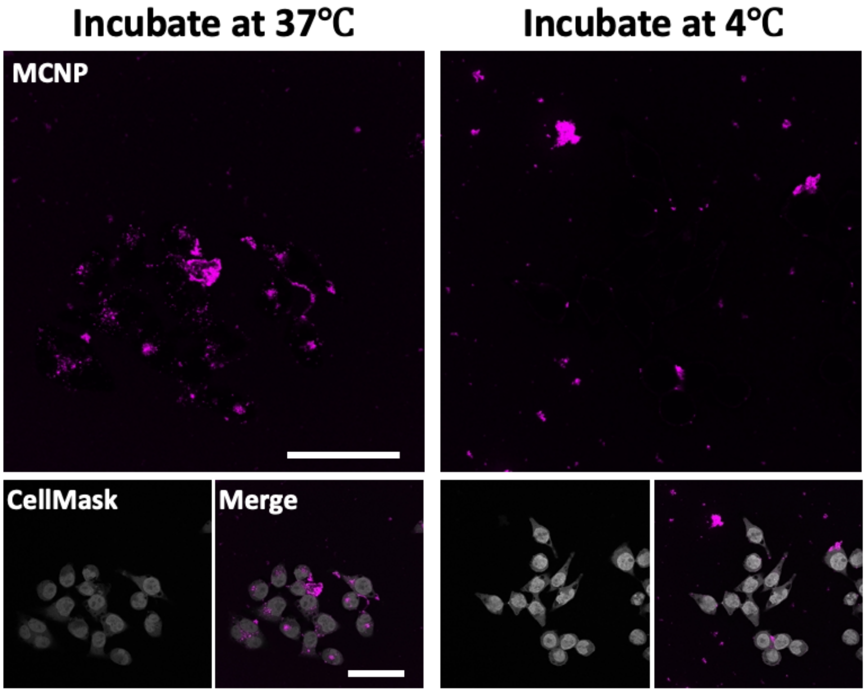

Figure S 5.4 CLSM on MCNPs

5.9.4 Endocytic Inhibitor Assay

Experimental Details

Cells were seeded at 0.05 x 10^6 per well in 4-well Nunc™ Lab-Tek™ II Chamber Slide™prior to incubation with nanoparticles. After overnight growing, at ~70% confluency, the old DMEM medium was removed and 0.5 mL original serum-free DMEM medium was added in each well.

Pretreatment of the cells with endocytic inhibitors was achieved by adding the inhibitor stock solution to a final concentration of 25 µM EIPA (5-[N-ethyl-N-isopropyl] amiloride), 20 µM CPZ (chlorpromazine), 50 µM Nys (Nystatin), 5000 µM

MβCD (methyl-β-cyclodextrin), 0.35 μM wort (Wortmannin[1]) and 80 μM Dyn (Dynasore[2]). Cells were incubated with the inhibitors for 30 min at 37°C before washing twice with PBS and the medium was replaced with PBS prior to addition of SCNPs. 1 μL AF 647-labelled SCNP samples solution (1 mg/mL) was added to each well to for incubation at 37°C 5% CO_2 for 2 hours. Afterwards, cells were thoroughly washed with PBS twice then enzymatically detached with trypsin and resuspended in buffer for flow cytometry analysis. Studies were done in triplicate.

FACS Results

The median value of the fluorescence intensity was determined and normalized with the blank control (SCNP+, inhibitor-) to show the down regulation effect of inhibitors, if there's any.

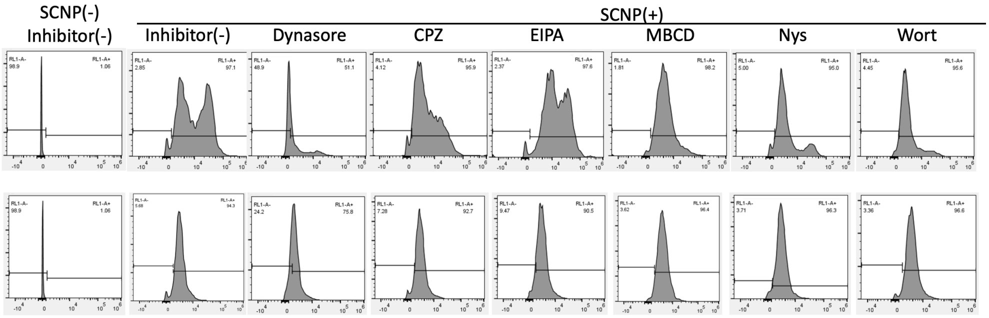

Figure S 5.5 FACS results showing AF647 signal as histogram.

5.9.5 GIGT Assay

Plasmid transfection

Transfection of HeLa cells with the plasmid pK7-GR-GFP[3] (Addgene plasmid #15534) was performed with Lipofectamine™ 3000 the day before the treatments, following the manufacturer's protocol. In brief, cells were seeded and cultured in 6-well ThermoFisher cell culture plate to be 50% confluency prior to transfection. For each well, 5 μL Lipofectamine™ 3000 Reagent was diluted into 125 μL Opti-MEM® reduced serum medium. Mix by vortexing 2~3 seconds. The 2.5 μg plasmid solution was diluted into 125 μL Opti-MEM® reduced serum medium, followed by adding 5 μL P3000™ reagent. Mix gently. Then the 125 μL diluted DNA solution was added to the 125 μL diluted Lipofectamine™ 3000 Reagent. The mixture was incubated for 10~15 minutes at room temperature. The cells' culture medium was replaced with DMEM supplemented with 10% FBS without antibiotics. The 250 μL DNA-

Lipofectamine™ 3000 complex was added into each well to be incubated for ~24 hours 37°C.

Before treatment with DEX SCNPs, the cell culture medium was replaced with DMEM (10% FBS and 1% Penicillin-Streptomycin), 10 µL DEX-SCNP solution (1 mg/mL, final molarity ~0.3 µM) was added to each well to incubate for 2 hours. Finally, cells were then incubated for 30 min with 1 µM Hoechst 33342 in DMEM.

Image acquisition and processing

CLSM images of each sample were acquired with a Leica SP8 inverted microscope at 40x magnification. The sequential scanning was made with two filters, DAPI and GFP, to acquire fluorescent images from the Hoechst-stained nucleus and the expressed chimeric proteins, respectively.

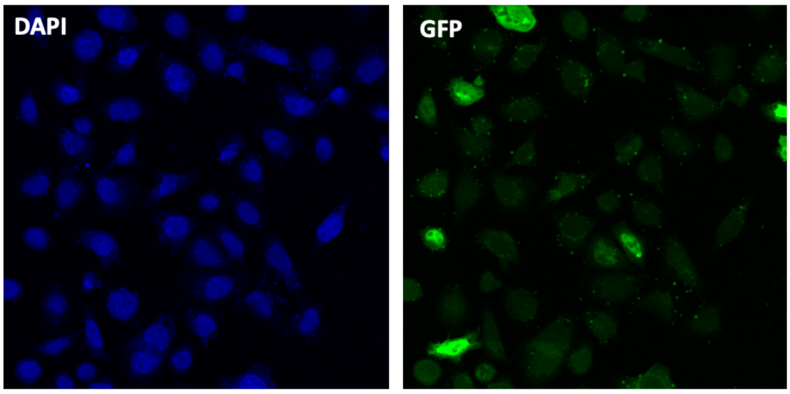

Figure S 5.6 Sample image to demonstrate the date processing in the GIGT assay

#1. Nuclei are identified as Hoechst-stained objects using the three-class thresholding Otsu method

#2. The first filter removes the objects with erroneous size and shape.

#3. The second filter identifies the successfully transfected cells based on the GFP intensity.

#4. The nuclei are enlarged by 15 pixels.

#5. The surround cytoplasmic region (CytoRing) is used to account for the cytosolic GFP intensity. It's obtained by subtracting Enlarged Nuclei region with the Filtered Nuclei region.

#6. Calculation of GFP(N/C) as shown in Figure below.

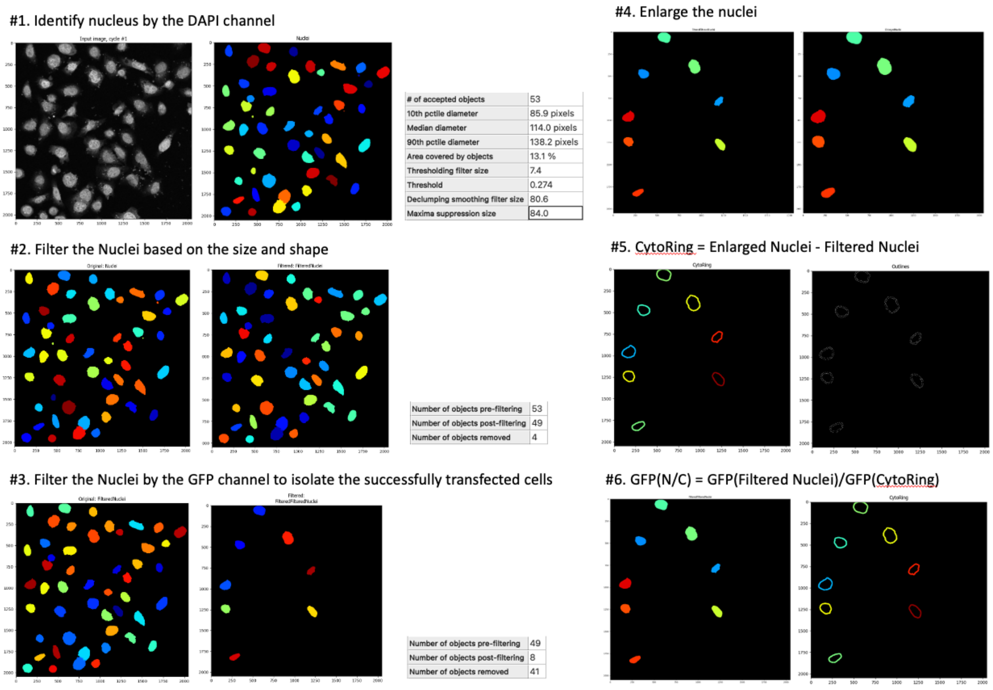

#1. Identify nucleus by the DAPI channel

# of accepted objects	53
10th pctile diameter	85.9 pixels
Median diameter	114.0 pixels
90th pctile diameter	138.2 pixels
Area covered by objects	13.1 %
Thresholding filter size	7.4
Threshold	0.274
Declumping smoothing filter size	80.6
Maxima suppression size	84.0

#2. Filter the Nuclei based on the size and shape

Number of objects pre-filtering	53
Number of objects post-filtering	49
Number of objects removed	4

#3. Filter the Nuclei by the GFP channel to isolate the successfully transfected cells

Number of objects pre-filtering	49
Number of objects post-filtering	8
Number of objects removed	41

#4. Enlarge the nuclei

#5. CytoRing = Enlarged Nuclei - Filtered Nuclei

#6. GFP(N/C) = GFP(Filtered Nuclei)/GFP(CytoRing)

Figure S 5.7 The workflow of using CellProfiler to calculate the translocation efficiency.

Representative CLSM images

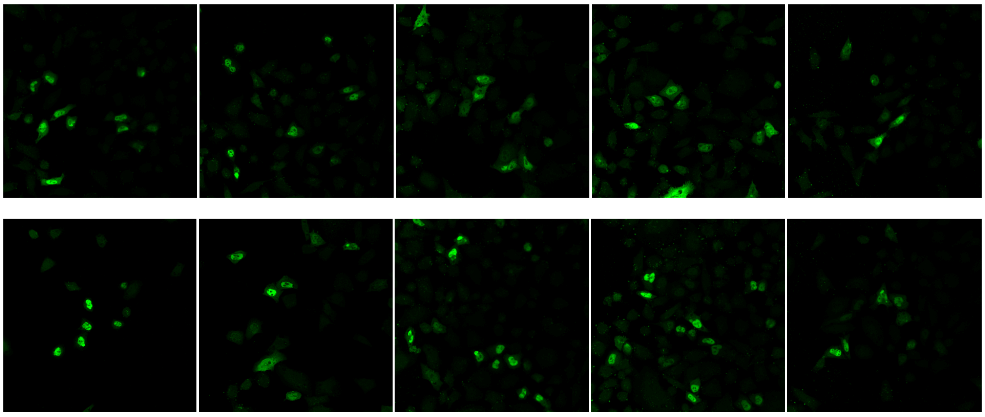

Figure S 5.8 Representative CLSM images from DEX-SCNPs reshuffled into two topologies. Upper: sparse; Lower: Compact.

5.10 REFERENCE

(1) Varkouhi, A. K.; Scholte, M.; Storm, G.; Haisma, H. J. Endosomal Escape Pathways for Delivery of Biologicals. *Journal of Controlled Release* **2011**, *151* (3), 220–228. https://doi.org/10.1016/j.jconrel.2010.11.004.

(2) Chithrani, B. D.; Ghazani, A. A.; Chan, W. C. W. Determining the Size and Shape Dependence of Gold Nanoparticle Uptake into Mammalian Cells. *Nano Lett.* **2006**, *6* (4), 662–668. https://doi.org/10.1021/nl052396o.

(3) Rejman, J.; Oberle, V.; Zuhorn, I. S.; Hoekstra, D. Size-Dependent Internalization of Particles via the Pathways of Clathrin- and Caveolae-Mediated Endocytosis. *Biochemical Journal* **2004**, *377* (1), 159–169. https://doi.org/10.1042/bj20031253.

(4) Dasgupta, S.; Auth, T.; Gompper, G. Shape and Orientation Matter for the Cellular Uptake of Nonspherical Particles. *Nano Lett.* **2014**, *14* (2), 687–693. https://doi.org/10.1021/nl403949h.

(5) Vácha, R.; Martinez-Veracoechea, F. J.; Frenkel, D. Receptor-Mediated Endocytosis of Nanoparticles of Various Shapes. *Nano Lett.* **2011**, *11* (12), 5391–5395. https://doi.org/10.1021/nl2030213.

(6) Cong, V. T.; Wang, W.; Tilley, R. D.; Sharbeen, G.; Phillips, P. A.; Gaus, K.; Gooding, J. J. Can the Shape of Nanoparticles Enable the Targeting to Cancer Cells over Healthy Cells? *Advanced Functional Materials n/a* (n/a), 2007880. https://doi.org/10.1002/adfm.202007880.

(7) Jiang, W.; Kim, B. Y. S.; Rutka, J. T.; Chan, W. C. W. Nanoparticle-Mediated Cellular Response Is Size-Dependent. *Nature Nanotechnology* **2008**, *3* (3), 145–150. https://doi.org/10.1038/nnano.2008.30.

(8) Schmidt, B. V. K. J.; Fechler, N.; Falkenhagen, J.; Lutz, J.-F. Controlled Folding of Synthetic Polymer Chains through the Formation of Positionable Covalent Bridges. *Nature Chemistry* **2011**, *3* (3), 234–238. https://doi.org/10.1038/nchem.964.

(9) Rabbel, H.; Breier, P.; Sommer, J.-U. Swelling Behavior of Single-Chain Polymer Nanoparticles: Theory and Simulation. *Macromolecules* **2017**, *50* (18), 7410–7418. https://doi.org/10.1021/acs.macromol.7b01379.

(10) Wang, J.; Wang, R.; Gu, Y.; Sourakov, A.; Olsen, B. D.; Johnson, J. A. Counting Loops in Sidechain-Crosslinked Polymers from Elastic Solids to Single-Chain Nanoparticles. *Chem. Sci.* **2019**, *10* (20), 5332–5337. https://doi.org/10.1039/C9SC01297D.

(11) Liao, S.; Wei, L.; Abriata, L. A.; Stellacci, F. Control and Characterization of the Compactness of Single-Chain Nanoparticles. *Macromolecules* **2021**. https://doi.org/10.1021/acs.macromol.1c02071.

(12) Arbe, A.; Pomposo, J. A.; Moreno, A. J.; LoVerso, F.; González-Burgos, M.; Asenjo-Sanz, I.; Iturrospe, A.; Radulescu, A.; Ivanova, O.; Colmenero, J. Structure and Dynamics of Single-Chain Nano-Particles in Solution. *Polymer* **2016**, *105*, 532–544. https://doi.org/10.1016/j.polymer.2016.07.059.

(13) Yu, P.; Liu, B.; Kodadek, T. A High-Throughput Assay for Assessing the Cell Permeability of Combinatorial Libraries. *Nat Biotechnol* **2005**, *23* (6), 746–751. https://doi.org/10.1038/nbt1099.

(14) Vandevyver, S.; Dejager, L.; Libert, C. On the Trail of the Glucocorticoid Receptor: Into the Nucleus and Back. *Traffic* **2012**, *13* (3), 364–374. https://doi.org/10.1111/j.1600-0854.2011.01288.x.

(15) Luo, Z.; Zhang, G. Sedimentation of Polyelectrolyte Chains in Aqueous Solutions. *Macromolecules* **2010**, *43* (23), 10038–10044. https://doi.org/10.1021/ma101324j.

(16) Saraste, J.; Palade, G. E.; Farquhar, M. G. Temperature-Sensitive Steps in the Transport of Secretory Proteins through the Golgi Complex in Exocrine Pancreatic Cells. *PNAS* **1986**, *83* (17), 6425–6429. https://doi.org/10.1073/pnas.83.17.6425.

(17) Iacopetta, B. J.; Morgan, E. H. The Kinetics of Transferrin Endocytosis and Iron Uptake from Transferrin in Rabbit Reticulocytes. *Journal of Biological Chemistry* **1983**, *258* (15), 9108–9115. https://doi.org/10.1016/S0021-9258(17)44637-0.

(18) Lesniak, A.; Salvati, A.; Santos-Martinez, M. J.; Radomski, M. W.; Dawson, K. A.; Åberg, C. Nanoparticle Adhesion to the Cell Membrane and Its Effect on Nanoparticle Uptake Efficiency. *J. Am. Chem. Soc.* **2013**, *135* (4), 1438–1444. https://doi.org/10.1021/ja309812z.

(19) Francia, V.; Reker-Smit, C.; Boel, G.; Salvati, A. Limits and Challenges in Using Transport Inhibitors to Characterize How Nano-Sized Drug Carriers Enter Cells. *Nanomedicine* **2019**, *14* (12), 1533–1549. https://doi.org/10.2217/nnm-2018-0446.

(20) Lostalé-Seijo, I.; Louzao, I.; Juanes, M.; Montenegro, J. Peptide/Cas9 Nanostructures for Ribonucleoprotein Cell Membrane Transport and Gene Edition. *Chem. Sci.* **2017**, *8* (12), 7923–7931. https://doi.org/10.1039/C7SC03918B.

(21) Holub, J. M.; LaRochelle, J. R.; Appelbaum, J. S.; Schepartz, A. Improved Assays for Determining the Cytosolic Access of Peptides, Proteins, and Their Mimetics. *Biochemistry* **2013**, *52* (50), 9036–9046. https://doi.org/10.1021/bi401069g.

(22) Li, M.; Tao, Y.; Shu, Y.; LaRochelle, J. R.; Steinauer, A.; Thompson, D.; Schepartz, A.; Chen, Z.-Y.; Liu, D. R. Discovery and Characterization of a Peptide That Enhances Endosomal Escape of Delivered Proteins in Vitro and in Vivo. *J. Am. Chem. Soc.* **2015**, *137* (44), 14084–14093. https://doi.org/10.1021/jacs.5b05694.

(23) Carey, K. L.; Richards, S. A.; Lounsbury, K. M.; Macara, I. G. Evidence Using a Green Fluorescent Protein-Glucocorticoid Receptor Chimera That the Ran/TC4 GTPase Mediates an Essential Function Independent of Nuclear Protein Import. *Journal of Cell Biology* **1996**, *133* (5), 985–996. https://doi.org/10.1083/jcb.133.5.985.

(24) Bus, T.; Traeger, A.; Schubert, U. S. The Great Escape: How Cationic Polyplexes Overcome the Endosomal Barrier. *J. Mater. Chem. B* **2018**, *6* (43), 6904–6918. https://doi.org/10.1039/C8TB00967H.

Chapter 6 Summary and Outlook

6.1 CONTRIBUTIONS OF THIS THESIS

Control topology via geometrical approach

This thesis makes contribution to the field of SCNPs by first discussing the difference between geometry and topology and points out that the latter provides more robust description of the structure of SCNPs. It has been shown that we can gain certain control on the global topology of SCNPs via geometrical approaches, namely, choosing crosslinkers of certain lengths or tuning the precursor chains' conformation via their interaction with solvent molecules.

Introduce AUC into SCNP characterization

To the best knowledge of the candidate, the works from the thesis are one of the first to apply AUC for the characterization of SCNPs. The results have shown that AUC holds huge potential in resolving the topological nuances of SCNPs.

New topology-property paradigm

When one tries to understand particles' structure-property relationship, the current paradigm assumes the "structure" to be related to geometrical features, due to the vast literature based on rigid inorganic nanoparticles. By investigating the cellular interaction with SCNPs of various topologies, this thesis reveals the new paradigm of topology-property relationship.

6.2 OUTSTANDING QUESTIONS

To directly characterize the topology, is it mission impossible?

The characterizing tasks from this thesis were performed to evaluate various aspects of SCNPs' structure to ensure robust interpretation of their global topology. As mentioned, in the strictest pure mathematical sense, topology deals with the connectivity. Is there an approach to directly characterize the topology instead of inferring the topology based on geometrical characterization? Moreover, is it possible to even probe the local topology? Current progress on structural biology might give inspiration to the solution of these problems.

How far are we from protein mimicking? Is it worth the sweat?

While SCNPs bear some resemblance to proteins, the former is regarded as the poor brothers of the latter and they differ in many ways, as summarized by Table 6.1.

Table 6.1 Comparison between proteins and SCNPs

	Proteins	SCNPs
MW dispersity	monodisperse	polydisperse
Sequence	defined	random
Size range/nm	< 20	< 20
Surface property	heterogenous	mostly homogenous
Intra-chain interaction	Non-covalent and disulfide	Covalent or non-covalent
Folding/cross-linking concentration (mg/mL)	~300	<1

To ensure the correct protein folding, amino acids from the polypeptide backbone provides a variety of interaction (hydrophobic, Van de Waals, hydrogen bonding, salt bridges, disulfide, etc.) as driving force to guide the compaction. The state-of-the-art of polymer chemistry lacks the ability to endow polymer chains with the suitable functionality at the right position. Protein folding is usually achieved at very crowded intracellular environment (300~400 mg/ml) yet maintains its robustness whereas single-chain reaction usually requires ultra-low concentration (<1 mg/ml), where the intra-chain interaction dominates, and this poses a challenge for the efficient production of SCNPs.

There's a long way ahead before polymer chemists can translate the structure-property relationship, learnt from proteins, onto synthetic polymeric nanoparticles. To this end, current limitations are from both sides of polymer and protein. From the side of polymer science, the current polymerization technologies do not allow us to construct sequence-defined synthetic polymer chains. From the protein side, our knowledge on protein folding limits our ability to reproduce the process.

Where do we place SCNPs via supramolecular interactions?

The topological discussion from this thesis is based on the classical model where the one crosslinking event creates one loop, representing well most of the scenarios where bifunctional external crosslinkers are applied or the internal crosslinking moieties are mono-valent. For the type of SCNPs via supramolecular chemistries, including hydrogen bonds, host-guest interaction, pi interactions, metal coordination, and hydrophobic interactions, some of the topological concepts should be adapted.

Curriculum Vitae

SUIYANG LIAO

Materials Scientist at EPFL
Avenue de Lonay 11, 1110 Morges, Switzerland
(+41) 78 732 20 47
suiyang.liao@epfl.ch
LinkedIn | Skype | Google Scholar

Strengths

- Characterization of polymeric nanoparticles, proteins, oligonucleotides and etc.
- Developing in vitro assays
- Data analysis: Simulation and visualization via Python

Education

École polytechnique fédérale de Lausanne (EPFL) *Lausanne, Switzerland*
PhD candidate in Materials Science *2017-Present*
Thesis: Single-chain nanoparticles and its applications in intracellular drug delivery

Tsinghua University *Beijing, China*
Bachelor of Engineering in Materials Science and Engineering *2011-2016*
Bachelor of Business Administration *2013-2016*

Core Experience

Supramolecular Nano-Materials and Interfaces Laboratory (EPFL) *Lausanne, Switzerland*
PhD candidate

Project 1: Protein corona on Au nanoparticles *2017-2018*
We developed AUC to understand the protein corona formation on Au nanoparticles covered with various ligands.

Project 2: Surface Characterization of bimetallic nanoparticles via MALDI-TOF *2018-2019*
MALDI-TOF was developed as a tool to characterize the surface composition and morphology of AuAg bimetallic nanoparticles.

Project 3: Single-chain folding *2019-2021*
Establish experimental validation on single-chain folding and develop a set of methods to characterize the conformation of single-chain nanoparticles

Project 4: Single-chain nanoparticles for intracellular delivery of biologics *2020-2022*
Developing single-chain nanoparticles for the intracellular delivery of peptides and siRNA

Additional Experience

ETH Zurich *Zürich, Switzerland*
Guest Student
Collaboration in the group of Prof. Renato Zenobi to learn MALDI-TOF *2019 Summer*

The University of Tokyo *Tokyo, Japan*
Summer Intern
Developing polymeric micelle for in-vivo protein delivery *2018 Summer*

University of Oxford *Oxford, UK*
Summer Intern *2015 Summer*

Languages

English (fluent), Chinese (native), French (A1)

Professional skills

Lab experience

Chemistry lab (Nano2)
Biological lab (BSL-2)

Chemistry

Synthesis and ligand exchange of gold nanoparticles;
thiolene click reaction;
Protein surface engineering;

Purification

Extraction; Dialysis; Vacuum; filtration; Lyophilization

Biological assay

Cell penetration assay;
Cytotoxicity test via MTS/MTT assay;
Transfection of pDNA and siRNA

Analytical skills

Mass spectrometry: MALDI-TOF, ESI;
NMR: Proton, DOSY, HSQC, relaxation;
Analytical Ultracentrifugation
Size exclusion chromatography
Spectroscopy: XPS; FTIR; uv-vis
Microscopy: CLSM; AFM; TEM; SEM
Scattering: DLS; SAXS
Other:
CLSM; Flow cytometry; Zeta-potential; thermal gravimetric analysis; Viscometery; Densimetery; SDS-page

Data analysis and visualization

MatLab; Python (NumPy, Pandas, Matplotlib, Seaborn);
Origin; ImageJ

Hobbies

Basketball; Badminton; Ski; Hiking; Swimming; Acoustic guitar

Extracurricular Activities

Lecturer at Business School, Hohai University	*Nanjing, China*
Organized a graduation party for ~200 students, School of Economy and Management, Tsinghua University	*Bejing, China*
Teaching assistant for EPFL master student course, Soft Matter	*Lausanne, Switzerland*
Supervising eight EPFL master students for lab immersion	*Lausanne, Switzerland*

Journal Publications:

(during PhD study)

1. Liao, S.*, Wei, L., Abriata, L., Stellacci, F.*, 2021. Control and Characterization of the Compactness of Single-Chain Nanoparticles. Macromolecules 54, 24, 11459–11467
2. Liao, S., Luo, Z., Metternich, J., Zenobi, R., Stellacci, F., 2020. Quantification of surface composition and segregation on AuAg bimetallic nanoparticles by MALDI MS. Nanoscale 12, 22639–22644.
3. Yang, Y., Liao, S., Luo, Z., Qi, R., Mac Fhionnlaoich, N., Stellacci, F., Guldin, S., 2020. Comparative characterisation of non-monodisperse gold nanoparticle populations by X-ray scattering and electron microscopy. Nanoscale 12, 12007–12013.
4. Tao, A., Huang, G.L., Igarashi, K., Hong, T., Liao, S., Stellacci, F., Matsumoto, Y., Yamasoba, T., Kataoka, K., Cabral, H., 2020. Polymeric Micelles Loading Proteins through Concurrent Ion Complexation and pH-Cleavable Covalent Bonding for In Vivo Delivery. Macromol. Biosci. 20, 1900161.
5. Bekdemir, A., Liao, S., Stellacci, F., 2019. On the effect of ligand shell heterogeneity on nanoparticle/protein binding thermodynamics. Colloids Surf. B Biointerfaces 174, 367–373.

(before PhD study)

6. Bai, X., Liao, S., Huang, Y., Song, J., Liu, Z., Fang, M., Xu, C., Cui, Y., Wu, H., 2017. Continuous Draw Spinning of Extra-Long Silver Submicron Fibers with Micrometer Patterning Capability. Nano Lett. 17, 1883–1891.
7. Huang, Y., Bai, X., Zhou, M., Liao, S., Yu, Z., Wang, Y., Wu, H., 2016a. Large-Scale Spinning of Silver Nanofibers as Flexible and Reliable Conductors. Nano Lett. 16, 5846–5851.
8. Huang, Y., Liao, S., Ren, J., Khalid, B., Peng, H., Wu, H., 2016b. A transparent, conducting tape for flexible electronics. Nano Res. 9, 917–924.
9. Liao, S., Bai, X., Song, J., Zhang, Q., Ren, J., Zhao, Y., Wu, H., 2017a. Draw-Spinning of Kilometer-Long and Highly Stretchable Polymer Submicrometer Fibers. Adv. Sci. 4, 1600480.
10. Wang, H., Liao, S., Bai, X., Liu, Z., Fang, M., Liu, T., Wang, N., Wu, H., 2016. Highly Flexible Indium Tin Oxide Nanofiber Transparent Electrodes by Blow Spinning. ACS Appl. Mater. Interfaces 8, 32661–32666.

Book Chapter:

Liao, S., Huang, Y., Wu, H., 2017b. Functional Nanofibers for Flexible Electronics, in: Kyung, C.-M., Yasuura, H., Liu, Y., Lin, Y.-L. (Eds.), Smart Sensors and Systems: Innovations for Medical, Environmental, and IoT Applications. Springer International Publishing, Cham, pp. 335–358.

Patent:

Wu, H., Bai, X., Huang, Y., Liao, S. (China Patent No. CN106637679)